Distribution Agreement

In presenting this thesis or dissertation as a partial fulfillment of the requirements for an advanced degree from Emory University, I hereby grant to Emory University and its agents the non-exclusive license to archive, make accessible, and display my thesis or dissertation in whole or in part in all forms of media, now or hereafter known, including display on the world wide web. I understand that I may select some access restrictions as part of the online submission of this thesis or dissertation. I retain all ownership rights to the copyright of the thesis or dissertation. I also retain the right to use in future works (such as articles or books) all or part of this thesis or dissertation.

Signature:

_____ _____

Irving Martinez Date

Mathematical modeling and simulation of coronary stents

By

Irving Martinez
Doctor of Philosophy

Mathematics

Alessandro Veneziani, Ph.D.
Advisor

Talea Mayo, Ph.D.
Committee Member

Yuanzhe Xi, Ph.D.
Committee Member

Accepted:

Kimberly Jacob Arriola, Ph.D.
Dean of the James T. Laney School of Graduate Studies

Date

Mathematical modeling and simulation of coronary stents

By

Irving Martinez

Advisor: Alessandro Veneziani, Ph.D.

An abstract of
A dissertation submitted to the Faculty of the
James T. Laney School of Graduate Studies of Emory University
in partial fulfillment of the requirements for the degree of
Doctor of Philosophy
in Mathematics
2023

Abstract

Mathematical modeling and simulation of coronary stents
By Irving Martinez

Every year approximately 3 million people in the US suffer from atherosclerosis, which is the condition in which one or more arteries get clogged up from excessive cholesterol and other residue build up. In spite of being introduced into the market decades ago, coronary stents remain the most popular solution, given their low surgery risk. However, stents are prone to malfunction after some time, with each type having its own set of complications. The introduction of newer types of stents to resolve the problems of their predecessors comes at the expense of creating different drawbacks. To have better insight into the physiological consequences of stent development, we give a contribution to fully understand stents through rigorous mathematical theory and modeling.

In this work, we emphasize the understanding and application of PDEs such as Navier-Stokes and advection-diffusion equations in the context of hemodynamics to explore the blood velocity and pressure, the concentration of solutes, and the dissipation of drug across the stented artery system. Given the presence of lumen, wall, and stent regions, it is necessary to develop domain decomposition techniques through adaptations of Gauss-Seidel and Jacobi solvers. We extend Steklov-Poincaré theory to multiple domains by taking into account the interplay of distinct meshed domains. And meshing reassignment methods are elaborated with the purpose of sculpting geometries or transforming meshes over time. Overall, the composition and combination of our methods provides a theoretical and numerical groundwork to model different types of stent.

Mathematical modeling and simulation of coronary stents

By

Irving Martinez

Advisor: Alessandro Veneziani, Ph.D.

A dissertation submitted to the Faculty of the
James T. Laney School of Graduate Studies of Emory University
in partial fulfillment of the requirements for the degree of
Doctor of Philosophy
in Mathematics
2023

Acknowledgments

Words cannot express my gratitude to my PhD advisor and chair of my committee Professor Alessandro Veneziani for his invaluable patience and guidance. I also could not have undertaken this journey without my defense committee, Dr. Talea Mayo and Dr. Yuanzhe Xi, who generously provided knowledge and expertise. Additionally, this endeavor would not have been possible without the generous support from Emory University, in particular the mathematics department and Laney Graduate School.

I would like to thank my research group peers for their support and ideas: Leonardo Molinari, Imran Shah, and Jimena Martin Tempestti, and Francesco Brarda. I am grateful to my cohort members for their companionship and moral support: Marcelo Sales, Kelvin Kan, Jack Barlow, and Chris Keyes. Thanks should also go to my office and department mates: Ayush Basu, Vishwanath Segeri, Shilpi Mandal, Davide Evangelista, and Jennifer Wang.

Lastly, I would be remiss in not mentioning my family, especially my parents Martha Acosta Varela and René Ramón Martínez Arroyo, my sister Paloma Vianey, my uncle Jorge Martinez, and my aunt Silvia Martinez. I also want to express eternal gratitude, in no particular order to my following friends for always believing in me, supporting me, and keeping my spirits and motivation high during this process: Genaro Andazola, Guillermo Lopez, Ismael Acevedo, Anna Barker, René Mata, Hector Zepeda, Vincent Bornert, Walter Marroquin, Valeria Labrado, Xavier Villaseñor, Franco Treviño, Andrea Caraveo, Silvia Spadoni, Oriane Brossard, Denise Pinheiro, Natalia Gonzalez, Julia Martin, Johanna Rauls, Ana Victoria Valenzuela, Aline Martins, Eulora Skelton, AnnMarie Sullivan, Estefany Palma, Citlali Cardenas, Christian Esparza, Daniel Gabillo, Carolina Barraza, Ryan Salchert, Eddie Dragone, Mumi Velez, Yazmin Osornio, Jenna Gowell, Andrés Flores, Mariana Ospina, Sofia Michelle, Lizeth Martinez, Nancy Moya, Alejandra Apodaca, my Milwaukee friends, my Juarez friends, and my Emory and Atlanta friends.

Contents

List of Figures

Chapter 1

Introduction and Mathematical Preliminaries

1.1 Introduction

Atherosclerosis is a condition in which blood vessels become narrow and constricted over time due to excessive cholesterol plaque and residue buildup, preventing blood from flowing smoothly.[10] It is common as more than three million cases in the United States are reported per year, affecting mostly older people of ages 45 and 55 for women and men, respectively.[1]. Without treatment, atherosclerosis can result in other life-threatening conditions and diseases, including coronary artery disease, carotid artery disease, peripheral artery disease, aneurysms, and chronic kidney disease.[24] [13]
Several solutions have been proposed to prevent the danger of atherosclerosis such a healthy lifestyle, non-invasive surgeries like angioplasty, and even risky procedures of the coronary bypass surgery type.[46][17][8] Balloon angioplasty is a non-invasive percutaneous procedure to reopen an occluded coronary by deploying a balloon inflation; however, this measure is rather temporary as the affected passageway is more likely to become obstructed again.[21] On the other hand, a coronary bypass surgery requires open surgery to reroute some of the artery network around the blocked artery.[35]
In the quest for a minimally invasive and more permanent procedure, the stent was developed.[31] A stent is a cylindrical mesh that is usually inserted through the leg and guided all the way internally until it reaches the damaged zone. Then, with enough pressure the stent is expanded and fixed in place, opening up the narrow area and allowing blood to flow again freely. However, the stent still suffered from par-

ticular complications. For instance, the first ever stents were called *bare metal stents* (BMS) and comprised of only a metal base, which proved to be quite damaging to the arterial tissue and produced unwanted clotting, resulting in a hardened constriction of the passageway.[55] To circumvent this, *drug eluting stents* (DES) were designed by adding a thick drug coating to aid with the tissue healing and prevent possible infections; but consequently, this provoked early thrombosis.[47] In spite of newer types of stents constantly being introduced, DESs remain the most popular prostheses.
While this is a consolidated technology, *bioresorbable stents* (BRS) were introduced (see e.g., [62]) to avoid the significant drawback of a metallic coil located lifelong in the patient. This was supposedly an ideal solution for young patients affected by acute (as opposed to chronic) diseases. However, the number of adverse events associated with BRS led to their withdrawal from the market. A common speculation is that the abnormal thickness required by the non-metallic structure to stand the pressure during deployment may trigger anomalous flow patterns downstream the struts; these patterns, in turn, may induce inflammations with a consequent re-occlusion of the artery.
This case study pinpoints the importance of a more accurate and massive numerical modeling behind the design of prostheses in biomedicine. Either for a deeper understanding of the complex dynamics (ranging from mechanics to biology related to the geometry of stented arteries) or for a rigorous shape-optimization (rooted in mathematical methods), the role of numerical modeling in this field cannot be underestimated. While the biomedical community still considers BRS an unmet clinical need [34], the role of mathematical modeling in developing next-generation prostheses is critical.

Recent studies [38] demonstrated the tremendous complexity of the morphology of stented arteries. At the bottom line, we have three different domains in this problem, the lumen (L) of the coronary, the wall (W), and the struts of the stent (S). They are in contact in various ways, ranging from struts completely embedded in the wall to struts floating in the lumen as in the case of so-called "malapposed stents". Numerical modeling of the erosion of the struts is a key factor for shape optimization and design; it must include the three domains in all the possible conformations that may happen in patients.
Modeling of the elution of DES was considered in several papers with a different complexity depending on the emphasis on the chemical elution process or on the numerical

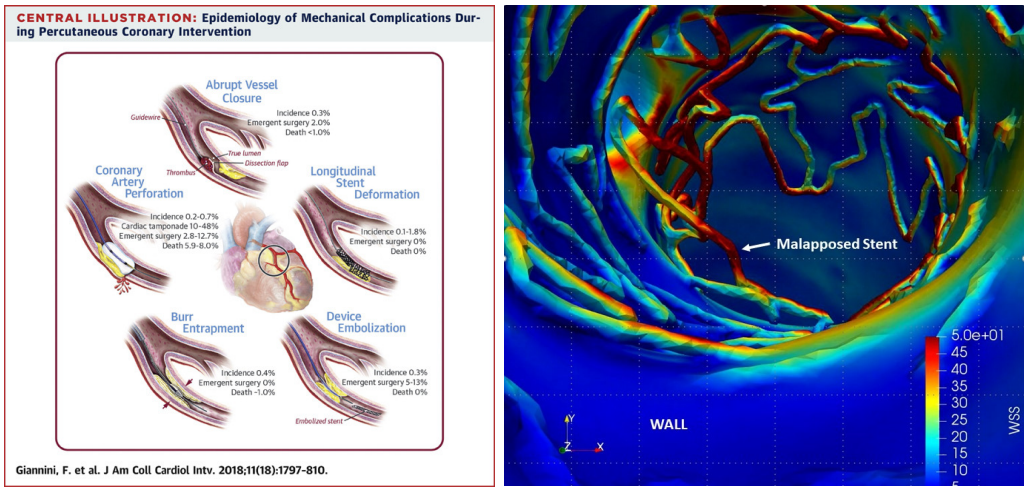

Figure 1.1: Left: deployment of a coronary stent [20]. Right: An internal reconstruction of a stented artery with a malapposed stent.

efficiency. For instance, in [15], the authors consider a pretty complex elution model only for cases when the struts are all embedded in the wall. In this way, there are 3 domains but they are never in contact altogether. Considering the general case where the three domains are all in contact is not just a mere geometrical extension. The time scale of the elution at the interface between the wall and the struts is generally slower, as the wall has a small convective field (the motion of water in the wall is minimal); on the contrary, the interface between the lumen and the strut features a much stronger convective field (the blood velocity), consequently a much faster erosion. When we assume to have both interfaces, the simultaneous presence of different scales may challenge the numerical solver.

In this work, we focus specifically on numerical methods for simplified elution models (inspired by the works for generic blood solutes in [52, 53]) involving all the possible positions among the different sub-domains. In the first chapter, we present standard mathematical preliminaries necessary for the theoretical background and undertaking of this project. In **Chapter 2**, we provide a multi-domain multi-interface formulation of the problem and a substructring iterative method for its effective solution. Numerical results of BMS modeling demonstrate the independence of the number of iterations of the mesh size. To better understand this property, we resort to a Steklov-Poincarè (SP) operator approach, leading to a system of three interface equations (LW, LS, SW). The extension of the basic SP formalism to a multi-domain setting presents some non-trivial novel aspects investigated here; it provides a key argument to explain the mesh-independence. We emulate BMS behavior through our simplified

geometries, parametric setup, and blood velocity and solute concentration behavior via Navier-Stokes and advection-diffusion, respectively. Then in **Chapter 3**, we expand the multi-domain notion in the context of drug movement and dynamics across the different domains, enabling us to model DESs. Moreover, in **Chapter 4**, we introduce meshing reassignment techniques with the objective of exploring remeshing-free geometry sculpture algorithms as well as for setting the groundwork to consider time-evolving domains. Finally, in **Chapter 5**, we emphasize future research stemming from the contents expounded here. This is the first step toward the construction of numerical and mathematical modeling to enable a shape-optimization analysis to identify engineering solution for the next generation of BRS.

1.2 Mathematical preliminaries

Definitions

We summarize some mathematical notation and results that will be useful for the contents presented in this work. Let Ω be a general an open set in $\mathbb{R}^d$. For $1 \leq p \leq \infty$, we will denote $L^p(\Omega)$ be the space of functions whose pth power is integrable in Ω, with norm $||\cdot||_{L^p(\Omega)}$. In the case of $p = \infty$, we let L^∞ be the space of functions in Ω that are essentially bounded. The scalar product of L^2 is indicated by $(\cdot, \cdot)$; and given $s \in \mathbb{N}$, $H^s(\Omega)$ is the Sobolev space of functions $v \in L^2$ such that their distributional derivatives of order up to s are L^2-integrable. Its norm is given by $||\cdot||_{H^s(\Omega)}$), and in the case of $s = 0$, H^s is simply L^2.

If we let Σ be an open and nonempty subset of $\partial\Omega$, then we define $H^{1/2}(\Sigma)$ to be the space of traces, defined on Σ, of functions belonging to $H^1(\Omega)$. Since we will be dealing constantly with mappings from traces in $H^{1/2}(\Sigma)$ to functions in $H^1(\Omega)$ and viceversa, we need to introduce necessary operators. We let $\gamma : H^1(\Omega) \to H^{1/2}(\Sigma)$ be a surjective and continuous operator; and on the other hand, the existence of a lifting map $\mathcal{L} : H^{1/2}(\Sigma) \to H^1(\Omega)$ such that it is injective, linear, and continuous and that for all $\lambda \in H^{1/2}(\Sigma)$ we have $\lambda = \gamma\mathcal{L}\lambda$ can be proven. Furthermore, we let $H^1_\Sigma(\Omega)$, more commonly written as $H^1_0(\Sigma)$, be the subspace of $H^1(\Omega)$ such that its functions have null traces on Σ. Now, for a $(d-1)$-dimensional manifold Γ in $\overline{\Omega}$ such that $\Gamma \cap \Sigma \neq \emptyset$, we allow $H^{1/2}_{00}(\Gamma)$ to be the subspace of $H^{1/2}(\Gamma)$ whose members consist of traces of $u \in H^1_\Sigma(\Omega)$. We will be dealing with this kind of space very often, so for simplicity we set $\Lambda = H^{1/2}_{00}(\Gamma)$, with Λ' being its dual. [6]

Important classic results

We now proceed with some established instrumental results.

Theorem 1.2.1 (Holder's Inequality)**.** Assume that $f \in L^p(\Omega)$ and $g \in L^q(\Omega)$ with $1 \leq p \leq \infty$ and such that q is the conjugate exponent of p (i.e. $\frac{1}{p} + \frac{1}{q} = 1$). Then $fg \in L^1$ and

$$\int_\Omega |fg| d\omega \leq \|f\|_{L^p(\Omega)} \|g\|_{L^q(\Omega)}.[6]$$

Theorem 1.2.2 (Trace theorem)**.** Assume Ω is bounded and Σ is C^1. Then there exists a bounded linear operator

$$\gamma : H^1(\Omega) \to H^{1/2}(\Sigma)$$

such that

$$\gamma u = u|_\Sigma \quad \text{if} \quad u \in H^1(\Omega) \cap C(\overline{\Omega}),$$

and

$$||\gamma u||_{H^{1/2}(\Sigma)} \leq C_t ||u||_{H^1(\Omega)}, \tag{1.1}$$

for each $u \in H^1(\Omega)$ with the constant $C_t > 0$ depending only on Ω.[12]

Theorem 1.2.3 (Poincare's inequality)**.** Assume Ω is a bounded, open subset of $\mathbb{R}^d$ and suppose $u \in H^1_\Gamma(\Omega)$, where $\Gamma \subseteq \Sigma$. Then we have the inequality

$$||u||_{L^2(\Omega)} \leq C||\nabla u||_{L^2(\Omega)} \quad \forall u \in H^1_0(\Omega),$$

with $C > 0$ depending only on Ω.[6]

For two Banach spaces, X and Y, we say that Y is continuously embedded into X, denoted by $Y \hookrightarrow X$, if for any $u \in Y$, we have also that $u \in X$, and if the embedding map is continuous; that is, for all $u \in Y$

$$\|u\|_X \leq C\|u\|_Y,$$

where $C > 0$.

Theorem 1.2.4 (Sobolev embedding theorem)**.** Let $1 \leq p \leq \infty$, $k \in \mathbb{Z}_+$, and Ω be a bounded open set in $\mathbb{R}^d$ with non-empty and Lipschitz-continuous boundary. Then we have the following statements:

1. For $kp > d$, $W^{k,p}(\Omega) \hookrightarrow C(\overline{\Omega})$;
2. For $kp = d$, $W^{k,p}(\Omega) \hookrightarrow L^q(\Omega)$, for all $q \in [1, \infty)$.
   Furthermore
   $$W^{d,1}(\Omega) \hookrightarrow C(\overline{\Omega}).$$
3. For $kp < d$, $W^{k,p}(\Omega) \hookrightarrow L^q(\Omega)$, with $\frac{1}{q} = \frac{1}{p} - \frac{k}{p}$.[12]

Let ζ be a positive function in $L^2(\Sigma)$ and consider $\lambda, \rho \in H^{1/2}(\Sigma)$. Then by Theorem 1.2.4, we observe that λ and ρ belong to $L^4(\Sigma)$, so that using Cauchy-Schwarz inequality gives

$$\left(\int_\Sigma |\lambda\rho|^2 d\gamma\right)^{1/2} \leq \left(\int_\Sigma |\lambda|^4 d\gamma\right)^{1/4} \left(\int_\Sigma |\rho|^4 d\gamma\right)^{1/4} = ||\lambda||^2_{L^4(\Sigma)} ||\rho||^2_{L^4(\Sigma)},$$

thus $\lambda\rho \in L^2(\Sigma)$. Letting $\mathcal{L}\lambda$ and $\mathcal{L}\rho$ be continuous liftings of λ and ρ from Σ to Ω, we get

$$\begin{aligned} \left|\int_\Sigma \zeta\lambda\rho d\gamma\right| &\leq \left(\int_\Sigma |\zeta|^2 d\gamma\right)^{1/2} \left(\int_\Sigma |\rho\lambda|^2 d\gamma\right)^{1/2} \\ &= ||\zeta||_{L^2} ||\lambda||_{L^4(\Sigma)} ||\rho||_{L^4(\Sigma)} \\ &\leq C_e^2 ||\zeta||_{L^2} ||\lambda||_{H^{1/2}(\Sigma)} ||\rho||_{H^{1/2}(\Sigma)} \\ &\leq C^2 ||\mathcal{L}\lambda||_{H^1(\Omega)} ||\mathcal{L}\rho||_{H^1(\Omega)}, \end{aligned} \tag{1.2}$$

where $C^2 = C_e^2 C_t^2 ||\zeta||_{L^2(\Sigma)}$, C_e the embedding constant from the Sobolev embedding theorem, and C_t the constant of the trace inequality (1.1). With this in mind, we can make the following definitions:

$$\begin{aligned} (\rho, \lambda)_\zeta = \int_\Sigma \zeta\rho\lambda = \left(\sqrt{\zeta}\lambda, \sqrt{\zeta}\rho\right) \quad \forall \lambda, \rho, \in H^{1/2}(\Sigma). \\ ||\lambda||_\zeta = (\lambda, \lambda)_\zeta = ||\sqrt{\zeta}\lambda||^2_{L^2(\Sigma)} \quad \forall \lambda \in H^{1/2}(\Sigma). \text{[52]} \end{aligned} \tag{1.3}$$

Furthermore, if $\zeta(\cdot) > 0$ almost everywhere, $\|\lambda\|_\zeta$ is a norm of λ equivalent to $\|\lambda\|_{H^{1/2}(\Sigma)}$.

Space-time functions. For space-time functions $v : (0,T) \times \Omega \to \mathbb{R}$, we consider the following space

$$L^2(0,T;L^2(\Omega)) := \left\{ v : (0,T) \to H^s \mid v(t) \text{ is measurable, } \int_0^T \|v(t)\|^2_{H^s(\Omega)} dt < \infty \right\}$$

with the norm

$$\|v\|_{L^2(0,T;H^s(\Omega))} := \left(\int_0^T \|v(t)\|^2_{H^s(\Omega)} dt \right)^{1/2}.$$

Similarly, we establish

$$\begin{aligned} L^\infty(0,T;L^2(\Omega)) := \{ & v : (0,T) \to H^s \mid v(t) \text{ is measurable and} \\ & \|v(t,\cdot)\|^2_{L^2(\Omega)} \text{ is essentially bounded in } (0,T) \} \end{aligned}$$

endowed with the norm

$$\|v\|_{L^\infty(0,T;L^2(\Omega))} := \inf \left\{ M > 0 \mid \|v(t,\cdot)\|^2_{L^2(\Omega)} \leq M \text{ almost everywhere in } (0,T) \right\}.$$

Chapter 2

Steklov-Poincaré analysis of the basic three-domain stent problem

2.1 Stent geometry

We initially consider a simple stent geometry $\overline{\Omega} \subset \mathbb{R}^d, (d = 2, 3)$ conformed by three subdomains Ω_l, Ω_w, and Ω_s, all of them belonging to $\mathbb{R}^d$ and any two of which sharing a boundary interface. $\overline{\Omega}$ corresponds to a cardiovascular structure, with Ω_l, Ω_w, and Ω_s denoting the lumen, artery wall, and stent, respectively (See Figure 2.1).

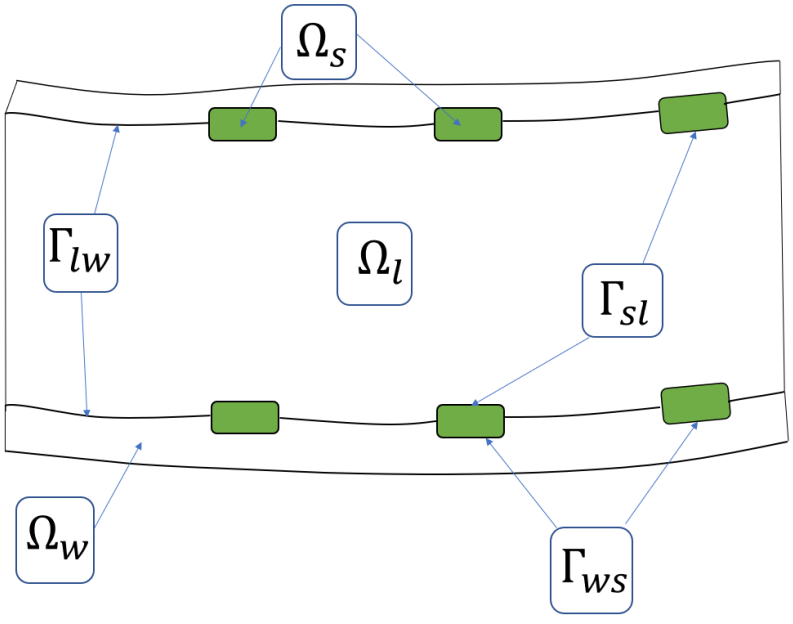

Figure 2.1: Diagram of simple stent domain

The boundary $\partial\Omega$ of $\overline{\Omega}$ is divided into proximal sections $\partial\Omega_{in}$ for incoming flow, distal sections $\partial\Omega_{out}$ for outgoing flow, and the external longitudinal boundary $\partial\Omega_{ext}$. In general, we let the entire domain $\overline{\Omega}$ be split into Ω_l, Ω_w, and Ω_s as follows.

- The domain Ω_w is the outermost shell of $\overline{\Omega}$ such that its outer surface $\partial\Omega_{w,ext}$ along the longitudinal axis of $\overline{\Omega}$ equals the outer surface $\partial\Omega_{ext}$ of $\overline{\Omega}$. Its closure intersects intermittently both Ω_l and Ω_s at $(d-1)$-manifolds Γ_{lw} and Γ_{ws}, respectively. In other words, these intersections are such that $\Gamma_{lw} = \overline{\Omega_w} \cap \overline{\Omega_l}$ and $= \Gamma_{sw} = \overline{\Omega_w} \cap \overline{\Omega_s}$. Solutes, but not blood, will flow through the incoming boundary $\partial\Omega_{w,in}$ and exit through the outgoing boundary $\partial\Omega_{w,out}$, located along the radial axis.

- Ω_l is the lumen of the artery, covered by the wall interface Γ_{lw} and stent boundary Γ_{sl}. Blood passes through the lumen from $\partial\Omega_{l,in}$ and leave through $\partial\Omega_{l,out}$. This is the convective part of the geometry responsible for the velocity of blood and oxygen.

- The third domain Ω_s inside $\overline{\Omega}$ is the stent of the artery. In the case of our simplified stent, it is merely blocks between the artery wall and lumen, but in actuality a stent is more realistically comprised by a net-like structure wrapped around the lumen (See Figure 2.2).[9] The important feature of Ω_s is that no fluid passes through it but rather around it. Specifically, solutes pass around both manifolds Γ_{ws} and Γ_{sl} while blood only surrounds Γ_{sl}.

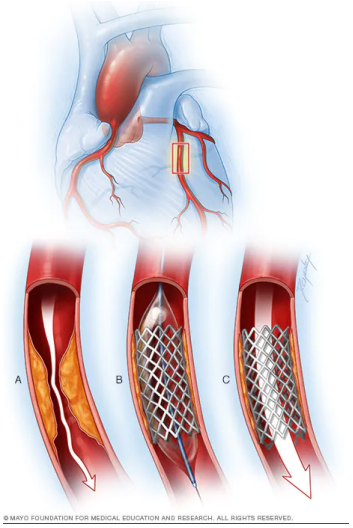

Figure 2.2: Illustration of coronary stent

In reality, the material of the stent can be of metallic or polymeric nature, or both.[19] In this first part, we assume that the struts are of bare metal, so that its volume is consistent over time. Furthermore, we will denote the intersection of Γ_{lw} and Γsl by Γ_{lws}, and notice that this is also the intersection of either with Γ_{ws}.

2.2 Mathematical analysis of simplified stent

The mathematical undertaking of the lumen and wall structure has already been explored with numerical results of two-dimensional simulations.[53] We illustrate an expansion of this model by adding a simplified stent in the form of a third domain as well as by implementing numerical schemes in three dimensions.

2.2.1 Blood and concentration equations

Given the sufficiently large artery channel and the natural composition of blood, it is reasonable to assume blood to have constant viscosity ν and to possess Newtonian fluid properties as well as to allow it circulate through rigid walls, then we can solve the blood velocity and pressure through incompressible Navier-Stokes.[2] For $\mathbf{x} \in \Omega_l$ and $t > 0$ we let $\mathbf{u}(t, \mathbf{x}) \in \mathbb{R}^d$ be the velocity of blood and $P(t, \mathbf{x})$ its pressure. Through momentum and mass conservation the following Navier-Stokes equations can be derived and applied in a cardiovascular setting:

$$
\left\{
\begin{array}{l}
\rho \frac{\partial \mathbf{u}}{\partial t} + \rho(\mathbf{u} \cdot \nabla)\mathbf{u} - \nu \Delta \mathbf{u} + \nabla P = \mathbf{f} \quad x \in \Omega_l, \qquad t > 0, \\
\nabla \cdot \mathbf{u} = 0 \quad \mathbf{x} \in \Omega_l, \qquad t > 0, \\
\mathbf{u} = \mathbf{b} \quad \text{on} \quad \partial\Omega_{l,in}, \quad t > 0 \\
\mathbf{u} = \mathbf{0} \quad \text{on} \quad \Gamma_{lw}, t > 0 \\
\mathbf{u} = \mathbf{0} \quad \text{on} \quad \Gamma_{sl}, t > 0, \\
P\mathbf{n} - \rho\nu \nabla \mathbf{u} \cdot \mathbf{n} = P_{ext}\mathbf{n} \quad \text{on} \quad \partial\Omega_{l,out} \qquad t > 0, \\
\mathbf{u}(\mathbf{x}, \mathbf{t}) = \mathbf{u}_0 \quad \text{with} \quad \nabla \cdot \mathbf{u}_0 = 0, \quad \mathbf{x} \in \Omega_l, \quad t = 0.
\end{array}
\right. \tag{2.1}
$$

Here $\mathbf{f}$ is a local source function, such as gravity, $\mathbf{b}$ is the inflow blood velocity function, $\mathbf{u}_0$ is the initial blood velocity in Ω_l at time $t = 0$, P_{ext} is the external pressure, and $\mathbf{n}$ is the normal to the boundaries of Ω_l, including the interfaces Γ_{lw} and Γ_{sl}.
However, while blood is constrained to the lumen part of $\overline{\Omega}$, the concentration of

solutes $C(\mathbf{x}, t)$ exhibits convective flow behavior in Ω_l and advection-diffusion movement in Ω_w.[53] The dynamics of $C_i(t, \mathbf{x})$ $(i = l, w, s)$ are described by the following system of equations

$$\frac{\partial C_l}{\partial t} - \mu_l \Delta C_l + \mathbf{u} \cdot \nabla C_l = s_l \quad \text{in} \quad \Omega_l, \quad t > 0, \tag{2.2}$$

$$\frac{\partial C_w}{\partial t} - \mu_w \Delta C_w = s_w \quad \text{in} \quad \Omega_w, \quad t > 0, \tag{2.3}$$

$$\frac{\partial C_s}{\partial t} - \mu_s \Delta C_s = s_s \quad \text{in} \quad \Omega_s, \quad t > 0, \tag{2.4}$$

Here, the s_i represent source (forcing) functions, μ_i are diffusivity terms. Furthermore, the following interface conditions hold as well:

$$\begin{cases} \mu_l \frac{\partial C_l}{\partial \mathbf{n}_l} + \zeta(C_l - C_w) = 0 \quad \text{on} \quad \Gamma_{lw}, \\ \mu_w \frac{\partial C_w}{\partial \mathbf{n}_w} + \zeta(C_w - C_l) = 0 \quad \text{on} \quad \Gamma_{lw}, \end{cases} \tag{2.5}$$

$$\begin{cases} \mu_s \frac{\partial C_s}{\partial \mathbf{n}_s} + \zeta(C_s - C_l) = 0 \quad \text{on} \quad \Gamma_{sl}, \\ \mu_l \frac{\partial C_l}{\partial \mathbf{n}_l} + \zeta(C_l - C_s) = 0 \quad \text{on} \quad \Gamma_{sl}, \end{cases} \tag{2.6}$$

$$\begin{cases} \mu_w \frac{\partial C_w}{\partial \mathbf{n}_w} + \zeta(C_w - C_s) = 0 \quad \text{on} \quad \Gamma_{ws}, \\ \mu_s \frac{\partial C_s}{\partial \mathbf{n}_s} + \zeta(C_s - C_w) = 0 \quad \text{on} \quad \Gamma_{ws}, \end{cases} \tag{2.7}$$

Notice that continuity at the interfaces allows us to express (2.5), (2.6), and (2.7) in the following equivalent form:

$$\mu_l \frac{\partial C_l}{\partial \mathbf{n}_l} = -\mu_w \frac{\partial C_w}{\partial \mathbf{n}_w} \quad \text{on} \quad \Gamma_{lw} \tag{2.8}$$

$$\mu_s \frac{\partial C_s}{\partial \mathbf{n}_s} = -\mu_l \frac{\partial C_l}{\partial \mathbf{n}_l} \quad \text{on} \quad \Gamma_{sl} \tag{2.9}$$

$$\mu_w \frac{\partial C_w}{\partial \mathbf{n}_w} = -\mu_s \frac{\partial C_s}{\partial \mathbf{n}_s} \quad \text{on} \quad \Gamma_{ws} \tag{2.10}$$

Finally, we prescribe the initial conditions

$$C_l(\mathbf{x}, t) = C_{f0}(\mathbf{x}), \quad \mathbf{x} \in \Omega_l, \quad C_w(\mathbf{x}, t) = C_{w0}(\mathbf{x}), \quad \mathbf{x} \in \Omega_w, \quad \mathbf{x} \in \Omega_s, \quad t = 0.$$

2.2.2 Definitions

Let ζ_{lw}, ζ_{sl}, and ζ_{ws} be positive functions in $L^2(\Gamma_{lw})$, $L^2(\Gamma_{sl})$, and $L^2(\Gamma_{ws})$, respectively, such that the properties in (1.3) are satisfied with Γ_{lw}, Γ_{sl}, and Γ_{ws} taking the role of Σ. Then, we can define $\Lambda_{lw} = H_{00}^{1/2}(\Gamma_{lw})$, $\Lambda_{sl} = H_{00}^{1/2}(\Gamma_{sl})$, $\Lambda_{ws} = H_{00}^{1/2}(\Gamma_{ws})$, and $\Lambda_{lws} = H_{00}^{1/2}(\Gamma_{lws})$ with Λ'_{lw}, Λ'_{sl}, Λ'_{ws}, and Λ'_{lws} being their respective dual spaces.

2.2.3 Weak formulation and analysis of the NS problem

For the purpose of extending the theory found in [52] and [53] to the three-domain stents we briefly recall some results about Navier-Stokes equations. To obtain $\mathbf{u}(t, \mathbf{x})$ and $C_i(t, \mathbf{x})$ in (2.1), (2.2),(2.3), and (2.4), we proceed by obtaining the weak form of each. Let $\mathbf{v} \in [H_0^1(\Omega_l)]^d$ and $q \in L^2(\Omega_l)$. Then multiplying the first and second equations by $\mathbf{v}$ and q, respectively, and integrating by parts where possible, we obtain the unsteady Navier-Stokes weak formulation problem:

Problem 1. *Given* $\mathbf{u}_0 \in (L^2(\Omega_l))^d$ *with* $\nabla \cdot \mathbf{u}_0 = 0$ *and* $f \in L^2(0, T; (L^2(\Omega_l))^d)$, *find* $\mathbf{u} \in L^2(0, T; (H^1(\Omega_l))^d) \cap L^\infty(0, T; (L^2(\Omega_l))^d)$ *and* $P \in L^2(0, T; L^2(\Omega_l))$ *such that for all* $t > 0$

(2.11)
$$\begin{cases} \left(\frac{\partial \mathbf{u}}{\partial t}, \mathbf{v}\right) + \nu(\nabla \mathbf{u}, \nabla \mathbf{v}) + ((\mathbf{u} \cdot \nabla)\mathbf{u}, \mathbf{v}) - (\nabla \cdot \mathbf{v}, P) = (\mathbf{f}, \mathbf{v}) \quad \forall \mathbf{v} \in (H_0^1(\Omega_l))^d, \\ (\nabla \cdot \mathbf{u}, q) = 0 \quad \forall q \in L^2(\Omega_l), \\ \mathbf{u} = \mathbf{b} \quad on \quad \partial\Omega_l \backslash (\Gamma_{lw} \cup \Gamma_{sl}), \quad \mathbf{u} = 0 \quad on \quad \Gamma_{lw} \cup \Gamma_{sl}, \end{cases}$$

with $\mathbf{u}(0) = \mathbf{u}_0$ *for* $t = 0$.

The existence of the solution has been proved by Leray [39, 40, 41] and Hopf [29]; the uniqueness has been proved in the two-dimensional case but remains an open problem in three dimensions [57, 56]. However, if the boundary of $\partial\Omega_l$ and the initial datum $\mathbf{u}_0$ are regular, then it can be proved that the solution is regular. From [27] and [26], we state the following useful results.

Theorem 2.2.1. *Let* $\mathbf{u}_0 \in H^2(\Omega_l)$ *and* $\mathbf{f}$ *be smooth enough(e.g.,* $\mathbf{f} \in L^\infty(\Omega_l)$ *and* $\nabla \mathbf{f} \in L^\infty(\Omega_l)$*). Assume that*

- *(Cattabriga assumption on the domain* Ω_l*) for a given* $\mathbf{g} \in \mathbf{L}^2(\Omega_l)$, *the steady*

Stokes problem

$$-\Delta \mathbf{v} + \nabla q = \mathbf{g}, \quad \nabla \cdot \mathbf{v} = 0 \quad in \quad \Omega_l, \quad \mathbf{v}|_{\partial\Omega_l} = \mathbf{0},$$

has a unique solution that satisfies the inequality

$$\|\mathbf{v}\|_{H^2(\Omega_l)} + \|q\|_{H^1(\Omega_l)\setminus\mathbb{R}} \leq c\|\mathbf{g}\|_{L^2(\Omega_l)},$$

where c is a constant;

- *there exists a time T, $0 < T < \infty$ and a constant A such that the solution of the Navier-Stokes problem* (2.11) *satisfies*

$$\sup_{0<t<T} \|\nabla \mathbf{u}(\cdot, t)\|_{H^2(\Omega_l)} \leq A.$$

Then there exists a constant B such that the solution of the Navier-Stokes problem (2.11) *satisfies*

$$\sup_{0<t<T} \|\mathbf{u}(\cdot, t)\|_{H^2(\Omega_l)} \leq B.$$

Theorem 2.2.2. *Suppose that the hypotheses of the previous theorem hold. Assume that Ω_l be any three-dimensional domain whose boundary is uniformly of class C^3. Suppose that the boundary value prescribed can be extended to a solenoidal function $\mathbf{g}$ smooth enough and that $\mathbf{f} \in C^2((0,\infty) \times \overline{\Omega}_l)$. Then, on some interval $[0, T]$, there exists a solution $\mathbf{u}$, P of the Navier-Stokes problem such that , in particular, $\mathbf{u} \in C([0, T) \times \overline{\Omega}_l \cap C^2((0, T) \times \Omega_l)$.*

We assume that $\mu_i \leq M_i$ are positive constants and that we have solved for blood velocity and pressure. Then we want to find the solute concentrations $C_i(t, \mathbf{x})$ in Ω_i, for $i = l, w, s$. Like we did for Navier-Stokes, we seek to solve in terms of weak formulation of this problem. We consider test functions in corresponding Sobolev spaces and integrate by parts to define the following bilinear forms:

$$\begin{aligned} a_l(u_l, v_l) &= \mu_l \int_{\Omega_l} \nabla u_l \nabla v_l d\omega + \int_{\Omega_l} (\mathbf{u} \cdot \nabla) u_l v_l d\omega \\ &= (\mu_l \nabla u_l, \nabla v_l) + ((\mathbf{u} \cdot \nabla) u_l, v_l) \quad \forall u_l, v_l \in H^1_{\partial\Omega_l \setminus (\Gamma_{lw} \cup \Gamma_{sl})}(\Omega_l) \end{aligned} \tag{2.12}$$

$$
\begin{aligned}
a_w(u_w, v_w) &= \mu_w \int_{\Omega_w} \nabla u_w \nabla v_w d\omega \\
&= (\mu_w \nabla u_w, \nabla v_w) \quad \forall u_w, v_w \in H^1_{\partial\Omega_w \setminus (\Gamma_{ws} \cup \Gamma_{lw})}(\Omega_w)
\end{aligned} \tag{2.13}
$$

$$
\begin{aligned}
a_s(u_s, v_s) &= \mu_s \int_{\Omega_s} \nabla u_s \nabla v_s d\omega \\
&= (\mu_l \nabla u_s, \nabla v_s) \quad \forall u_s, v_s \in H^1_{\partial\Omega_s \setminus (\Gamma_{sl} \cup \Gamma_{ws})}(\Omega_s)
\end{aligned} \tag{2.14}
$$

Properties of each bilinear form are explored in the following lemma.[53]

Lemma 1. *The bilinear forms a_l, a_w, and a_s are well-defined, continuous, and coercive with coercivity constants α_l, α_w, and α_s, respectively. Furthermore, a_w and a_s are symmetric.*

Proof. For any $u_l, v_l \in H^1_{\partial\Omega_l \setminus (\Gamma_{lw} \cup \Gamma_{sl})}(\Omega_l)$, we get

$$
\begin{aligned}
|a_l(u_l, v_l)| &\leq M_l \|\nabla u_l\|_{L^2(\Omega_l)} \|\nabla v_l\|_{L^2(\Omega_l)} + \|\mathbf{u}\|_{L^4(\Omega_l)} \|v_l\|_{L^4(\Omega_l)} \|\nabla u_l\|_{L^2(\Omega_l)} \\
&\leq (M_l + \|\mathbf{u}\|_{H^1(\Omega_l)}) \|u_l\|_{H^1(\Omega_l)} \|v_l\|_{H^1(\Omega_l)}
\end{aligned}
$$

Similarly, for a_w and a_s:

$$
\begin{aligned}
|a_w(u_w, v_w)| &\leq M_w \|\nabla u_w\|_{L^2(\Omega_w)} \|\nabla v_w\|_{L^2(\Omega_w)} \\
&\leq M_w \|u_w\|_{H^1(\Omega_w)} \|v_w\|_{H^1(\Omega_w)}
\end{aligned}
$$

and

$$
\begin{aligned}
|a_s(u_s, v_s)| &\leq M_s \|\nabla u_s\|_{L^2(\Omega_s)} \|\nabla v_s\|_{L^2(\Omega_s)} \\
&\leq M_s \|u_s\|_{H^1(\Omega_s)} \|v_s\|_{H^1(\Omega_s)}
\end{aligned}
$$

This establishes that the bilinear forms are well-defined and continuous. For the coercivity of a_l, we rely on $\nabla \cdot \mathbf{u} = 0$ and $\mathbf{u}|_\Gamma = 0$:

$$
\begin{aligned}
a_l(u_l, u_l) &= \mu_l \int_{\Omega_l} \nabla u_l \nabla u_l d\omega + \int_{\Omega_l} (\mathbf{u} \cdot \nabla) u_l u_l d\omega \\
&= \mu_l \|\nabla u_l\|^2_{L^2(\Omega_l)} + \int_{\Omega_l} (\mathbf{u} \cdot \nabla) u_l u_l d\omega \quad u_l \in H^1_{\partial\Omega_l \setminus (\Gamma_{lw} \cup \Gamma_{sl})}(\Omega_l)
\end{aligned}
$$

Observe that

$$\begin{aligned}\int_{\Omega_l}(\mathbf{u}\cdot\nabla)u_l u_l d\omega &= -\int_{\Omega_l} u_l(\nabla\cdot(\mathbf{u}u_l))d\omega + \int_{\partial\Omega}(\mathbf{u}u_l^2)\cdot\mathbf{n}d\gamma \\ &= -\int_{\Omega_l} u_l^2(\nabla\cdot\mathbf{u})d\omega - \int_{\Omega_l} u_l(\mathbf{u}\cdot\nabla)u_l d\omega \\ 2\int_{\Omega_l}(\mathbf{u}\cdot\nabla)u_l u_l d\omega &= -\int_{\Omega_l} u_l^2(\nabla\cdot\mathbf{u})d\omega = 0.\end{aligned}$$

So for any $u_l \in H^1_{\partial\Omega_l\setminus(\Gamma_{lw}\cup\Gamma_{sl})}(\Omega_l)$

$$a_l(u_l,u_l) = \mu_l\|\nabla u_l\|^2_{L^2(\Omega_l)};$$

then using the Poincaré inequality with constant C_1, we get

$$\begin{aligned}a_l(u_l,u_l) &\geq C_1\mu_l\|u_l\|^2_{L^2(\Omega_l)}; \\ (C_1+1)a_l(u_l,u_l) &\geq C_1\mu_1(\|u_l\|^2_{L^2(\Omega_l)} + \|\nabla u_l\|^2_{L^2(\Omega_l)}) \\ a_l(u_l,u_l) &\geq \frac{C_1\mu_1}{C_1+1}\|u_l\|^2_{H^1(\Omega_l)},\end{aligned}$$

letting $\alpha_l = \frac{C_1\mu_1}{C_1+1}$ we can guarantee the existence of a positive constant such that coercivity is established. We can proceed similarly with a_w and a_s obtaining coercivity constants α_w and α_s, respectively. Finally, we trivially notice that for any $u_w, v_w \in H^1_{\partial\Omega_w\setminus(\Gamma_{ws}\cup\Gamma_{lw})}(\Omega_w)$

$$a_w(u_w,v) = a_w(v_w,u_w),$$

so it is symmetric.
This applies for a_s as well since it has the same structure as a_w. □

We now give a statement of the weak formulation of (2.2), (2.3), and (2.4).

Problem 2. *Given the initial condition* $C_l(t=0,\mathbf{x}) = C_{l,0} \in H^1_{\partial\Omega_l\setminus(\Gamma_{lw}\cup\Gamma_{sl})}(\Omega_l)$, $C_w(t=0,\mathbf{x}) = C_{w,0} \in H^1_{\partial\Omega_w\setminus(\Gamma_{ws}\cup\Gamma_{lw})}(\Omega_w)$, *and* $C_s(t=0,\mathbf{x}) = C_{s,0} \in H^1_{\partial\Omega_s\setminus(\Gamma_{sl}\cup\Gamma_{ws})}(\Omega_s)$, *and given positive functions* $\zeta_{lw} \in L^2(\Gamma_{lw})$, $\zeta_{ws} \in L^2(\Gamma_{ws})$, *and* $\zeta_{sl} \in L^2(\Gamma_{sl})$, *find* $C_l \in L^2(0,T,H^1_{\partial\Omega_l\setminus(\Gamma_{lw}\cup\Gamma_{sl})}(\Omega_l))$, $C_w \in L^2(0,T,H^1_{\partial\Omega_w\setminus(\Gamma_{ws}\cup\Gamma_{lw})}(\Omega_w))$, *and* $C_s \in L^2(0,T,H^1_{\partial\Omega_s\setminus(\Gamma_{sl}\cup\Gamma_{ws})}(\Omega_s))$ *such that for all* $\phi_l \in H^1_{\partial\Omega_l\setminus(\Gamma_{lw}\cup\Gamma_{sl})}(\Omega_l)$,

$\phi_w \in H^1_{\partial\Omega_w\setminus(\Gamma_{ws}\cup\Gamma_{lw})}(\Omega_w)$, *and* $\phi_s \in H^1_{\partial\Omega_s\setminus(\Gamma_{sl}\cup\Gamma_{ws})}(\Omega_s)$ *we get*

$$\begin{cases} \left(\frac{\partial C_l}{\partial t}, \phi_l\right) + a_l(C_l, \phi_l) + (C_l - C_w, \phi_l)_{\zeta_{lw}} + (C_l - C_s, \phi_s)_{\zeta_{sl}} = (s_l, \phi_l), \\ \left(\frac{\partial C_w}{\partial t}, \phi_w\right) + a_w(C_w, \phi_w) + (C_w - C_s, \phi_w)_{\zeta_{ws}} + (C_w - C_l, \phi_w)_{\zeta_{lw}} = (s_w, \phi_w), \\ \left(\frac{\partial C_s}{\partial t}, \phi_s\right) + a_s(C_s, \phi_s) + (C_s - C_l, \phi_s)_{\zeta_{sl}} + (C_s - C_w, \phi_s)_{\zeta_{ws}} = (s_s, \phi_s), \end{cases}$$

Theorem 2.2.3. *Under the hypotheses of Theorem* 2.2.2, *Problem* 2 *admits a unique solution which depends continuously on the data.*

Proof. From Lemma 1, we know that $a_l(\cdot,\cdot)$, $a_w(\cdot,\cdot)$, $a_s(\cdot,\cdot)$ are continuous and coercive for every $t > 0$. Then, we notice that for $\phi_l \in H^1_{\partial\Omega_l\setminus(\Gamma_{lw}\cup\Gamma_{sl})}(\Omega_l)$, $\phi_w \in H^1_{\partial\Omega_w\setminus(\Gamma_{ws}\cup\Gamma_{lw})}(\Omega_w)$, and $\phi_s \in H^1_{\partial\Omega_s\setminus(\Gamma_{sl}\cup\Gamma_{ws})}(\Omega_s)$

$$\begin{aligned} (\phi_l - \phi_w, \phi_l - \phi_w)_{\zeta_{lw}} &= \|\phi_l - \phi_w\|^2_{\zeta_{lw}} \\ (\phi_w - \phi_s, \phi_w - \phi_s)_{\zeta_{ws}} &= \|\phi_w - \phi_s\|^2_{\zeta_{ws}} \\ (\phi_s - \phi_l, \phi_s - \phi_l)_{\zeta_{sl}} &= \|\phi_s - \phi_l\|^2_{\zeta_{sl}}, \end{aligned}$$

resulting in coercivity. Adding up the equations in Problem 2 and rearranging the terms

$$\begin{aligned} (C_l - C_w, \phi_l)_{\zeta_{lw}} + (C_w - C_l, \phi_w)_{\zeta_{lw}} &= (C_l - C_w, \phi_l - \phi_w)_{\zeta_{lw}} \\ (C_w - C_s, \phi_w)_{\zeta_{ws}} + (C_s - C_w, \phi_s)_{\zeta_{ws}} &= (C_w - C_s, \phi_w - \phi_s)_{\zeta_{ws}} \\ (C_s - C_l, \phi_s)_{\zeta_{sl}} + (C_l - C_s, \phi_l)_{\zeta_{sl}} &= (C_s - C_l, \phi_s - \phi_l)_{\zeta_{sl}} \end{aligned}$$

gives

$$\left(\frac{\partial \mathbf{C}}{\partial t}, \mathbf{\Phi}\right) + \mathcal{A}(\mathbf{C}, \mathbf{\Phi}) = (\mathbf{S}, \mathbf{\Phi}), \tag{2.15}$$

where

$$\begin{aligned} \mathbf{C} = [C_l, C_w, C_l]^T, \quad \mathbf{\Phi} = [\phi_l, \phi_w, \phi_s]^T, \quad \mathbf{S} = [s_l, s_w, s_s]^T, \quad \text{and} \\ \mathcal{A}(\mathbf{C}, \mathbf{\Phi}) := a_l(C_l, \phi_l) + a_w(C_w, \phi_w) + a_s(C_s, \phi_s) + \\ + (C_l - C_w, \phi_l - \phi_w)_{\zeta_{lw}} + (C_w - C_s, \phi_w - \phi_s)_{\zeta_{ws}} + (C_s - C_l, \phi_s - \phi_l)_{\zeta_{sl}} \end{aligned}$$

Now, the bilinear form $\mathcal{A}(\cdot,\cdot)$ is continuous and coercive with constant α since each

one of its terms is continuous and coercive. Since the right-hand side of (2.15) is a linear and continuous functional in $H^1_{\partial\Omega_l\setminus(\Gamma_{lw}\cup\Gamma_{sl})}(\Omega_l) \times H^1_{\partial\Omega_w\setminus(\Gamma_{ws}\cup\Gamma_{lw})}(\Omega_w) \times H^1_{\partial\Omega_s\setminus(\Gamma_{sl}\cup\Gamma_{ws})}(\Omega_s)$, we can establish the well-posedness of Problem 2 through the Faedo-Galerkin method. □

2.2.4 Time Discretization

To solve for the concentration of solutes we assume that we are given (i.e. have solved for) the velocity and pressure of blood. We consider a semi-discretization in terms of time of Problem 2. We let the time interval $[0, T]$ be divided into N subintervals of uniform length $\Delta t > 0$ such that $t^n = n\Delta t$ for $n = 0, 1, ..., N$. Then we reformulate Problem 2 with implicit semi-discretization, using $\chi = \frac{1}{\Delta t}$ and the following definitions:

$$\hat{a}_l(u_l, v_l) = \chi(u_l, v_l) + a_l(u_l, v_l) \quad \forall u_l, v_l \in H^1_{\partial\Omega_l\setminus(\Gamma_{lw}\cup\Gamma_{sl})}(\Omega_l) \tag{2.16}$$

$$\hat{a}_w(u_w, v_w) = \chi(u_w, v_w) + a_w(u_w, v_w) \quad \forall u_w, v_w \in H^1_{\partial\Omega_w\setminus(\Gamma_{ws}\cup\Gamma_{lw})}(\Omega_w) \tag{2.17}$$

$$\hat{a}_s(u_s, v_s) = \chi(u_s, v_s) + a_l(u_s, v_s) \quad \forall u_s, v_s \in H^1_{\partial\Omega_s\setminus(\Gamma_{sl}\cup\Gamma_{ws})}(\Omega_s) \tag{2.18}$$

Observe that each of these are bilinear and coercive, with $\hat{a}_w$ and $\hat{a}_s$ being additionally symmetric.

Problem 3. *Given* C_l^0, C_w^0, *and* C_s^0 *for every* $n = 0, 1, ..., N-1$ *find* $C_l^{n+1} \in H^1_{\partial\Omega_l\setminus(\Gamma_{lw}\cup\Gamma_{sl})}(\Omega_l)$, $C_w^{n+1} \in H^1_{\partial\Omega_w\setminus(\Gamma_{ws}\cup\Gamma_{lw})}(\Omega_w)$, *and* $C_s^{n+1} \in H^1_{\partial\Omega_s\setminus(\Gamma_{sl}\cup\Gamma_{ws})}(\Omega_s)$ *such that for all* ϕ_l *in* $H^1_{\partial\Omega_l\setminus(\Gamma_{lw}\cup\Gamma_{sl})}(\Omega_l)$, ϕ_w *in* $H^1_{\partial\Omega_w\setminus(\Gamma_{ws}\cup\Gamma_{lw})}(\Omega_w)$, *and*

ϕ_s in $H^1_{\partial\Omega_s\setminus(\Gamma_{sl}\cup\Gamma_{ws})}(\Omega_s)$ we have

$$
\begin{cases}
\hat{a}_l(C_l^{n+1},\phi_l)+(C_l^{n+1},\phi_l)_{\zeta_{lw}}+(C_l^{n+1},\phi_l)_{\zeta_{sl}} \\
\qquad -(C_w^{n+1},\phi_l)_{\zeta_{lw}}-(C_s^{n+1},\phi_l)_{\zeta_{sl}}=\chi(C_l^n,\phi_l)+(s_l^{n+1},\phi_l) \\
\hat{a}_w(C_w^{n+1},\phi_w)+(C_w^{n+1},\phi_w)_{\zeta_{ws}}+(C_w^{n+1},\phi_w)_{\zeta_{lw}} \\
\qquad -(C_s^{n+1},\phi_w)_{\zeta_{ws}}-(C_l^{n+1},\phi_w)_{\zeta_{lw}}=\chi(C_w^n,\phi_w)+(s_w^{n+1},\phi_w) \\
\hat{a}_s(C_s^{n+1},\phi_s)+(C_s^{n+1},\phi_s)_{\zeta_{sl}}+(C_s^{n+1},\phi_s)_{\zeta_{ws}} \\
\qquad -(C_l^{n+1},\phi_s)_{\zeta_{sl}}-(C_w^{n+1},\phi_s)_{\zeta_{ws}}=\chi(C_s^n,\phi_s)+(s_s^{n+1},\phi_s),
\end{cases}
\tag{2.19}
$$

where $s_l^{n+1}=s_l(t^{n+1})$, $s_w^{n+1}=s_w(t^{n+1})$, $s_s^{n+1}=s_s(t^{n+1})$, and C_l^0, C_w^0, and C_s^0 are the initial data.

2.2.5 Full discretization

We now consider a space discretization of the problem by using the finite element method (FEM). For this purpose, we let $\mathcal{T}_{h,l}$ and $\mathcal{T}_{h,w}$, and $\mathcal{T}_{h,s}$ be admissible triangulations of $\overline{\Omega}_l$, $\overline{\Omega}_w$, and $\overline{\Omega}_s$, respectively. Furthermore, we assume that $\mathcal{T}_{h,l}$, $\mathcal{T}_{h,w}$, and $\mathcal{T}_{h,s}$ are conforming triangulations on the interfaces Γ_{lw}, Γ_{sl}, and Γ_{ws}, as well as the boundary Γ_{lws}. As a result, $\mathcal{T}_h=\mathcal{T}_{h,l}\cup\mathcal{T}_{h,w}\cup\mathcal{T}_{h,s}$ is an admissible triangulation for $\overline{\Omega}_l\cup\overline{\Omega}_w\cup\overline{\Omega}_s$.

Now we set h to represent the length of the elements K of $\mathcal{T}_h$. $V_{l,h}$, $V_{w,h}$, and $V_{s,h}$ are finite-dimensional subspaces of $H^1_{\partial\Omega_l\setminus(\Gamma_{lw}\cup\Gamma_{sl})}(\Omega_l)$, $H^1_{\partial\Omega_w\setminus(\Gamma_{ws}\cup\Gamma_{lw})}(\Omega_w)$, and $H^1_{\partial\Omega_s\setminus(\Gamma_{sl}\cup\Gamma_{ws})}(\Omega_s)$, respectively. Analogously, define $\Lambda_{lw,h}$, $\Lambda_{ws,h}$, and $\Lambda_{sl,h}$ to be corresponding finite-dimensional subspaces of Λ_{lw}, Λ_{sl}, and Λ_{ws} such that the traces on Γ_{lw}, Γ_{sl}, and Γ_{ws} of functions in $V_{l,h}$, $V_{w,h}$, or $V_{s,h}$ belong to either $\Lambda_{lw,h}$, $\Lambda_{sl,h}$, or $\Lambda_{ws,h}$, respectively.

Let N_l be the dimension of $V_{l,h}$, N_w the dimension of $V_{w,h}$, N_s the dimension of $V_{s,h}$, N_{lw} the dimension of $\Lambda_{lw,h}$, N_{sl} the dimension of $\Lambda_{sl,h}$, and N_{ws} the dimension of $\Lambda_{ws,h}$. Then, we allow $\{\phi_{i,l}\}(i=1,2,...,N_l)$ be a basis for $V_{l,h}$, $\{\phi_{i,w}\}(i=1,2,...,N_w)$ be a basis for $V_{w,h}$, $\{\phi_{i,s}\}(i=1,2,...,N_s)$ be a basis for $V_{s,h}$, $\{\lambda_{i,lw}\}(i=1,2,...,N_{lw})$ be a basis for $\Lambda_{lw,h}$, $\{\lambda_{i,sl}\}(i=1,2,...,N_{sl})$ be a basis for $\Lambda_{sl,h}$, and $\{\lambda_{i,ws}\}(i=1,2,...,N_{ws})$ be a basis for $\Lambda_{ws,h}$. From now on, adding the subscript h will refer to the space discrete solution.

Problem 4. *Given the initial data $C_{l,h}^0$, $C_{w,h}^0$, and $C_{s,h}^0$, for every $n=0,1,...N-$*

1 (*being* $N\Delta t = T$ *the final time*), *find* $C_{l,h}^{n+1} \in V_{l,h}$, $C_{w,h}^{n+1} \in V_{w,h}$, $, C_{s,h}^{n+1} \in V_{s,h}$ *such that for all* $i_l = 1, ..., N_l$, $i_w = 1, ..., N_w$, *and* $i_s = 1, ..., N_s$

$$
\begin{cases}
\hat{a}_l(C_{l,h}^{n+1}, \phi_{i_l,l}) + (C_{l,h}^{n+1}, \phi_{i_l,l})_{\zeta_{lw}} + (C_{l,h}^{n+1}, \phi_{i_l,l})_{\zeta_{sl}} \\
\qquad -(C_{w,h}^{n+1}, \phi_{i_l,l})_{\zeta_{lw}} - (C_{s,h}^{n+1}, \phi_{i_l,l})_{\zeta_{sl}} = \chi(C_{l,h}^{n}, \phi_{i_l,l}) + (s_l^{n+1}, \phi_{i_l,l}) \\
\hat{a}_w(C_{w,h}^{n+1}, \phi_{i_w,w}) + (C_{w,h}^{n+1}, \phi_{i_w,w})_{\zeta_{ws}} + (C_{w,h}^{n+1}, \phi_{i_w,w})_{\zeta_{lw}} \\
\qquad -(C_{s,h}^{n+1}, \phi_{i_w,w})_{\zeta_{ws}} - (C_{l,h}^{n+1}, \phi_{i_w,w})_{\zeta_{lw}} = \chi(C_{w,h}^{n}, \phi_{i_w,w}) + (s_w^{n+1}, \phi_{i_w,w}) \\
\hat{a}_s(C_{sh}^{n+1}, \phi_{i_s,s}) + (C_{s,h}^{n+1}, \phi_{i_s,s})_{\zeta_{sl}} + (C_{s,h}^{n+1}, \phi_{i_s,s})_{\zeta_{ws}} \\
\qquad -(C_{l,h}^{n+1}, \phi_{i_s,s})_{\zeta_{sl}} - (C_{w,h}^{n+1}, \phi_{i_s,s})_{\zeta_{ws}} = \chi(C_{s,h}^{n}, \phi_{i_s,s}) + (s_s^{n+1}, \phi_{i_s,s}),
\end{cases} \tag{2.20}
$$

It is important to note that due to the convection dominating in the problem, this problem is conditionally unstable so that only a sufficiently fine triangulation will result in a stable solution. However, in our analysis and numerical implementation we used streamline upwing Petrov Galerkin to counteract the local Péclet number and have it be less than 1.

2.2.6 Convergence analysis of Two-domain Problems

Before considering a complete scheme involving all three domains and interfaces, we motivate the overall structure by setting up three smaller problems by every two domains. We initialize the iterative method by having initial guesses for C_l^{n+1}, C_s^{n+1} and C_w^{n+1}, which are respectively denoted by $C_{s,0}^{n+1}$ and $C_{w,0}^{n+1}$. Then, we find a sequence of functions $[C_{l,k}^{n+1}, C_{w,k}^{n+1}, C_{s,k}^{n+1}]$ by solving the following sets of equations for $k = 0, 1, ...$

$$
\begin{aligned}
&\hat{a}_l(C_{l,k+1}^{n+1}, \phi_l) + (C_{l,k+1}^{n+1}, \phi_l)_{\zeta_{lw}} + (C_{l,k+1}^{n+1}, \phi_l)_{\zeta_{sl}} \\
&\quad = \chi(C_l^n, \phi_l) + (C_{w,k}^{n+1}, \phi_l)_{\zeta_{lw}} + (C_{s,k}^{n+1}, \phi_l)_{\zeta_{sl}} + (s_l^{n+1}, \phi_l) \quad \forall \phi_l \in H^1_{\partial\Omega_l \setminus (\Gamma_{lw} \cup \Gamma_{sl})}(\Omega_l), \\
&\hat{a}_s(C_{s,k+1}^{n+1}, \phi_s) + (C_{s,k+1}^{n+1}, \phi_s)_{\zeta_{sl}} + (C_{s,k+1}^{n+1}, \phi_s)_{\zeta_{ws}} \\
&\quad = \chi(C_s^n, \phi_s) + (C_{l,k+1}^{n+1}, \phi_s)_{\zeta_{sl}} + (C_{w,k}^{n+1}, \phi_s)_{\zeta_{ws}} + (s_s^{n+1}, \phi_s) \quad \forall \phi_s \in H^1_{\partial\Omega_s \setminus (\Gamma_{sl} \cup \Gamma_{ws})}(\Omega_s),
\end{aligned}
$$

$$\hat{a}_l(C_{l,k+1}^{n+1},\phi_l)+(C_{l,k+1}^{n+1},\phi_l)_{\zeta_{lw}}+(C_{l,k+1}^{n+1},\phi_l)_{\zeta_{sl}}$$
$$=\chi(C_l^n,\phi_l)+(C_{w,k}^{n+1},\phi_l)_{\zeta_{lw}}+(C_{s,k}^{n+1},\phi_l)_{\zeta_{sl}}+(s_l^{n+1},\phi_l)\quad\forall\phi_l\in H^1_{\partial\Omega_l\setminus(\Gamma_{lw}\cup\Gamma_{sl})}(\Omega_l),$$
$$\hat{a}_w(C_{w,k+1}^{n+1},\phi_w)+(C_{w,k+1}^{n+1},\phi_w)_{\zeta_{lw}}+(C_{w,k+1}^{n+1},\phi_w)_{\zeta_{ws}}$$
$$=\chi(C_w^n,\phi_w)+(C_{l,k+1}^{n+1},\phi_w)_{\zeta_{lw}}+(C_{s,k+1}^{n+1},\phi_s)_{\zeta_{ws}}+(s_w^{n+1},\phi_w)\quad\forall\phi_w\in H^1_{\partial\Omega_w\setminus(\Gamma_{lw}\cup\Gamma_{ws})}(\Omega_s)$$

$$\hat{a}_s(C_{s,k+1}^{n+1},\phi_s)+(C_{s,k+1}^{n+1},\phi_s)_{\zeta_{sl}}+(C_{s,k+1}^{n+1},\phi_s)_{\zeta_{ws}}$$
$$=\chi(C_s^n,\phi_s)+(C_{l,k+1}^{n+1},\phi_s)_{\zeta_{sl}}+(C_{w,k}^{n+1},\phi_s)_{\zeta_{ws}}+(s_s^{n+1},\phi_s)\quad\forall\phi_s\in H^1_{\partial\Omega_s\setminus(\Gamma_{sl}\cup\Gamma_{ws})}(\Omega_s),$$
$$\hat{a}_w(C_{w,k+1}^{n+1},\phi_w)+(C_{w,k+1}^{n+1},\phi_w)_{\zeta_{lw}}+(C_{w,k+1}^{n+1},\phi_w)_{\zeta_{ws}}$$
$$=\chi(C_w^n,\phi_w)+(C_{l,k+1}^{n+1},\phi_w)_{\zeta_{lw}}+(C_{s,k+1}^{n+1},\phi_s)_{\zeta_{ws}}+(s_w^{n+1},\phi_w)\quad\forall\phi_w\in H^1_{\partial\Omega_w\setminus(\Gamma_{lw}\cup\Gamma_{ws})}(\Omega_s)$$

We want the sequence $[C_{l,k}^{n+1},C_{w,k}^{n+1},C_{s,k}^{n+1}]$ to pairwise converge to $[C_l^{n+1},C_w^{n+1},C_s^{n+1}]$ for each time step $n+1$. Within each time step, we seek to obtain convergence of the solution along all interfaces, which we now drop for notation simplicity (i.e. the supercript of each function), with the time index only being used when referring to another time step. We introduce the splitting error as follows:

$$e_{l,k}:=C_l-C_{l,k},\quad e_{w,k}:=C_w-C_{w,k},\quad e_{s,k}:=C_s-C_{s,k},$$
$$\lambda_{lw,k}:=\gamma_{wl}e_{w,k},\quad \lambda_{sl,k}:=\gamma_{ls}e_{l,k},\quad \lambda_{ws,k}:=\gamma_{sw}e_{s,k},\tag{2.21}$$

where $[C_l,C_w,C_s]$ is the solution to Problem 3. If we substract 2.20 from in terms of the solution, with initial guesses $\lambda_{lw,0}$, $\lambda_{sl,0}$, and $\lambda_{ws,0}$, we obtain

(2.22)
$$\hat{a}_l(e_{l,k+1},\phi_l)+(e_{l,k+1},\phi_l)_{\zeta_{lw}}+(e_{l,k+1},\phi_l)_{\zeta_{sl}}=(\lambda_{lw,k},\phi_l)_{\zeta_{lw}}+(\gamma_{sl}e_{s,k+1},\phi_l)_{\zeta_{sl}}$$
(2.23)
$$\hat{a}_w(e_{w,k+1},\phi_w)+(e_{w,k+1},\phi_w)_{\zeta_{ws}}+(e_{w,k+1},\phi_w)_{\zeta_{lw}}=(\lambda_{ws,k},\phi_w)_{\zeta_{ws}}+(\gamma_{lw}e_{l,k+1},\phi_w)_{\zeta_{lw}}$$
(2.24)
$$\hat{a}_s(e_{s,k+1},\phi_s)+(e_{s,k+1},\phi_s)_{\zeta_{sl}}+(e_{s,k+1},\phi_s)_{\zeta_{ws}}=(\lambda_{sl,k},\phi_s)_{\zeta_{sl}}+(\gamma_{ws}e_{w,k+1},\phi_s)_{\zeta_{ws}}$$

We consider splitting up by interface contribution

$$\frac{1}{2}\hat{a}_l(e_{l,k+1},\phi_l)+(e_{l,k+1},\phi_l)_{\zeta_{lw}}=(\lambda_{lw,k},\phi_l)_{\zeta_{lw}}\tag{2.25}$$
$$\frac{1}{2}\hat{a}_l(e_{l,k+1},\phi_l)+(e_{l,k+1},\phi_l)_{\zeta_{sl}}=(\gamma_{sl}e_{s,k+1},\phi_l)_{\zeta_{sl}}\tag{2.26}$$

$$\frac{1}{2}\hat{a}_w(e_{w,k+1},\phi_w)+(e_{w,k+1},\phi_w)_{\zeta_{ws}}=(\lambda_{ws,k},\phi_w)_{\zeta_{ws}} \tag{2.27}$$

$$\frac{1}{2}\hat{a}_w(e_{w,k+1},\phi_w)+(e_{w,k+1},\phi_w)_{\zeta_{lw}}=(\gamma_{wl}e_{l,k+1},\phi_w)_{\zeta_{lw}} \tag{2.28}$$

$$\frac{1}{2}\hat{a}_s(e_{s,k+1},\phi_s)+(e_{s,k+1},\phi_s)_{\zeta_{sl}}=(\lambda_{sl,k},\phi_s)_{\zeta_{sl}} \tag{2.29}$$

$$\frac{1}{2}\hat{a}_s(e_{s,k+1},\phi_s)+(e_{s,k+1},\phi_s)_{\zeta_{ws}}=(\gamma_{sw}e_{w,k+1},\phi_s)_{\zeta_{ws}} \tag{2.30}$$

Notice that adding each pair of equations recovers our original system. However, proving overall convergence requires a more rigorous approach and construction of a global contraction to fulfill fixed point arguments. Instead, we prove how pairwise the solutions converge by assuming the third solution in place. We now set up iteration schemes and prove corresponding results.

Let $\mathcal{R}_{lw}:\Lambda_{lw}\to\Lambda_{lw}$ be the operator such that given a function $\psi_{lw}\in\Lambda_{lw}$, we have $\mathcal{R}_{lw}\psi_{lw}=\gamma_{lw}u_l$, where $u_l\in H^1_{\partial\Omega_l\setminus\Gamma_{lw}}(\Omega_l)$ satisfies

$$\frac{1}{2}\hat{a}_l(u_{l,k+1},\phi_l)+(u_{l,k+1},\phi_l)_{\zeta_{lw}}=(\psi_{lw},\phi_l)_{\zeta_{lw}}\quad\forall\phi_l\in H^1_{\partial\Omega_l\setminus\Gamma_{lw}}(\Omega_l). \tag{2.31}$$

Let $\mathcal{R}_{wl}:\Lambda_{lw}\to\Lambda_{lw}$ be the operator such that given a function $\xi_{lw}\in\Lambda_{lw}$, we have $\mathcal{R}_{wl}\psi_{lw}=\gamma_{wl}u_w$, where $u_l\in H^1_{\partial\Omega_l\setminus\Gamma_{lw}}(\Omega_w)$ satisfies

$$\frac{1}{2}\hat{a}_w(u_{w,k+1},\phi_w)+(u_{w,k+1},\phi_w)_{\zeta_{lw}}=(\xi_{lw},\phi_w)_{\zeta_{lw}}\quad\forall\phi_l\in H^1_{\partial\Omega_w\setminus\Gamma_{lw}}(\Omega_w). \tag{2.32}$$

Then, the iterative scheme corresponding to (2.25) and (2.28) can be seen as a fixed-point iteration:

$$\lambda_{lw,k+1}=T_{lw}\lambda_{lw,k},\quad k=0,1,...,\quad\text{where } T=\mathcal{R}_{wl}\circ\mathcal{R}_{lw}.$$

We prove the following lemma, where we proceed just as in [53]:

Lemma 2. There exists a constant $K_{lw}<1$ depending on Ω_l, Ω_w, and ζ_{lw} such that

$$\|T_{lw}\psi_{lw}\|_{\zeta_{lw}}\le K_{lw}\|\psi_{lw}\|_{\zeta_{lw}}\quad\forall\psi_{lw}\in\Lambda_{lw}. \tag{2.33}$$

Proof. Let u_l be a function related to ψ_{lw} through (2.31). We define $\xi_{lw}=\mathcal{R}_{lw}\psi_{lw}$ so that $\xi_{lw}=\gamma_{lw}u_l$. Also, let $\lambda_{lw}=\mathcal{R}_{wl}\xi_{lw}$, which is $\lambda_{lw}=T_{lw}\psi_{lw}$. Choose $\phi_l=u_l$ in

(2.31), so that

$$\frac{1}{2}\hat{a}_l(u_l,u_l)+(u_l,u_l)_{\zeta_{lw}}=(\psi_{lw},u_l)_{\zeta_{lw}}$$
$$\frac{1}{2}\hat{\alpha}_l\|u_l\|_{H^1(\Omega_l)}+\|\xi_{lw}\|^2_{\zeta_{lw}}\leq\|\psi_{lw}\|_{\zeta_{lw}}\|\xi_{lw}\|_{\zeta_{lw}},$$

where $\hat{\alpha}_l$ is the coercivity constant of the bilinear form $\hat{a}_l$. Using (1.2), we have that for all $\xi_{lw}\in\Lambda_{lw}$

$$\|\xi_{lw}\|^2_{\zeta_{lw}}\leq K_1\|u_l\|^2_{H^1(\Omega_l)}, \tag{2.34}$$

with $K_1=C^2_{e,lw},C^2_{t,l}\|\zeta_{lw}\|^2_{L^2(\Gamma_{lw})}$, $C_{e,lw}$ being the embedding constant of Λ_{lw} in $L^4(\Gamma_{lw})$ and $C_{t,l}$ the constant of the trace inequality. Therefore, we have

$$\left(\frac{\hat{\alpha}_l}{2K_1}+1\right)\|\xi_{lw}\|_{\zeta_{lw}}\leq\|\psi_{lw}\|_{\zeta_{lw}},$$

resulting in

$$\|\xi_{lw}\|_{\zeta_{lw}}\leq K_{l1}\|\psi_{lw}\|_{\zeta_{lw}}\quad\forall\psi_{lw}\in\Lambda_{lw}, \tag{2.35}$$

with $K_{l1}=\frac{2K_1}{2K_1+\hat{\alpha}_l}<1$. Now, in (2.32), let $\phi_w=u_w$, so that with $\lambda_{lw}=\gamma_{wl}u_w$ we obtain

$$\frac{1}{2}\hat{a}_w(u_w,u_w)+(u_w,u_w)_{\zeta_{lw}}=(\xi_{lw},u_w)_{\zeta_{lw}}$$
$$\frac{1}{2}\hat{\alpha}_w\|u_w\|_{H^1(\Omega_w)}+\|\lambda_{lw}\|_{\zeta_{lw}}\leq\|\xi_{lw}\|_{\zeta_{lw}}\|\lambda_{lw}\|_{\zeta_{lw}},$$

where $\hat{\alpha}_w$ is the coercivity constant of the bilinear form $\hat{u}_w$. Again, using (1.2), we have for all $\lambda_{lw}\in\Lambda_{lw}$

$$\|\lambda_{lw}\|^2_{\zeta_{lw}}\leq K_2\|u_w\|^2_{H^1(\Omega_w)} \tag{2.36}$$

where $K_2=C^2_{e,lw}C^2_{t,w}\|\zeta_{lw}\|^2_{L^2(\Gamma_{lw})}$ and $C_{t,w}$ is the constant of the trace inequality. Thus, we get

$$\left(\frac{\hat{\alpha}_w}{2K_2}+1\right)\|\lambda_{lw}\|_{\zeta_{lw}}\leq\|\xi_{lw}\|_{\zeta_{lw}},$$

resulting in

$$\|\lambda_{lw}\|_{\zeta_{lw}} \leq K_{w1}\|\xi_{lw}\|_{\zeta_{lw}} \quad \forall \xi_{lw} \in \Lambda_{lw}, \tag{2.37}$$

with $K_{w1} = \frac{2K_2}{2K_2+\hat{\alpha}_w} < 1$. Putting (2.35) and (2.37) together, we have the desired result

$$\|\lambda_{lw}\|_{\zeta_{lw}} \leq K_{lw}\|\psi_{lw}\|_{\zeta_{lw}} < \|\psi_{lw}\|_{\zeta_{lw}},$$

with $K_{lw} = K_{w1}K_{l1}$. □

We proceed similarly for the convergence in the Γ_{sl} interface.

Let $\mathcal{R}_{sl} : \Lambda_{sl} \to \Lambda_{sl}$ be the operator such that given a function $\psi_{sl} \in \Lambda_{sl}$, we have $\mathcal{R}_{sl}\psi_{sl} = \gamma_{sl}u_s$, where $u_s \in H^1_{\partial\Omega_s\setminus\Gamma_{sl}}(\Omega_s)$ satisfies

$$\frac{1}{2}\hat{a}_s(u_{s,k+1}, \phi_s) + (u_{s,k+1}, \phi_s)_{\zeta_{sl}} + = (\psi_{sl}, \phi_s)_{\zeta_{sl}} \quad \forall \phi_s \in H^1_{\partial\Omega_l\setminus\Gamma_{sl}}(\Omega_s). \tag{2.38}$$

Let $\mathcal{R}_{ls} : \Lambda_{sl} \to \Lambda_{sl}$ be the operator such that given a function $\xi_{sl} \in \Lambda_{sl}$, we have $\mathcal{R}_{sl}\psi_{sl} = \gamma_{sl}u_l$, where $u_l \in H^1_{\partial\Omega_l\setminus\Gamma_{sl}}(\Omega_l)$ satisfies

$$\frac{1}{2}\hat{a}_l(u_{l,k+1}, \phi_l) + (u_{l,k+1}, \phi_l)_{\zeta_{sl}} = (\xi_{sl}, \phi_l)_{\zeta_{sl}} \quad \forall \phi_l \in H^1_{\partial\Omega_l\setminus\Gamma_{sl}}(\Omega_l). \tag{2.39}$$

Then, the iterative scheme corresponding to (2.26) and (2.29) can be seen as a fixed-point iteration:

$$\lambda_{sl,k+1} = T_{sl}\lambda_{sl,k}, \quad k = 0, 1, ..., \quad \text{where } T = \mathcal{R}_{ls} \circ \mathcal{R}_{sl}.$$

We prove a lemma similar to Lemma 2.

Lemma 3. There exists a constant $K_{sl} < 1$ depending on Ω_l, Ω_s, and ζ_{sl} such that

$$\|T_{sl}\psi_{sl}\|_{\zeta_{sl}} \leq K_{sl}\|\psi_{sl}\|_{\zeta_{sl}} \quad \forall \psi_{sl} \in \Lambda_{sl}. \tag{2.40}$$

Proof. Let u_s be a function related to ψ_{sl} through (2.38). We define $\xi_{sl} = \mathcal{R}_{sl}\psi_{sl}$ so that $\xi_{sl} = \gamma_{sl}u_s$. Also, let $\lambda_{sl} = \mathcal{R}_{ls}\xi_{sl}$, which is $\lambda_{sl} = T_{sl}\psi_{sl}$. Choose $\phi_s = u_s$ in

(2.31), so that

$$\frac{1}{2}\hat{a}_s(u_s,u_s)+(u_s,u_s)_{\zeta_{sl}}=(\psi_{sl},u_s)_{\zeta_{sl}}$$
$$\frac{1}{2}\hat{\alpha}_s\|u_s\|_{H^1(\Omega_s)}+\|\xi_{sl}\|^2_{\zeta_{sl}}\leq\|\psi_{sl}\|_{\zeta_{sl}}\|\xi_{sl}\|_{\zeta_{sl}},$$

where $\hat{\alpha}_s$ is the coercivity constant of $\hat{a}_s$. Using (1.2), we have that for all $\xi_{sl}\in\Lambda_{sl}$

$$\|\xi_{sl}\|^2_{\zeta_{sl}}\leq K_3\|u_s\|^2_{H^1(\Omega_s)}, \tag{2.41}$$

with $K_3=C^2_{e,sl}C^2_{t,s}\|\zeta_{sl}\|^2_{L^2(\Gamma_{sl})}$, C_e being the embedding constant of Λ_{sl} in $L^4(\Gamma_{sl})$ and $C_{t,s}$ the constant of the trace inequality. Therefore, we have

$$\left(\frac{\hat{\alpha}_s}{2K_3}+1\right)\|\xi_{sl}\|_{\zeta_{sl}}\leq\|\psi_{sl}\|_{\zeta_{sl}},$$

resulting in

$$\|\xi_{sl}\|_{\zeta_{sl}}\leq K_{s1}\|\psi_{sl}\|_{\zeta_{sl}}\quad\forall\psi_{sl}\in\Lambda_{sl}, \tag{2.42}$$

with $K_{s1}=\frac{2K_3}{2K_3+\hat{\alpha}_s}<1$. Now, in (2.39), let $\phi_l=u_l$, so that with $\lambda_{sl}=\gamma_{ls}u_l$ we obtain

$$\frac{1}{2}\hat{a}_l(u_l,u_l)+(u_l,u_l)_{\zeta_{sl}}=(\xi_{sl},u_l)_{\zeta_{sl}}$$
$$\frac{1}{2}\hat{\alpha}_l\|u_l\|_{H^1(\Omega_l)}+\|\lambda_{sl}\|_{\zeta_{sl}}\leq\|\xi_{sl}\|_{\zeta_{sl}}\|\lambda_{sl}\|_{\zeta_{sl}}$$

Using (1.2), we have for all $\lambda_{sl}\in\Lambda_{sl}$

$$\|\lambda_{sl}\|^2_{\zeta_{sl}}\leq K_4\|u_l\|^2_{H^1(\Omega_l)} \tag{2.43}$$

where $K_4=C^2_{e,sl}C^2_{t,l}\|\zeta_{sl}\|^2_{L^2(\Gamma_{sl})}$. Thus, we get

$$\left(\frac{\hat{\alpha}_l}{2K_4}+1\right)\|\lambda_{sl}\|_{\zeta_{sl}}\leq\|\xi_{sl}\|_{\zeta_{sl}},$$

resulting in

$$\|\lambda_{sl}\|_{\zeta_{sl}}\leq K_{l2}\|\xi_{sl}\|_{\zeta_{sl}}\quad\forall\xi_{sl}\in\Lambda_{sl}, \tag{2.44}$$

with $K_{l2} = \frac{2K_4}{2K_4+\hat{\alpha}_l} < 1$. Overall, we obtain

$$\|\lambda_{sl}\|_{\zeta_{sl}} \leq K_{sl}\|\psi_{sl}\|_{\zeta_{sl}} < \|\psi_{sl}\|_{\zeta_{sl}},$$

with $K_{sl} = K_{l2}K_{s1}$. □

Finally, we repeat for interface Γ_{ws}.

Let $\mathcal{R}_{ws} : \Lambda_{ws} \to \Lambda_{ws}$ be the operator such that given a function $\psi_{ws} \in \Lambda_{ws}$, we have $\mathcal{R}_{ws}\psi_{ws} = \gamma_{ws}u_w$, where $u_w \in H^1_{\partial\Omega_s\setminus\Gamma_{ws}}(\Omega_w)$ satisfies

$$\frac{1}{2}\hat{a}_w(u_{w,k+1}, \phi_w) + (u_{w,k+1}, \phi_w)_{\zeta_{ws}} += (\psi_{ws}, \phi_w)_{\zeta_{ws}} \quad \forall \phi_w \in H^1_{\partial\Omega_l\setminus\Gamma_{ws}}(\Omega_w). \tag{2.45}$$

Let $\mathcal{R}_{sw} : \Lambda_{ws} \to \Lambda_{ws}$ be the operator such that given a function $\xi_{ws} \in \Lambda_{ws}$, we have $\mathcal{R}_{ws}\psi_{ws} = \gamma_{ws}u_s$, where $u_s \in H^1_{\partial\Omega_s\setminus\Gamma_{ws}}(\Omega_s)$ satisfies

$$\frac{1}{2}\hat{a}_s(u_{s,k+1}, \phi_s) + (u_{s,k+1}, \phi_s)_{\zeta_{ws}} = (\xi_{ws}, \phi_s)_{\zeta_{ws}} \quad \forall \phi_s \in H^1_{\partial\Omega_s\setminus\Gamma_{ws}}(\Omega_s). \tag{2.46}$$

Then, the iterative scheme corresponding to (2.27) and (2.30) can be seen as a fixed-point iteration:

$$\lambda_{ws,k+1} = T_{ws}\lambda_{ws,k}, \quad k = 0, 1, ..., \quad \text{where } T = \mathcal{R}_{sw} \circ \mathcal{R}_{ws}.$$

We prove a lemma similar to Lemma 3.

Lemma 4. There exists a constant $K_{ws} < 1$ depending on Ω_w, Ω_s, and ζ_{ws} such that

$$\|T_{ws}\psi_{ws}\|_{\zeta_{ws}} \leq K_{ws}\|\psi_{ws}\|_{\zeta_{ws}} \quad \forall \psi_{ws} \in \Lambda_{ws}. \tag{2.47}$$

Proof. Let u_s be a function related to ψ_{ws} through (2.45). We define $\xi_{ws} = \mathcal{R}_{ws}\psi_{ws}$ so that $\xi_{ws} = \gamma_{ws}u_s$. Also, let $\lambda_{ws} = \mathcal{R}_{sw}\xi_{ws}$, which is $\lambda_{ws} = T_{ws}\psi_{ws}$. Now, in (2.45), let $\phi_w = u_w$, so that with $\lambda_{ws}u_w$ we obtain

$$\begin{aligned}
&\frac{1}{2}\hat{u}_w(u_w, u_w) + (u_w, u_w)_{\zeta_{ws}} = (\xi_{ws}, u_w)_{\zeta_{ws}} \\
&\frac{1}{2}\hat{\alpha}_w\|u_w\|_{H^1(\Omega_w)} + \|\lambda_{ws}\|_{\zeta_{ws}} \leq \|\xi_{ws}\|_{\zeta_{ws}}\|\lambda_{ws}\|_{\zeta_{ws}}
\end{aligned}$$

Using (1.2), we have for all $\lambda_{ws} \in \Lambda_{ws}$

$$\|\lambda_{ws}\|^2_{\zeta_{ws}} \leq K_5 \|u_w\|^2_{H^1(\Omega_w)} \tag{2.48}$$

where $K_5 = C^2_{e,ws} C^2_{t,w} \|\zeta_{ws}\|^2_{L^2(\Gamma_{ws})}$, where $C_{e,ws}$ is the embedding constant of Λ_{ws} in $L^4(\Gamma_{ws})$. We then obtain

$$\left(\frac{\hat{\alpha}_s}{2K_5} + 1 \right) \|\lambda_{ws}\|_{\zeta_{ws}} \leq \|\xi_{ws}\|_{\zeta_{ws}},$$

resulting in

$$\|\lambda_{ws}\|_{\zeta_{ws}} \leq K_{w2} \|\xi_{ws}\|_{\zeta_{ws}} \quad \forall \xi_{ws} \in \Lambda_{ws}, \tag{2.49}$$

with $K_{w2} = \frac{2K_5}{2K_5 + \beta_w \hat{\alpha}_w} < 1$. For (2.46), let $\phi_s = u_s$, so that with $\lambda_{ws} = \gamma_{sw} u_s$ we obtain

$$\begin{aligned} \frac{1}{2} \hat{u}_s(u_s, u_s) + (u_s, u_s)_{\zeta_{ws}} &= (\xi_{ws}, u_s)_{\zeta_{ws}} \\ \frac{1}{2} \hat{\alpha}_s \|u_s\|_{H^1(\Omega_s)} + \|\lambda_{ws}\|_{\zeta_{ws}} &\leq \|\xi_{ws}\|_{\zeta_{ws}} \|\lambda_{ws}\|_{\zeta_{ws}}. \end{aligned}$$

Again, using (1.2), we have for all $\lambda_{ws} \in \Lambda_{ws}$

$$\|\lambda_{ws}\|^2_{\zeta_{ws}} \leq K_6 \|u_s\|^2_{H^1(\Omega_s)} \tag{2.50}$$

where $K_6 = C^2_{e,ws}, C^2_{t,s} \|\zeta_{ws}\|^2_{L^2(\Gamma_{ws})}$. Thus, we get

$$\left(\frac{\hat{\alpha}_s}{2K_6} + 1 \right) \|\lambda_{ws}\|_{\zeta_{ws}} \leq \|\xi_{ws}\|_{\zeta_{ws}},$$

resulting in

$$\|\lambda_{ws}\|_{\zeta_{ws}} \leq K_{s2} \|\xi_{ws}\|_{\zeta_{ws}} \quad \forall \xi_{ws} \in \Lambda_{ws}, \tag{2.51}$$

with $K_{s2} = \frac{2K_6}{2K_6 + \hat{\alpha}_s} < 1$. Assembling everything gives

$$\|\lambda_{ws}\|_{\zeta_{ws}} \leq K_{ws} \|\psi_{ws}\|_{\zeta_{ws}} < \|\psi_{ws}\|_{\zeta_{ws}},$$

with $K_{ws} = K_{w2} K_{s2}$. □

Consequently, from Lemma 2, Lemma 3, and Lemma 4 we see that

$$\lim_{k\to\infty} \|\lambda_{lw,k}\|_{\zeta_{lw}} = 0 \tag{2.52}$$

$$\lim_{k\to\infty} \|\lambda_{sl,k}\|_{\zeta_{sl}} = 0 \tag{2.53}$$

$$\lim_{k\to\infty} \|\lambda_{ws,k}\|_{\zeta_{ws}} = 0 \tag{2.54}$$

Corollary 1. The scheme (2.22), (2.23), and (2.24) is convergent, in particular

$$\lim_{k\to\infty} \left(\|e_{l,k}\|_{H^1(\Omega_l)} + \|e_{w,k}\|_{H^1(\Omega_w)} + \|e_{s,k}\|_{H^1(\Omega_s)}\right) = 0. \tag{2.55}$$

Proof. This is direct consequence of (2.52), (2.53), and (2.54). Consider (2.25), (2.27), and (2.29) with $\phi_l = e_{l,k+1}$, $\phi_w = e_{w,k+1}$, and $\phi_s = e_{s,k+1}$, respectively. Then, by Poincaré inequality we have

$$\begin{aligned}
\frac{1}{2}\hat{\alpha}_l\|e_{l,k+1}\|^2_{H^1(\Omega_l)} &\leq \|\lambda_{lw,k}\|_{\zeta_{lw}}\|\gamma_{lw}e_{l,k+1}\|_{\zeta_{lw}} \\
\frac{1}{2}\hat{\alpha}_w\|e_{w,k+1}\|^2_{H^1(\Omega_w)} &\leq \|\lambda_{ws,k}\|_{\zeta_{ws}}\|\gamma_{ws}e_{w,k+1}\|_{\zeta_{ws}} \\
\frac{1}{2}\hat{\alpha}_s\|e_{s,k+1}\|^2_{H^1(\Omega_s)} &\leq \|\lambda_{sl,k}\|_{\zeta_{sl}}\|\gamma_{sl}e_{s,k+1}\|_{\zeta_{sl}}.
\end{aligned}$$

Through inequalities (2.34), (2.41), and (2.48), we obtain that for all $k > 0$ there exist constants K_7, K_8, and K_9 such that

$$\begin{aligned}
\|e_{l,k+1}\|_{H^1(\Omega_l)} &\leq K_7\|\lambda_{lw,k}\|_{\zeta_{lw}} \\
\|e_{w,k+1}\|_{H^1(\Omega_w)} &\leq K_8\|\lambda_{ws,k}\|_{\zeta_{ws}} \\
\|e_{s,k+1}\|_{H^1(\Omega_s)} &\leq K_9\|\lambda_{sl,k}\|_{\zeta_{sl}}
\end{aligned}$$

.

Similarly for (2.26), (2.28), and (2.30), using $\phi_s = e_{s,k+1}$, $\phi_w = e_{w,k+1}$, and $\phi_l = e_{l,k+1}$, respectively, we can guarantee that for all $k > 0$, there exist constants K_{10}, K_{11}, and

K_{12} such that

$$\begin{aligned}\|e_{w,k+1}\|_{H^1(\Omega_w)} &\leq K_{10}\|e_{l,k+1}\|_{H^1(\Omega_l)}\\ \|e_{s,k+1}\|_{H^1(\Omega_s)} &\leq K_{11}\|e_{w,k+1}\|_{H^1(\Omega_w)}\\ \|e_{l,k+1}\|_{H^1(\Omega_l)} &\leq K_{12}\|e_{s,k+1}\|_{H^1(\Omega_s)}\end{aligned},$$

and the conclusion is reached. □

2.2.7 Convection dominated case considerations

In the presence of convection dominated problems, stabilization of the solution is required. This requires $\hat{a}_l$ to be substituted by

$$\hat{a}_{l,stab}(C_l,\phi_l) = \hat{a}_l(C_l,\phi_l) + a_{l,h}(C_l,\phi_l), \tag{2.56}$$

where $a_{l,h}(C_l,\phi_l)$ depends on specific stabilization methods. Setting

$$L_sC = -\nabla\cdot\mu_l\nabla C, \quad L_{ss}C = \frac{1}{2}\nabla\cdot\mathbf{u}C + \frac{1}{2}\mathbf{u}\cdot\nabla C \quad (L_l = L_s + L_{ss})$$

as the symmetric and skew-symmetric parts of the fluid differential operator L_s, respectively, then common strongly consistent stabilization methods are of the form

$$a_{l,h}(C_l,\phi_l) = \sum_{K\in\mathcal{T}_h}\sigma\left(LC_l, \frac{h_K}{|\mathbf{u}|}(L_{ss}+\kappa L_s)\phi_l\right)_K,$$

with K being the generic element of the triangulation $\mathcal{T}_h$ having diameter h_K, $(\cdot,\cdot)_K$ the $L^2(K)$ scalar product, δ a parameter to be chosen, and κ the correspondence to different stabilization techniques [49]. For instance, SUPG is established when letting $\kappa = 0$, and Galerkin least squares (GaLS) is invoked for $\kappa = 1$. For the numerical simulations, we chose SUPG since if δ is suitably chosen it can be directly proved that $\hat{a}_{l,stab}$ is coercive, with their coercivity constants independent of h.

2.3 Iterative-by-subdomain solution of the problem

To solve our problem, we perform the following iterative method based on the solution of the following problems. We state first the strong formulation, then the weak one. We do not explicitly specify the boundary conditions on the input/output sections. Also, for the sake of notation, the time index $n+1$ is understood, and the index k refers to the substructuring iterations.

Let us assume that the initial guesses $C_l^{(0)}$, $C_w^{(0)}$ and $C_s^{(0)}$ are given (they may coincide with the converged value at the previous time step).

1. **Lumen problem:** Solve

$$\begin{aligned}
\chi C_l^{(k+1)} - \mu_l \Delta C_l^{(k+1)} + \cdot\nabla C_l^{(k+1)} &= f_l \quad \text{on} \quad \Omega_l \\
\mu_l \frac{\partial C_l^{(k+1)}}{\partial \boldsymbol{n}_l} + \zeta_{ls}(C_l^{(k+1)} - C_s^{(k)}) &= 0 \quad \text{on} \quad \Gamma_{ls} \\
\mu_l \frac{\partial C_l^{(k+1)}}{\partial \boldsymbol{n}_l} + \zeta_{lw}(C_l^{(k+1)} - C_w^{(k)}) &= 0 \quad \text{on} \quad \Gamma_{lw}
\end{aligned}$$

   In weak terms: find $C_l^{(k+1)} \in V_l$ s.t.

$$\hat{a}_l(C_l^{(k+1)}, \phi_l) + \left(C_l^{(k+1)} - C_s^{(k)}, \phi_l\right)_{ls} + \left(C_l^{(k+1)} - C_w^{(k)}, \phi_l\right)_{lw} = (f_l, \phi_l) \tag{2.57}$$

   for all $\phi_l \in V_l$.

2. **Wall problem:** Solve

$$\begin{aligned}
\chi C_w^{(k+1)} - \mu_w \Delta C_w^{(k+1)} &= f_w \quad \text{in} \quad \Omega_w \\
\mu_w \frac{\partial C_w^{(k+1)}}{\partial \boldsymbol{n}_w} + \zeta_{lw}(C_w^{(k+1)} - C_l^{(k+1)}) &= 0 \quad \text{on} \quad \Gamma_{lw} \\
\mu_w \frac{\partial C_w^{(k+1)}}{\partial \boldsymbol{n}_w} + \zeta_{sw}(C_w^{(k+1)} - C_s^{(k)}) &= 0 \quad \text{on} \quad \Gamma_{sw}
\end{aligned}$$

   In weak terms: find $C_w^{(k+1)} \in V_w$ s.t.

$$\hat{a}_w(C_w^{(k+1)}, \phi_w) + \left(C_w^{(k+1)} - C_l^{(k+1)}, \phi_w\right)_{lw} + \left(C_w^{(k+1)} - C_s^{(k)}, \phi_w\right)_{sw} = (f_w, \phi_w) \tag{2.58}$$

for all $\phi_w \in V_w$.

3. **Strut problem:** Solve

$$\begin{aligned} ll\chi C_s^{(k+1)} - \mu_s \Delta C_s^{(k+1)} &= f_s \quad \text{in} \quad \Omega_s \\ \mu_s \frac{\partial C_s^{(k+1)}}{\partial \boldsymbol{n}_s} + \zeta_{ls}(C_s^{(k+1)} - C_l^{(k+1)}) &= 0 \quad \text{on} \quad \Gamma_{ls} \\ \mu_s \frac{\partial C_s^{(k+1)}}{\partial \boldsymbol{n}_w} + \zeta_{sw}(C_s^{(k+1)} - C_w^{(k+1)}) &= 0 \quad \text{on} \quad \Gamma_{sw} \end{aligned}$$

In weak terms: find $C_s^{(k+1)} \in V_s$ s.t.

(2.59)

$$\hat{a}_s(C_s^{(k+1)}, \phi_s) + \left(C_s^{(k+1)} - C_l^{(k+1)}, \phi_s\right)_{ls} + \left(C_s^{(k+1)} - C_w^{(k+1)}, \phi_s\right)_{sw} = (f_s, \phi_s)$$

for all $\phi_s \in V_s$.

4. Relaxation: Set

$$C_i^{(k+1)} := \omega_i C_i^{(k+1)} + (1 - \omega_i) C_i^{(i)}, i = l, w, s$$

where ω_i are real numbers generally in the interval $(0, 1]$.

Remark: In the sequence of problems we solve (lumen-wall-strut), we select the Lumen first because we preliminary solve the Navier-Stokes equations to compute the convective field in the lumen. It seems reasonable to use this convective field immediately. For the other problems in the sequence there is no specific reason to choose one or the other. It is promptly written a scheme solving the sequence lumen-strut-wall problems. From the convergence point of view, the two methods are equivalent.

2.3.1 The Jacobi variant

The previous iterative scheme uses the guess of the solution C_l, C_w, C_s as soon as it is available, like in the Gauss-Seidel method for solving linear systems. For this reason, we will call it the "Gauss-Seidel" variant.

A natural variant, oriented to the parallel computation, is to use the information available at one iteration only when all the subdomain solvers have completed their

process. This resembles the Jacobi method for solving linear systems and reads as follows.

Let's assume that $C_l^{(0)}$, $C_w^{(0)}$ and $C_s^{(0)}$ are given (they may coincide with the converged value at the previous time step).

1. **Lumen problem:** Solve

$$\begin{aligned}
\chi C_l^{(k+1)} - \mu_l \Delta C_l^{(k+1)} + \cdot\nabla C_l^{(k+1)} &= f_l \quad \text{in} \quad \Omega_l \\
\mu_l \frac{\partial C_l^{(k+1)}}{\partial \boldsymbol{n}_l} + \zeta_{ls}(C_l^{(k+1)} - C_s^{(k)}) &= 0 \quad \text{on} \quad \Gamma_{ls} \\
\mu_l \frac{\partial C_l^{(k+1)}}{\partial \boldsymbol{n}_l} + \zeta_{lw}(C_l^{(k+1)} - C_w^{(k)}) &= 0 \quad \text{on} \quad \Gamma_{lw}
\end{aligned}$$

   In weak terms: find $C_l^{(k+1)} \in V_l$ s.t.

$$\hat{a}_l(C_l^{(k+1)}, \phi_l) + \left(C_l^{(k+1)} - C_s^{(k)}, \phi_l\right)_{ls} + \left(C_l^{(k+1)} - C_w^{(k)}, \phi_l\right)_{lw} = (f_l, \phi_l) \tag{2.60}$$

   for all $\phi_l \in V_l$.

2. **Wall problem:** Solve

$$\begin{aligned}
\chi C_w^{(k+1)} - \mu_w \Delta C_w^{(k+1)} &= f_w \quad \text{in} \quad \Omega_w \\
\mu_w \frac{\partial C_w^{(k+1)}}{\partial \boldsymbol{n}_w} + \zeta_{lw}(C_w^{(k+1)} - C_l^{(k)}) &= 0 \quad \text{on} \quad \Gamma_{lw} \\
\mu_w \frac{\partial C_w^{(k+1)}}{\partial \boldsymbol{n}_w} + \zeta_{sw}(C_w^{(k+1)} - C_s^{(k)}) &= 0 \quad \text{on} \quad \Gamma_{sw}
\end{aligned}$$

   In weak terms: find $C_w^{(k+1)} \in V_w$ s.t.

$$\hat{a}_w(C_w^{(k+1)}, \phi_w) + \left(C_w^{(k+1)} - C_l^{(k)}, \phi_w\right)_{lw} + \left(C_w^{(k+1)} - C_s^{(k)}, \phi_w\right)_{sw} = (f_w, \phi_w) \tag{2.61}$$

   for all $\phi_w \in V_w$.

3. **Strut problem:** Solve

$$\begin{aligned} \chi C_s^{(k+1)} - \mu_s \Delta C_s^{(k+1)} &= f_s \quad \text{in} \quad \Omega_s \\ \mu_s \frac{\partial C_s^{(k+1)}}{\partial \boldsymbol{n}_s} + \zeta_{ls}(C_s^{(k+1)} - C_l^{(k)}) &= 0 \quad \text{on} \quad \Gamma_{ls} \\ \mu_s \frac{\partial C_s^{(k+1)}}{\partial \boldsymbol{n}_w} + \zeta_{sw}(C_s^{(k+1)} - C_w^{(k)}) &= 0 \quad \text{on} \quad \Gamma_{sw} \end{aligned}$$

In weak terms: find $C_s^{(k+1)} \in V_s$ s.t.

$$\hat{a}_s(C_s^{(k+1)}, \phi_s) + \left(C_s^{(k+1)} - C_l^{(k)}, \phi_s\right)_{ls} + \left(C_s^{(k+1)} - C_w^{(k)}, \phi_s\right)_{sw} = (f_s, \phi_s) \tag{2.62}$$

for all $\phi_s \in V_s$.

4. Relaxation: Set

$$C_i^{(k+1)} := \omega_i C_i^{(k+1)} + (1 - \omega_i) C_i^{(i)}, i = l, w, s$$

where ω_i are real numbers generally in the interval $(0, 1]$.

This Jacobi approach is immediately parallelizable, since the three problems Lumen, Wall, Strut can be solved simultaneuosly.

2.4 Domain decomposition methodology through Steklov-Poincaré operators

We briefly out the methodology and techniques of domain decomposition in the advection-diffusion problem that will be important in the following chapters. Let Ω be a bounded domain in $\mathbb{R}^d$, $d = 2, 3$ with Lipschitz boundary $\partial\Omega$ and non-overlapping domains Ω_1 and Ω_2, having Γ as their common boundary. On the boundary, we set $\mathbf{n}$ to be the normal at Γ oriented outwardly from $\partial\Omega_1 \cap \Gamma$.

We wish to reformulate the Poisson problem on Ω

$$\begin{cases} -\Delta u = f \quad \text{in} \quad \Omega \\ u = 0 \quad \text{on} \quad \partial\Omega, \end{cases}$$

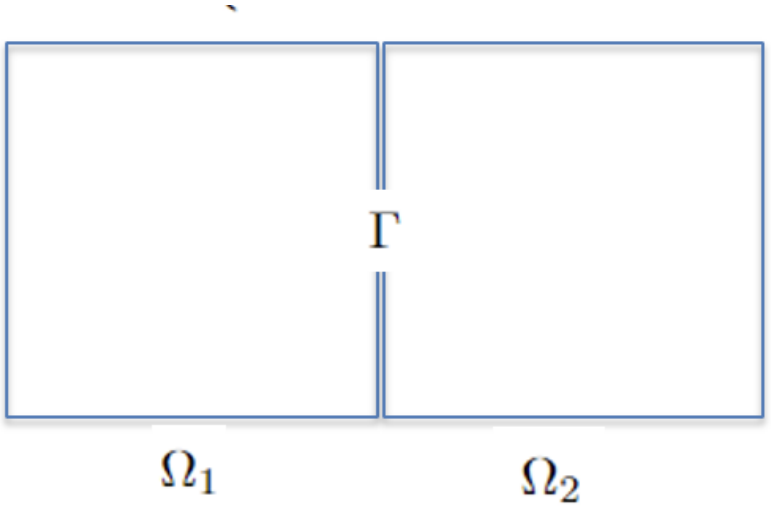

Figure 2.3: Non-overlapping partitions of Ω

If we assume f and u to be sufficiently smooth, and letting u_i be the restrictions of u to Ω_i, for $i = 1, 2$, then the Poisson problem becomes:

$$\begin{cases} -\Delta u_1 = f \quad \text{in} \quad \Omega_1 \\ u_1 = 0 \quad \text{on} \quad \partial\Omega_1 \cap \partial\Omega \\ u_1 = u_2 \quad \text{on} \quad \Gamma \\ \frac{\partial u_2}{\partial n} = \frac{\partial u_1}{\partial n} \quad \text{on}\Gamma \\ u_2 = 0 \quad \text{on} \quad \partial\Omega_2 \cap \partial\Omega \\ -\Delta u_2 = f \quad \text{in} \quad \Omega_2. \end{cases}$$

The conditions on Γ are called the interface, or transmission, conditions, and have boundary behavior with respect to u_1 or u_2. The strategy is to develop iteration by subdomain methods to update the overall system of solutions, with emphasis on Γ. In general, two sequences of functions $\{u_1^k\}$ and $\{u_2^k\}$ are generated with initial guess u_1^0, u_2^0 with the hope of converging to u_1 and u_2. The following are popular approaches:

- *Dirichlet/Neumann method* It consists of splitting the problem into Dirichlet and Neumann conditions for u_1 and u_2, respectively without loss of generality.

So for each $k \geq 0$, we seek to solve

$$\begin{cases} -\Delta u_1^{k+1} = f \quad \text{in} \quad \Omega_1 \\ u_1^{k+1} = 0 \quad \text{on} \quad \partial\Omega_1 \cap \partial\Omega \\ u_1^{k+1} = \lambda^k \quad \text{on} \quad \Gamma, \end{cases}$$

and then

$$\begin{cases} -\Delta u_2^{k+1} = f \quad \text{in} \quad \Omega_1 \\ u_2^{k+1} = 0 \quad \text{on} \quad \partial\Omega_2 \cap \partial\Omega \\ \frac{\partial u_2^{k+1}}{\partial n} = \frac{\partial u_1^{k+1}}{\partial n} \quad \text{on} \quad \Gamma, \end{cases}$$

with

$$\lambda^k := \theta u_{2|\Gamma}^k + (1-\theta) u_{1|\Gamma}^k,$$

θ being a positive acceleration parameter.

- *Neumann/Neumann method* Similar to the previous method but with initial values ψ_1^0 and ψ_2^0, we solve for $k \geq 0$

$$\begin{cases} -\Delta u_i^{k+1} = f \quad \text{in} \quad \Omega_i \\ u_i^{k+1} = 0 \quad \text{on} \quad \partial\Omega_i \cap \partial\Omega \\ u_i^{k+1} = \lambda^k \quad \text{on} \quad \Gamma, \end{cases}$$

and then

$$\begin{cases} -\Delta \psi_i^{k+1} = 0 \quad \text{in} \quad \Omega_i \\ \psi_i^{k+1} = 0 \quad \text{on} \quad \partial\Omega_i \cap \partial\Omega \\ \frac{\partial \psi_i^{k+1}}{\partial n} = \frac{\partial u_1^{k+1}}{\partial n} - \frac{\partial u_2^{k+1}}{\partial n} \quad \text{on} \quad \Gamma, \end{cases}$$

for $i = 1, 2$, with

$$\lambda^k := u_{1|\Gamma}^k - \theta(\alpha_1 \psi_{1|\Gamma}^k - \alpha_2 \psi_{2|\Gamma}^k),$$

where θ fulfills the same role as the previous instance and α_1 and α_2 are two

positive averaging coefficients. [50]

2.4.1 Steklov-Poincaré operators

With Steklov-Poincaré domain decomposition, we seek to split the problem into two Dirichlet problems wanting to solve for λ, which is the unknown value of u on Γ. Essentially, the problem is solved in terms of traces. Consider

$$\begin{cases} -\Delta w_i = f & \text{in} \quad \Omega_i \\ w_i = 0 & \text{on} \quad \partial\Omega_i \cap \partial\Omega \\ w_i = \lambda & \text{on} \quad \Gamma, \end{cases}$$

for $i = 1, 2$. Then letting

$$w_i = \mathcal{H}_i\lambda + \mathcal{G}_i f,$$

where

$$\begin{cases} -\Delta\mathcal{H}_i\lambda = 0 & \text{in} \quad \Omega_i \\ \mathcal{H}_i\lambda = 0 & \text{on} \quad \partial\Omega_i \cap \partial\Omega \\ \mathcal{H}_i\lambda = \lambda & \text{on} \quad \Gamma \end{cases}$$

and

$$\begin{cases} -\Delta\mathcal{G}_i f = f & \text{in} \quad \Omega_i \\ \mathcal{G}_i f = 0 & \text{on} \quad \partial\Omega_i \cap \partial\Omega \\ \mathcal{G}_i f = 0 & \text{on} \quad \Gamma. \end{cases}$$

For $i = 1, 2$, $\mathcal{H}_i\lambda$ is the harmonic extension of λ into Ω_i. We have that

$$w_i = u_i \text{ for } i = 1, 2 \text{ if and only if } \frac{\partial w_1}{\partial n} = \frac{\partial w_2}{\partial n} \text{ on } \Gamma.$$

A Steklov-Poincaré operator $\mathcal{S}$ is defined as

$$\mathcal{S}\mu := \frac{\partial}{\partial n}\mathcal{H}_1\mu - \frac{\partial}{\partial n}\mathcal{H}_2\mu$$

and acts between the space of trace functions $\Lambda := H_{00}^{1/2}(\Gamma) = \{v_{|\Gamma} | v \in H_0^1(\Omega)\}$ and its dual $\Lambda' = H_{00}^{-1/2}(\Gamma)$. [32]. Thus, in the context of the domain decomposition problem, we obtain that we have to solve for λ on Γ:

$$\mathcal{S}\lambda = \eta \quad \text{on} \quad \Gamma,$$

where

$$\eta := \frac{\partial}{\partial n}\mathcal{G}_2 f - \frac{\partial}{\partial n}\mathcal{G}_1 f.$$

Through weak formulation we get

$$\langle \mathcal{S}\gamma, \mu \rangle_{\Lambda',\Lambda} = (\nabla \mathcal{H}_1 \gamma, \nabla \mathcal{H}_1 \mu)_{\Omega_1} + (\nabla \mathcal{H}_2 \gamma, \nabla \mathcal{H}_2 \mu)_{\Omega_2} \quad \forall \gamma, \mu \in \Lambda.$$

We notice that $\mathcal{S}$ is symmetric and positive definite since

$$\langle \mathcal{S}\mu, \mu \rangle_{\Lambda',\Lambda} = \|\nabla \mathcal{H}_1 \mu\|_{0,\Omega_1}^2 + \|\nabla \mathcal{H}_2 \mu\|_{0,\Omega_2}^2 > 0 \quad \forall \mu \in \Lambda.$$

2.5 Steklov-Poincaré Analysis of the Stent Problem

The previous methodology required stronger continuity in the interfaces as we restrict the manifold interfaces. We attempt to curb this by considering a different direction, in which we employ slightly different terminology and notation.

In this section we provide an explanation to the mesh-independence demonstrated numerically for the Gauss-Seidel variant.

Following the path of the investigation for the wall-fluid problem (two domains, one interface) in [52, 53], we provide a reinterpretation of the problem and its numerical solver by interface equations and the so-called Steklov-Poincaré operators. While in the case with two domains, this leads to a single equation and to a neat interpretation of the segregated method as a preconditioned Richardson scheme, the extension to the multiples domain case is significantly more involved. Yet, it sheds a light on the convergence properties we obtain numerically.

2.5.1 Auxiliary Operators

Let us consider the following auxiliary problems. For the sake of readiness, we do not specify the conditions at the boundary (i.e., the portion of the boundaries that do not form the interfaces) here; they are intended to be consistent with the ones of the problems specified earlier (either homogeneous Dirichlet or homogeneous Neumann conditions). We focus only on the conditions of the interfaces.

When defining lifting operators, we introduce the same differential operators and functions extending trace functions from the interfaces in one of the domains insisting on that interface. The couple of indexes to denote the interfaces were ordered lexicographical (i.e., lw, ls, sw). In what follows, the lifting functions will have two indexes too, the second one refers to the domain where the function is extended, the first ones specifies at what interface. For instance, u_{sl} extends an interface function ρ_{ls} on Γ_{ls} into the s domain, while u_{ls} into the l one. Similarly, when we introduce the notation $\mathcal{H}_i^j$, the subscript recalls the domain i where the operator is solved, and j the interface where the corresponding function is defined.

Lifting operators

Struts operators Consider the following problems. Let ρ_{ls} and ρ_{sw} be two trace functions in Λ_{ls} and Λ_{sw}, respectively.

$$\begin{array}{l|l} \chi u_{ls} - \mu_s \Delta u_{ls} = 0 \quad \text{in} \quad \Omega_s, & \chi u_{ws} - \mu_s \Delta u_{ws} = 0 \quad \text{in} \quad \Omega_s, \\ u_{ls} = \rho_{ls} \qquad\qquad\quad \text{in } \Gamma_{ls}, & u_{ws} = 0 \qquad\qquad\quad \text{in } \Gamma_{ls} \\ u_{ls} = 0 \qquad\qquad\quad \text{in } \Gamma_{sw}, & u_{ws} = \rho_{sw} \qquad\qquad\quad \text{in } \Gamma_{sw}. \end{array} \tag{2.63}$$

We denote $\mathcal{H}_s^l \rho_{ls} \equiv u_{ls}$, $\mathcal{H}_w^s \rho_{sw} \equiv u_{ws}$ and $u_s \equiv u_{ls} + u_{sw}$.

Also, we introduce the problem

$$\begin{array}{ll} \chi g_s - \mu_s \Delta g_s = f_s & \text{in } \Omega_s, \\ g_s = 0 & \text{in } \partial\Gamma_{ls} \cup \Gamma_{sw}. \end{array} \tag{2.64}$$

Set $g_s \equiv \mathcal{G}_s f_s$.

Wall operators Let ρ_{lw} be a trace function in Λ_{lw}. We define the problems:

(2.65)

$$\begin{array}{l|l} \chi u_{lw} - \mu_w \Delta u_{lw} = 0 \quad \text{in } \Omega_w, & \chi u_{sw} - \mu_w \Delta u_{sw} = 0 \quad \text{in } \Omega_w, \\ u_{lw} = \rho_{lw} \quad \text{in } \Gamma_{lw}, & u_{sw} = 0 \quad \text{in } \Gamma_{ls} \\ \mu_w \nabla u_{lw} \cdot \mathbf{n}_w + \zeta_{sw} u_{lw} = 0 \quad \text{in } \Gamma_{sw}; & \mu_w \nabla u_{sw} \cdot \mathbf{n}_w + \zeta_{sw} u_{sw} = \zeta_{sw} \rho_{sw} \quad \text{in } \Gamma_{sw}, \end{array}$$

where ρ_{sw} is introduced in the previous paragraph. We denote $\mathcal{H}^l_w \rho_{lw} \equiv u_{lw}$, $\mathcal{H}^s_w \rho_{sw} \equiv u_{sw}$ and $u_w \equiv u_{lw} + u_{sw}$. Also, the operator $\mathcal{G}_w f_w$ is defined as the solution of:

$$\begin{array}{ll} \chi g_w - \mu_w \Delta g_w = f_w & \text{in } \Omega_w, \\ g_w = 0 & \text{on } \Gamma_{lw}, \\ \mu_w \nabla g_w \cdot \mathbf{n}_w + \zeta_{sw} g_w = 0 & \text{on } \Gamma_{sw}. \end{array} \tag{2.66}$$

Set $g_w \equiv \mathcal{G}_w f_w$.

Lumen operators Finally, we define the problems:

(2.67)

$$\begin{array}{l|l} \chi u_{wl} - \mu_w \Delta u_{wl} + \mathbf{u} \cdot \nabla u_{wl} = 0 \quad \text{in } \Omega_l, & \chi u_{sl} - \mu_w \Delta u_{sl} + \mathbf{u} \cdot \nabla u_{sl} = 0 \quad \text{in } \Omega_l, \\ \mu_l \nabla u_{wl} \cdot \mathbf{n}_l + \zeta_{wl} u_{wl} = \zeta_{lw} \rho_{wl} \rho_{wl} \quad \text{on } \Gamma_{lw}, & \mu_l \nabla u_{wl} \cdot \mathbf{n}_l + \zeta_{wl} u_{wl} = 0 \quad \text{on } \Gamma_{lw} \\ \mu_l \nabla u_{sl} \cdot \mathbf{n}_l + \zeta_{sl} u_{sl} = 0 \quad \text{on } \Gamma_{ls}; & \mu_l \nabla u_{sl} \cdot \mathbf{n}_l + \zeta_{sl} u_{sl} = \zeta_{ls} \rho_{sl} \quad \text{on } \Gamma_{ls}, \end{array}$$

where ρ_{ls} and ρ_{lw} were introduced in the previous paragraphs. We denote $\mathcal{H}^w_l \rho_{lw} \equiv u_{wl}$, $\mathcal{H}^s_l \rho_{ls} \equiv u_{sl}$ and $u_l \equiv u_{wl} + u_{sl}$. Finally, consider the problem

$$\begin{array}{ll} \chi g_l - \mu_l \Delta g_l + \mathbf{u} \cdot \nabla g_l = f_l & \text{in } \Omega_l \\ \mu_l \nabla g_l \cdot \mathbf{n}_l + \zeta_{wl} g_l = 0 & \text{on } \Gamma_{lw}, \\ \mu_l \nabla g_l \cdot \mathbf{n}_l + \zeta_{sl} g_l = 0 & \text{on } \Gamma_{ls}. \end{array} \tag{2.68}$$

We denote $\mathcal{G}_l f_l = g_l$.

Interface operators

Let us now consider the following operators acting at the interfaces. Traces ρ_{ls}, ρ_{sw} and ρ_{lw} are as in the previous paragraphs.

Wall-lumen interface Let us set

$$\left\{\begin{array}{l} \left.\begin{array}{l} \mathcal{S}^w_{11}\rho_{lw} \equiv \mu_w \frac{\partial \mathcal{H}^l_w \rho_{lw}}{\partial \boldsymbol{n}_w} + \zeta_{lw}\rho_{lw} \\ \mathcal{S}^l_{11}\rho_{lw} \equiv -\zeta_{lw}\gamma_{wl}\mathcal{H}^w_l \rho_{lw} \end{array}\right\} \\ \mathcal{S}_{12}\rho_{ls} \equiv -\zeta_{lw}\gamma_{wl}\mathcal{H}^s_l \rho_{ls} \\ \mathcal{S}_{13}\rho_{sw} \equiv \mu_w \frac{\partial \mathcal{H}^s_w \rho_{sw}}{\partial \mathbf{n}_w} \\ \eta_1 \equiv -\mu_w \frac{\mathcal{G}_w f_w}{\mathbf{n}_w} + \zeta_{lw}\gamma_{wl}\mathcal{G}_l f_l, \end{array}\right. \qquad \mathcal{S}_{11}\rho_{lw} \equiv \left(\mathcal{S}^w_{11} + \mathcal{S}^l_{11}\right)\rho_{lw} \tag{2.69}$$

where γ_{wl} is the trace operator $V_l \to \Lambda_{lw}$. Notice that

$$\mathcal{S}_{11}\rho_{lw} + \mathcal{S}_{12}\rho_{ls} + \mathcal{S}_{13}\rho_{sw} = \eta_1$$

implements the interface condition

$$\mu_w \frac{\partial(u_w + g_w)}{\partial \mathbf{n}_w} + \zeta_{lw}(u_w + g_w) = \zeta_{lw}(u_l + g_l).$$

Lumen-strut interface

$$\left\{\begin{array}{l} \left.\begin{array}{l} \mathcal{S}^s_{22}\rho_{ls} \equiv \mu_s \frac{\partial \mathcal{H}^l_s \rho_{ls}}{\partial \boldsymbol{n}_s}, \\ \mathcal{S}^l_{22}\rho_{ls} \equiv -\zeta_{ls}\gamma_{ls}\mathcal{H}^s_l \rho_{ls} \end{array}\right\} \\ \mathcal{S}_{21}\rho_{lw} \equiv -\zeta_{ls}\gamma_{sl}\mathcal{H}^w_l \rho_{lw} \\ \mathcal{S}_{23}\rho_{sw} \equiv \mu_s \partial \mathcal{H}^w_s \rho_{sw} \partial \mathbf{n}_s, \\ \eta_2 \equiv -\mu_s \frac{\mathcal{G}_s f_s}{\mathbf{n}_s} + \zeta_{ls}\gamma_{ls}\mathcal{G}_l f_l, \end{array}\right. \qquad \mathcal{S}_{22}\rho_{ls} = \left(\mathcal{S}^s_{11} + \mathcal{S}^l_{11}\right)\rho_{ls} \tag{2.70}$$

where γ_{sl} is the trace operator $V_l \to \Lambda_{ls}$.

By direct inspection, one verifies that:

$$\mathcal{S}_{22}\rho_{ls} + \mathcal{S}_{21}\rho_{lw} + \mathcal{S}_{23}\rho_{sw} = \eta_2$$

corresponds to the interface condition

$$\mu_s \partial(u_s + g_s)\partial \mathbf{n}_s + \zeta_{ls}(u_s + g_s) = \zeta_{ls}(u_l + g_l).$$

Wall-strut interface In this case, we introduce the notation:

$$
\left\{
\begin{array}{l}
\left.\begin{array}{l}
\mathcal{S}^s_{33}\rho_{sw} \equiv \mu_s \frac{\partial \mathcal{H}^w_s \rho_{sw}}{\partial \mathbf{n}_s} + \zeta_{sw}\rho_{sw} \\
\mathcal{S}^w_{33}\rho_{sw} \equiv -\zeta_{sw}\gamma_{sw}\mathcal{H}^s_w \rho_{sw}
\end{array}\right\} \qquad \mathcal{S}_{33}\rho_{sw} = \left(\mathcal{S}^s_{33} + \mathcal{S}^w_{33}\right)\rho_{sw} \\
\mathcal{S}_{31}\rho_{lw} \equiv -\zeta_{sw}\gamma_{sw}\mathcal{S}^l_w \rho_{lw} \\
\mathcal{S}_{32}\rho_{ls} \equiv \mu_s \frac{\partial \mathcal{S}sl\rho_{ls}}{\partial \mathbf{n}_s} \\
\eta_3 \equiv -\mu_s \frac{\partial \mathcal{G}_s f_s}{\mathbf{n}_s} + \zeta_{sw}\gamma_{sw}\mathcal{G}_w f_w,
\end{array}
\right. \tag{2.71}
$$

where γ_{sw} is the trace operator $V_w \to \Lambda_{sw}$.

Again, the equation

$$\mathcal{S}_{31}\rho_{lw} + \mathcal{S}32\rho_{ls} + \mathcal{S}33\rho_{sw} = \eta_3$$

corresponds to the wall-strut interface equation

$$\mu_s \frac{\partial(u_s + g_s)}{\partial \mathbf{n}_s} + \zeta_{ls}(u_s + g_s) = \zeta_{sw}(u_w + g_w).$$

The Steklov-Poincaré (SP) System

The operators introduced above form a system of interface equations in the form

$$\boldsymbol{\mathcal{S}}\boldsymbol{\rho} = \boldsymbol{\eta} \tag{2.72}$$

where

$$\boldsymbol{\mathcal{S}} \equiv \begin{bmatrix} \mathcal{S}_{11} & \mathcal{S}_{12} & \mathcal{S}_{13} \\ \mathcal{S}_{21} & \mathcal{S}_{22} & \mathcal{S}_{23} \\ \mathcal{S}_{31} & \mathcal{S}_{32} & \mathcal{S}_{33} \end{bmatrix}, \boldsymbol{\rho} \equiv \begin{bmatrix} \rho_{lw} \\ \rho_{ls} \\ \rho_{sw} \end{bmatrix}, \boldsymbol{\eta} \equiv \begin{bmatrix} \eta_1 \\ \eta_2 \\ \eta_3 \end{bmatrix}.$$

We will prove that this system of equations that we will call *Steklov-Poincaré* system amounts to the solution of the time-discrete Problem 4, and extends the problem previously considered in [52, 53] to the case of multiple (i.e., 3+) domains.

2.5.2 Weak formulation of the SP system

To find the weak formulation of (2.72), we notice that for a generic function $\lambda_{ls} \in \Lambda_{ls}$ and its extensions $\mathcal{L}_s\lambda_{ls}$ in Ω_s s.t. its trace on Γ_{sw} is 0 and $\mathcal{L}_l\lambda_{ls}$ in Ω_l s.t. its trace

on Γ_{lw} is 0,

$$
\begin{array}{l}
\left\langle \mu_s \frac{(\partial \mathcal{H}_s^l \rho_{ls} + \mathcal{H}_s^w \rho_{sw})}{\partial \mathbf{n}_s}, \lambda_{ls} \right\rangle_{ls} = \hat{a}_s(u_s, \mathcal{L}_s \lambda_{ls}) \\
(\rho_{ls} - \gamma_{ls} \mathcal{H}_l^s \rho_{ls} - \gamma_{ls} \mathcal{H}_l^w \rho_{lw}, \lambda_{ls})_{\zeta_{ls}} = \left\langle \mu_l \frac{\partial (\mathcal{H}_l^s \rho_{ls} + \mathcal{H}_l^w \rho_{lw})}{\partial \mathbf{n}_s}, \lambda_{ls} \right\rangle_{ls} = \hat{a}_l(u_l, \mathcal{L}_l \lambda_{ls}) \\
\left\langle \mu_s \frac{\partial \mathcal{G}_s f_s}{\mathbf{n}_s}, \lambda_{ls} \right\rangle_{ls} = \hat{a}_s(g_s, \mathcal{L}_s \lambda_{ls}) - (f_s, \mathcal{L}s \lambda_{ls}) \\
\left\langle \mu_l \frac{\partial \mathcal{G}_l f_l}{\partial \mathbf{n}_l}, \lambda_{ls} \right\rangle_{ls} = -(\gamma_{ls} \mathcal{G}s f_s, \lambda_{ls})_{\zeta_{ls}} = \hat{a}_l(g_l, \mathcal{L}_l \lambda_{ls}) - (f_l, \mathcal{L}_l \lambda_{ls})
\end{array}
\tag{2.73}
$$

With these positions, we verify that weak formulation of the second equation of the SP system reads $\forall \lambda_{ls} \in \Lambda_{ls}$

$$
\hat{a}_s(u_s + g_s, \mathcal{L}_s \lambda_{ls}) + \hat{a}_l(u_l + g_l, \mathcal{L}_l \lambda_{ls}) = (f_s, \mathcal{L}_s \lambda_{ls}) + (f_l, \mathcal{L}_l \lambda_{ls}). \tag{2.74}
$$

Here, $\langle \cdot, \cdot \rangle_{ls}$ denotes the duality pairing Λ_{ls} with its dual space.

With similar arguments and notation, it is possible to verify that the first and the third equations of the SP system read

$$
\begin{array}{l}
\hat{a}_w(u_w + g_w, \mathcal{L}_w \lambda_{lw}) + \hat{a}_l(u_l + g_l, \mathcal{L}_l \lambda_{lw}) = (f_w, \mathcal{L}_w \lambda_{lw}) + (f_l, \mathcal{L}_l \lambda_{lw}) \\
\hat{a}_s(u_s + g_s, \mathcal{L}_s \lambda_{sw}) + \hat{a}_w(u_w + g_w, \mathcal{L}_w \lambda_{sw}) = (f_s, \mathcal{L}s \lambda_{sw}) + (f_w, \mathcal{L}_w \lambda_{sw})
\end{array}
\tag{2.75}
$$

Now, if we sum the three equations and identify

$$
C_s = u_s + g_s, \quad C_w = u_w + g_w, \quad C_l = u_l + g_l,
$$

and

$$
\phi_s = \mathcal{L}_s \lambda_{ls} + \mathcal{L}_s \lambda_{ws}, \quad \phi_w = \mathcal{L}_w \lambda_{ws} + \mathcal{L}_w \lambda_{lw}, \quad \phi_l = \mathcal{L}_l \lambda_{ls} + \mathcal{L}_l \lambda_{lw},
$$

it follows that the SP system is equivalent to the multidomain Problem 3 when we sum the three equations.

2.5.3 Space-discretization of the SP system

For the space-discretization of the problem, let us consider again a conformal reticulation of the three domains, i.e., such that the reticulation in each subdomain shares the same degrees of freedom at the interfaces. Then, we introduce the finite-dimensional subspaces of $H^1(\Omega_l)$, $H^1(\Omega_w)$ and $H^1(\Omega_s)$, denoted by $V_{h,l}$, $V_{h,w}$ and $V_{h,s}$, respectively. Correspondingly, we introduce the finite-dimensional trace subspaces $\Lambda_{h,ls}$, $\Lambda_{h,sw}$ and $\Lambda_{h,lw}$ of Λ_{ls}, Λ_{sw} and Λ_{lw} respectively.

Following up on the weak formulation of the SP system provided above, the fully discrete formulation of the SP problem reads: find $\rho_{h,ls} \in \Lambda_{h,ls}$, $\rho_{h,ws} \in \Lambda_{h,sw}$, and $\rho_{h,ls} \in \Lambda_{h,ls}$ s.t.

$$
\begin{aligned}
&\hat{a}_s(u_{h,s} + g_{h,s}, \mathcal{L}_{h,s}\lambda_{h,ls}) + \hat{a}_w(u_{h,l} + g_{h,l}, \mathcal{L}_{h,l}\lambda_{h,ls}) = \\
&\qquad (f_s, \mathcal{L}_{h,s}\lambda_{h,ls}) + (f_l, \mathcal{L}_{h,l}\lambda_{h,ls}) \\
&\hat{a}_s(u_{h,s} + g_{h,s}, \mathcal{L}_{h,s}\lambda_{h,ws}) + \hat{a}_w(u_{h,w} + g_{h,w}, \mathcal{L}_{h,w}\lambda_{h,ws}) = \\
&\qquad (f_s, \mathcal{L}_{h,s}\lambda_{h,ws}) + (f_w, \mathcal{L}_{h,w}\lambda_{h,ws}) \\
&\hat{a}_w(u_{h,w} + g_{h,w}, \mathcal{L}_{h,w}\lambda_{h,lw}) + \hat{a}_l(u_{h,l} + g_{h,l}, \mathcal{L}_{h,l}\lambda_{h,lw}) = \\
&\qquad (f_w, \mathcal{L}_{h,w}\lambda_{h,lw}) + (f_l, \mathcal{L}_{h,l}\lambda_{h,lw})
\end{aligned}
\tag{2.76}
$$

for all $\lambda_{h,ls} \in \Lambda_{h,ls}$ $\lambda_{h,ws} \in \Lambda_{h,sw}$ and $\lambda_{h,lw} \in \Lambda_{h,lw}$ and with $\rho_{h,ls} = u_{h,s}(\Gamma_{ls})$, $\rho_{h,sw} = u_{h,s}(\Gamma_{sw})$ and $\rho_{h,lw} = u_{h,w}(\Gamma_{lw})$.

Summing up the three equations we obtain the sum of equations in Problem 4. This formulation will help to analyze the iterative-by-subdomain method we propose for the the solution of the problem. To this aim, we recall the Finite Element Uniform Extension Theorem (see [51], Theorem 4.1.3), that states that $\|\rho_{h,lw}\|_{\Lambda_{h,lw}}$ is equivalent to $\|u_{lw,h}\|_{1,w}$ with constants independent of h. Similarly, we state the uniform equivalence of $\|\rho_{h,ls}\|_{\Lambda_{h,ls}}$ with $\|u_{ls,h}\|_{1,s}$ and $\|\rho_{h,sw}\|_{\Lambda_{h,sw}}$ with $\|u_{ws,h}\|_{1,s}$. In particular,

$$
\|u_{s,h}\|^2_{1,s} \leq C_1 \left(\|\rho_{h,sw}\|^2_{\Lambda_{h,sw}} + \|\rho_{h,ls}\|^2_{\Lambda_{h,ls}} \right) \leq C_2 \|u_{ws,h}\|^2_{1,s}
$$

where the constants C_1 and C_2 are independent of h. Thanks to this Theorem, it is possible to prove the continuity of the operators forming the matrix $\boldsymbol{\mathcal{S}}$ and the positivity of the matrix, independently of the value of the discretization parameter h. More precisely, we can prove the following proposition.

Proposition 1. The following statements hold.

1. The operator $\mathcal{S}^w_{11,h}$ is symmetric and uniformly coercive.

2. The matrix
$$
\boldsymbol{\mathcal{S}} \equiv \mathcal{S}_{2,h} \equiv \begin{bmatrix} \mathcal{S}^s_{22,h} & \mathcal{S}_{23,h} \\ \mathcal{S}_{32,h} & \mathcal{S}^s_{33,h} \end{bmatrix},
$$
is continuous and uniformly positive.

3. The Steklov-Poincaré discrete matrix is continuous and uniformly positive.

The statements follow from the definition of each operator in the weak form. In particular, statement 3 implies that the discrete problem is well-posed.

2.5.4 The substructring method and the SP system

Let us consider the substructuring methods of the lumen, wall, and strut. In particular, we consider a function $\lambda_{lw} \in \Lambda_{lw}$ and its extensions $\mathcal{L}_l\lambda_{lw}$ such that $\mathcal{L}_l\lambda_{lw} = 0$ on Γ_{ls} and $\mathcal{L}_w\lambda_{lw}$ such that $\mathcal{L}w\lambda_{lw} = 0$ on Γ_{sw}.

Summing up in Ω_l for $\phi_l = \mathcal{L}_l\lambda_{lw}$ and Ω_w for $\phi_w = \mathcal{L}_w\lambda_{lw}$, we obtain

$$\begin{aligned} &\hat{a}_l(C_l^{(k+1)}, \mathcal{L}_l\lambda_{lw}) + \hat{a}_w(C_w^{(k+1)}, \mathcal{L}_w\lambda_{lw}) + \left(C_w^{(k+1)} - C_w^{(k)}, \lambda_{lw}\right)_{lw} \\ &\qquad = (f_l, \mathcal{L}_l\lambda_{lw}) + (f_w, \mathcal{L}_w\lambda_{lw})\,. \end{aligned} \tag{2.77}$$

Denote the trace of $C_w^{(k)}$ on Γ_{lw} as $\rho_{lw}^{(k)}$, likewise the trace of $C_s^{(k)}$ on Γ_{sw} as $\rho_{sw}^{(k)}$ and on Γ_{ls} as $\rho_{ls}^{(k)}$.

Then, consistently with the notation introduced earlier, we denote the solution by

$$C_l^{(k+1)} = \mathcal{H}_l^w\rho_{lw}^{(k)} + \mathcal{H}_l^s\rho_{ls}^{(k)} + g_l,$$

and

$$C_w^{(k+1)} = \mathcal{H}_l^w\rho_{lw}^{(k+1)} + \mathcal{H}_l^s\rho_{sw}^{(k)} + g_w.$$

With this notation, equation ((2.77)) reads

$$\begin{aligned} &\hat{a}_l(\mathcal{H}_l^w\rho_{lw}^{(k)} + \mathcal{H}_l^s\rho_{ls}^{(k)} + g_l, \mathcal{L}_l\lambda_{lw}) + \hat{a}_w\mathcal{H}_l^w\rho_{lw}^{(k+1)} + \mathcal{H}_l^s\rho_{sw}^{(k)} + g_w\mathcal{L}_w\lambda_{lw} + \\ &\left(\rho_{lw}^{(k+1)} - \rho_{lw}^{(k)}, \lambda_{lw}\right)_{lw} \qquad = (f_l, \mathcal{L}l\lambda_{lw}) + (f_w, \mathcal{L}w\lambda_{lw})\,. \end{aligned}$$

Formally, for the Steklov-Poincaré operators, this equation reads

$$\mathcal{S}_{11}^w\rho_{lw}^{(k+1)} = \eta_1 - \mathcal{S}_{11}^l\rho_{lw}^{(k)} - \mathcal{S}_{12}^l\rho_{ls}^{(k)} - \mathcal{S}_{13}^l\rho_{sw}^{(k)}$$

or, equivalently

$$\mathcal{S}_{11}^w(\rho_{lw}^{(k+1)} - \rho_{lw}^{(k)}) = \mathbf{r}_1^{(k)},$$

where $\mathbf{r}_1^{(k)}$ is the residual of the first equation.

Proceeding similarly, it is possible to find that the generic iteration of the unre-

laxed Gauss-Seidel substructuring iterative method reads

$$\boldsymbol{\mathcal{S}_P}\left(\boldsymbol{\rho}^{(k+1)}-\boldsymbol{\rho}^{(k)}\right)=\boldsymbol{\eta}-\boldsymbol{\mathcal{S}}\boldsymbol{\rho}^{(k)},$$

where

$$\boldsymbol{\mathcal{S}_P}\equiv\begin{bmatrix}\mathcal{S}_{11}^{w} & 0 & 0\\ 0 & \mathcal{S}_{22}^{s} & \mathcal{S}_{23}\\ \mathcal{S}_{31} & \mathcal{S}_{32} & \mathcal{S}_{33}^{s}\end{bmatrix}.$$

Alternatively, we get

$$\boldsymbol{\rho}^{(k+1)}=\boldsymbol{\mathcal{S}_P^{-1}}\boldsymbol{\eta}-\left(\mathcal{I}-\boldsymbol{\mathcal{S}_P^{-1}}\boldsymbol{\mathcal{S}}\right)\boldsymbol{\rho}^{(k)}$$

This is the generic iteration of an unrelaxed preconditioned Richardson scheme for the SP system, where $\boldsymbol{\mathcal{S}_P}$ is the preconditioner.

The relaxed version of the scheme promptly reads

$$\boldsymbol{\rho}^{(k+1)}=\boldsymbol{\rho}^{(k)}+\mathcal{W}\boldsymbol{\mathcal{S}_P^{-1}}\left(\boldsymbol{\eta}-\boldsymbol{\mathcal{S}}\boldsymbol{\rho}^{(k)}\right)$$

where $\mathcal{W}$ is the diagonal matrix with the coefficients $\omega_l, \omega_w, \omega_s$ on the main diagonal. Should we set $\omega_l=\omega_w=\omega_s=\omega$, the previous iteration reads

$$\boldsymbol{\rho}^{(k+1)}=\boldsymbol{\rho}^{(k)}+\omega\boldsymbol{\mathcal{S}_P^{-1}}\left(\boldsymbol{\eta}-\boldsymbol{\mathcal{S}}\boldsymbol{\rho}^{(k)}\right)$$

Discussion about the convergence of the preconditioned Richardson scheme

We can recall the following result, similar to what was done in [53].

Theorem 2.5.1 (see [51], Thm 4.4 and Remark 4.2.4)**.** Let X be a real Hilbert space, X' its dual and $\langle\cdot,\cdot\rangle$ the duality pairing them. Let $\mathcal{Q}: X\to X'$ a linear continuous operator split as $\mathcal{Q}=\mathcal{Q}_1+\mathcal{Q}_2$ where

1. $\mathcal{Q}_2$ is continuous, symmetric and coercive;
2. $\mathcal{Q}$ is continuous and coercive.

Let $\eta\in X'$ be given and consider the problem in the unknown ρ:

$$\mathcal{Q}\eta=\rho.$$

Then, there exists a real value θ_M, depending on the coercivity and continuity constants, such that $\forall\theta \in (0, \theta_M)$ the preconditioned Richardson iteration

$$\rho^{(k+1)} = \rho^{(k)} + \theta\mathcal{Q}_2^{-1}\left(\eta - \mathcal{Q}\rho^{(k)}\right)$$

converges in X to the solution of the problem for any initial guess $\rho^{(0)}$.

In the case of the wall-fluid problem considered in [53], this Theorem perfectly fits into the Steklov Poincaré formulation, leading straightforwardly to the proof of convergence of the iterative-by-subdomain method. In the case considered here with three interfaces, the case is more complicated, since the operator $\boldsymbol{\mathcal{S}_P}$ acting as preconditioner in the SP reinterpretation of the iterative method is not symmetric. However, notice that

$$\boldsymbol{\mathcal{S}_P} \equiv \begin{bmatrix} \mathcal{S}_{11} & 0 & 0 \\ 0 & \mathcal{S}_{22} & \mathcal{S}_{23} \\ 0 & \mathcal{S}_{32} & \mathcal{S}_{33} \end{bmatrix} + \begin{bmatrix} 0 & 0 & 0 \\ 0 & 0 & 0 \\ \mathcal{S}_{32} & 0 & 0 \end{bmatrix}$$

Let's denote by $\boldsymbol{\mathcal{Q}}_2$ the first term on the right hand side. This is a symmetric, continuous, and coercive operator by virtue of Proposition 1. The preconditioner $\boldsymbol{\mathcal{S}_P}$ associated with the Gauss-Seidel iterative method is therefore a *low-rank perturbation* of the symmetric operator $\boldsymbol{\mathcal{Q}}_2$. In particular, notice that

$$\begin{bmatrix} 0 & 0 & 0 \\ 0 & 0 & 0 \\ \mathcal{S}_{32} & 0 & 0 \end{bmatrix} \equiv \upsilon\psi^T, \quad \text{with} \quad \upsilon = \begin{bmatrix} 0 \\ 0 \\ \mathcal{I} \end{bmatrix}, \psi = \begin{bmatrix} \mathcal{S}_{31} \\ 0 \\ 0 \end{bmatrix}.$$

Notice that with this notation $\mathcal{I} + \psi^T\boldsymbol{\mathcal{Q}}_2^{-1}\upsilon = \mathcal{I}$, which is trivially invertible. This enables the use of the Sherman-Morrison Formula for operators:

$$\boldsymbol{\mathcal{S}_P}^{-1} = \boldsymbol{\mathcal{Q}}_2^{-1} - \boldsymbol{\mathcal{Q}}_2^{-1}\upsilon\left(\mathcal{I} + \psi^T\mathcal{Q}_2^{-1}\upsilon\right)^{-1}\psi\boldsymbol{\mathcal{Q}}_2^{-1}$$

that in our case reduces to

$$\boldsymbol{\mathcal{S}_P}^{-1} = \boldsymbol{\mathcal{Q}}_2^{-1} - \boldsymbol{\mathcal{Q}}_2^{-1}\upsilon\psi^T\boldsymbol{\mathcal{Q}}_2^{-1} = \boldsymbol{\mathcal{Q}}_2^{-1} - \begin{bmatrix} 0 & 0 & 0 \\ \star & 0 & 0 \\ \star & 0 & 0 \end{bmatrix}.$$

The symbol $\star$ denotes non-zero entries in the matrix operator. If we assume the same relaxation parameter for the three domains, our relaxed preconditioned Richardson scheme obtained by the iterative subdomain method reads therefore

$$\boldsymbol{\rho}^{(k+1)} = \boldsymbol{\rho}^{(k+1)} + \omega \boldsymbol{\mathcal{Q}}_2^{-1} \boldsymbol{r}^{(k)} + \boxed{\begin{bmatrix} 0 & 0 & 0 \\ \star & 0 & 0 \\ \star & 0 & 0 \end{bmatrix} . \boldsymbol{r}^{(k)}}.$$

The iteration scheme without the boxed term converges uniformly thanks to Theorem 5. On the other hand, the boxed term is a low-rank perturbation driven by a singular matrix with all zero eigenfunctions. We argue that the boxed term does not alter signifcantly the spectral behavior of the scheme with the symmetric preconditioner.

When we consider the space-discrete version of the operators, we get to the same point and the application of Proposition 1 explains why our results exhibit a mesh-independent convergence rate.

Remark. The previous analysis refers to the sequence lumen-wall-strut. It can be adjusted to the sequence lumen-strut-wall. It is enough to swap the operators marked by w and s in our definitions, since the wall and the strut problems are both symmetric.

Remark. The previous results promtply extend to the case of stabilized solvers (like SUPG) featuring a coercivity constant independent of the mesh size (see also [53]).

2.6 Numerical Results

The struts form a sequence of rings centered on the centerline of the pipe. We consider sequences of 1, 3 and 5 rings on a straight and a curved pipe. The pipe is 5 mm long, with an external radius of 1.2 mm (external wall); the wall-lumen interface is located at the radius $R_l = 1$ mm. The internal face of the struts (interfacing with the lumen) is a is at a distance of 0.9 mm from the centerline, the external face (interfacing with the wall) is at 1.08 mm, and the length of each ring is 0.2 mm.

We implemented our domain decomposition method within the NGSolve library [54], through Python scripts.

We wrote a simple monolithic unsteady Navier-Stokes solver for the flow in the lumen. The boundary conditions for the Navier-Stokes problem were set to be:

1. no-slip (i.e., homogeneous Dirichlet) at the interface of the lumen with either the wall or the struts;

2. non-homogeneous Dirichlet at the inflow with a Poiseuille flow at the inflow circular section;

3. traction-free (i.e., homogeneous Neumann) at the outflow.

At this proof-of-concept stage, we tested different diffusivities. In particular, when in Ω_l the convection is dominating over the diffusion we stabilized the solver with a strongly consistent method like SUPG [7]. In the following results, we set the diffusivities to be $\mu_l = 5.0 \times 10^{-5}$, $\mu_w = 5.0 \times 10^{-5}$, $\mu_s = 1.0 \times 10^{-9}$. The Robin constants ζ_{lw} and ζ_{ls}, in general, are functions of the shear stress $\nu(\nabla \mathbf{u} + \nabla^T \mathbf{u}) \cdot \boldsymbol{n} - \boldsymbol{n} \cdot \left(\nu(\nabla \mathbf{u} + \nabla^T \mathbf{u}) \cdot \boldsymbol{n}\right) \boldsymbol{n}$. For the sake of simplicity, we assume here these coefficients to be constant: $\zeta_{lw} = 3.42 \times 10^{-3}$, $\zeta_{ls} = 3.42 \times 10^{-3}$, and $\zeta_{sw} = 3.5 \times 10^{-3}$.

The initial conditions were set to be $C_{l,0} = 1$, $C_{w,0} = 0.5$ and $C_{s,0} = 0$. For the Jacobi, the system would solve in lumen, stent, and wall before updating to the next iteration; and for Gauss-Seidel, a domain would be solved and soon thereafter would the solutions of the other domains be updated without waiting for all three to be solved. In the latter, we considered a normal sequence of lumen-stent-wall iterated several times and a "snake" sequence that solves through the stent domain intermittently (e.g. lumen-stent-wall-stent-lumen-stent...).In our numerical results, we considered the two methods introduced above, the Gauss-Seidel and the Jacobi variants. For the Gauss-Seidel method we considered both the $l - w - s$ and the $l - s - w$ sequences with similar results. We set the relaxation parameters to 1. Also, we considered an additional case, the Symmetric Gauss-Seidel (SGS) case. This means that at the end of the iteration, we do not restart with the lumen, but we perform another solution of the wall problem in the $l - w - s$ sequence (or the strut problem in the $l - s - w$ sequence) to get back eventually to the lumen problem, similarly to what done for linear systems for the Symmetric Successive Over Relaxation (SSOR) scheme. The following shows a summary of the results, with L^2-norm and number of iterations per domain needed for convergence.

2-Ring Stent Results				
Solver	Number of elements	Time (s)	Iterations	L^2-norm
Jacobi	3022	3.9	5	2.12215
	23672	41.6	5	1.38647
	189376	1070	5	0.91845
GS (Normal)	3022	3.7	4	2.150887
	23672	41.8	5	1.3936
	189376	1055	5	0.92445
GS (Snake)	3022	3.4	5	2.150804
	23672	36	5	1.3934
	189376	819	5	0.92418

3-Ring Stent Results				
Solver	Number of elements	Time (s)	Iterations	L^2-norm
Jacobi	3437	4.52	5	2.9298
	27496	52	5	1.9749
	219968	2012	4	1.335885
GS (Normal)	3437	4.88	5	2.9534
	27496	49	6	1.9794
	219968	1923	4	1.33793
GS (Snake)	3437	4.48	5	2.9533
	27496	44	5	1.9794
	219968	1509	4	1.33793

5-Ring Stent Results				
Solver	Number of elements	Time (s)	Iterations	L^2-norm
Jacobi	4154	5.7	5	2.89657
	33232	94	5	1.93923
	265856	2570	5	1.30985
GS (Normal)	4154	5.3	5	2.93147
	33232	98	6	1.9474
	265856	2578	6	1.3132678
GS (Snake)	4154	5.15	5	2.931395
	33232	84	6	1.9474
	265856	2020	5	1.3132574

As can be seen, the numerical results are consistent with better convergence according to number of elements and iterations. Moreover, all of the schemes perform similarly numerically, with Jacobi being only slightly better. However, Gauss-Seidel has a better time complexity than Jacobi; in particular, the "snake" variation is faster since it acts as a pivot domain given its lighter element density and placement between the other two domains. Since the performance is similar to the other two, the snake Gauss-Seidel should be the favored numerical scheme in the future.

The results consistently confirm the convergence theorems we proved. However, regardless of the number of struts and the curvature of the geometry, we notice what follows.

1. The convergence rate of the methods is independent of the mesh: this is critical for the application to real problems, as we expect we need to resort to very fine meshes.

2. The fastest method in terms of CPU time is the SGS. This is arguably due to the fact that in the symmetric iterations the additional step reduces the time for solving each other subdomain thanks to a better transmission of the interface information through the subdomains.

Diffusivity observations

We implemented simulations by changing the diffusivity parameters in the lumen, wall, and stent to understand the interplay behavior among domains. Previously,

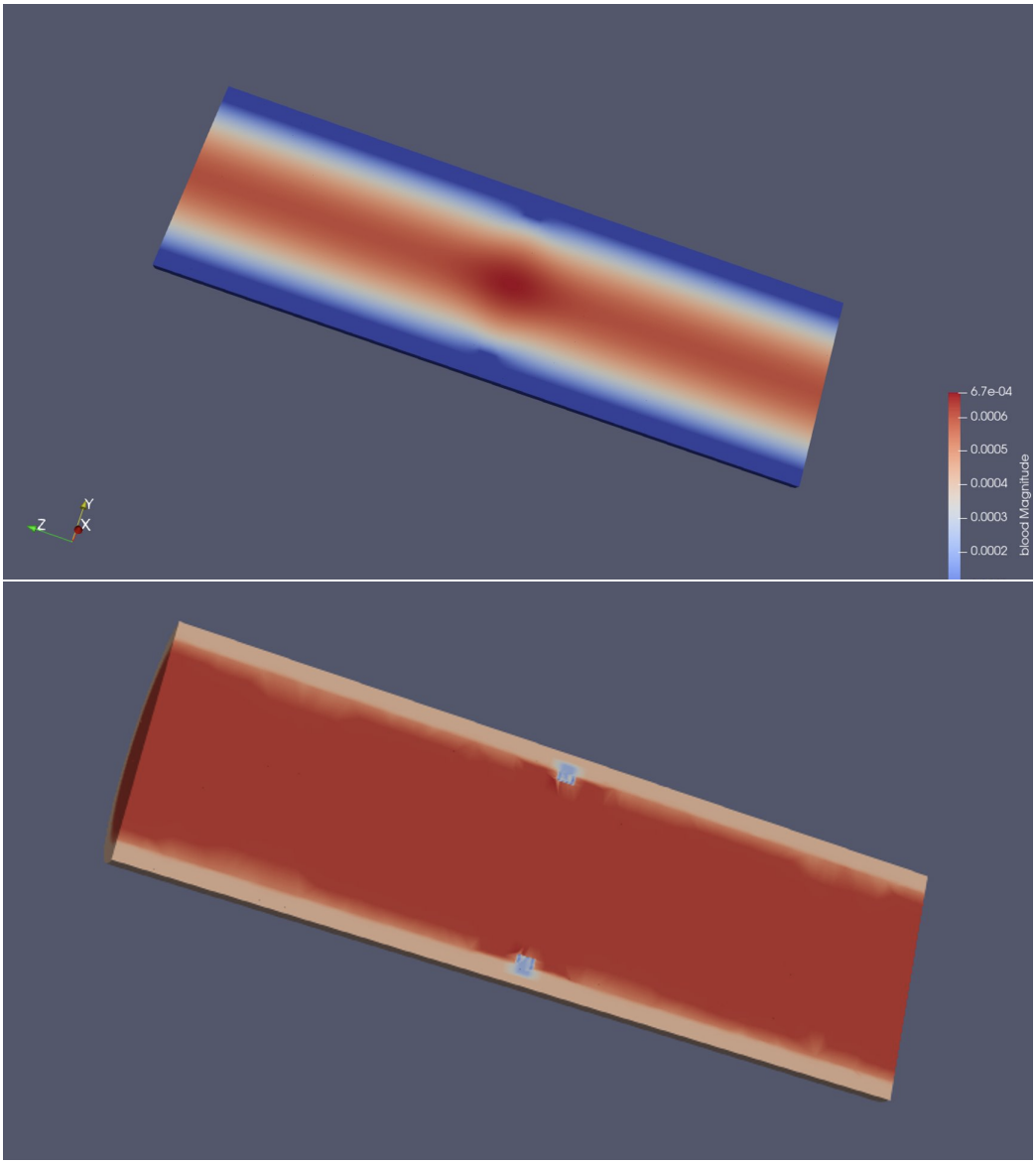

Figure 2.4: Upper: Blood velocity with one-ring stent. Bottom: Solute with one-ring stent

we had the same diffusivity in the wall and lumen, but for this part we set them two degrees of magnitude apart. We primarily considered the following cases: $\mu_w = 1.0 \times 10^{-3}$, $\mu_l = 1.0 \times 10^{-5}$, $\mu_s = 1.0 \times 10^{-9}$ (negligible permeability in the stent); $\mu_w = 1.0 \times 10^{-3}$, $\mu_l = 1.0 \times 10^{-5}$, $\mu_s = 1.0 \times 10^{-7}$ (low permeability in the stent); and $\mu_w = 1.0 \times 10^{-3}$, $\mu_l = 1.0 \times 10^{-5}$, $\mu_s = 1.0 \times 10^{-1}$ (high permeability in the stent). The results are visibly observed in Figures 2.8 and 2.6. In the first instance, there is a noticeable difference in the absorption from lumen to wall while only a small discrepancy can be observed from their respective interactions with the stent.

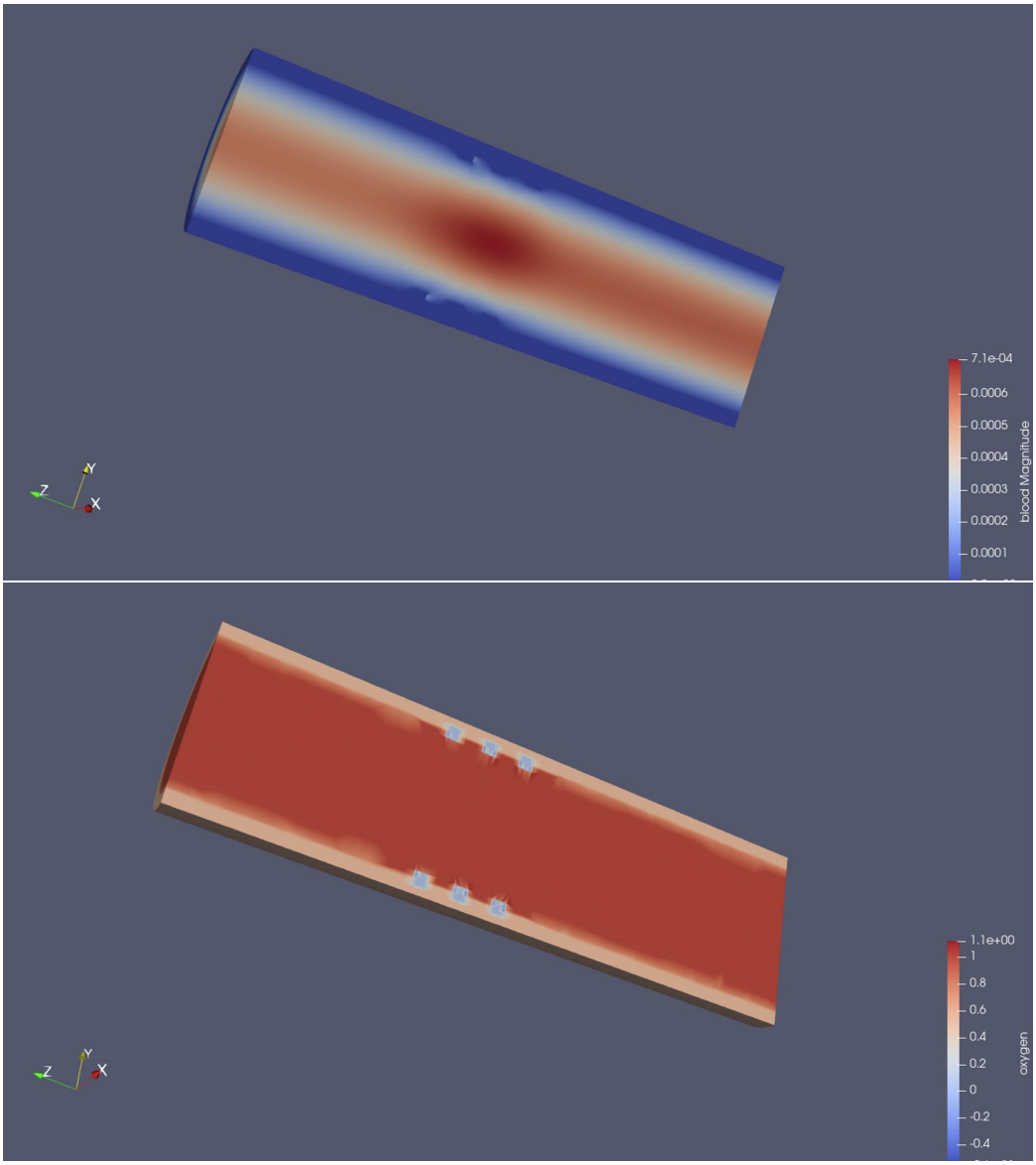

Figure 2.5: Upper: Blood velocity with three-ring stent. Bottom: Solute with three-ring stent

When it comes to low permeability in the stent, the concentration shifts more around the stent; and for high permeability in the stent, a more dynamic variability in all regions around the stent can be appreciated. Interestingly, there is a slightly inverse relationship between the maximum element concentration of solute in the overall geometry and the diffusivity of the stent. When the struts had higher diffusivity, the maximum concentration decreased, and viceversa. This is presumably due the fact that the concentration is spread across more regions, instead of becoming increasingly turbulent in fewer areas. There was no discernible change in the time complexity

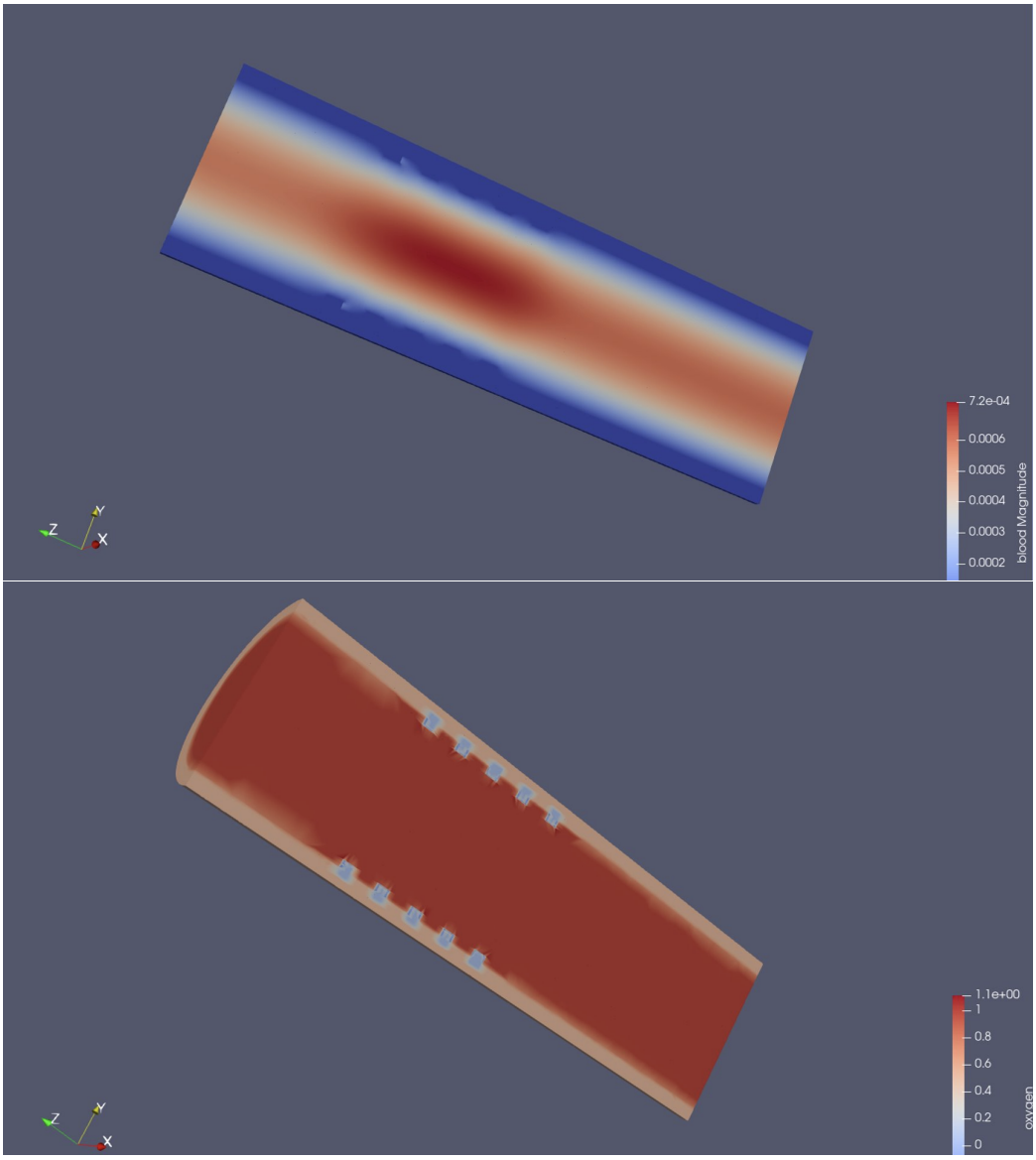

Figure 2.6: Upper: Blood velocity with five-ring stent. Bottom: Solute with five-ring stent

and convergence behavior explored in the aforementioned same diffusivity instances. Overall, the variational diffusivity could play an important role in the behavior of the solute concentration.

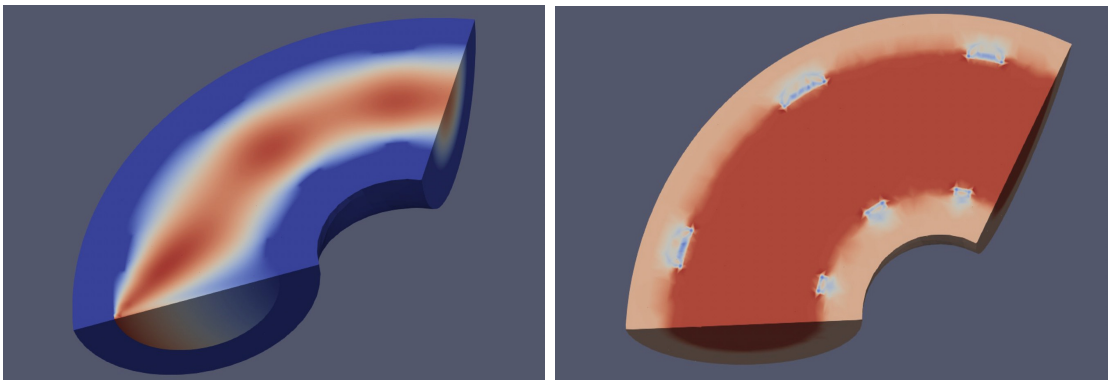

Figure 2.7: Left: Blood velocity with three-ring curved stent. Right: Solute with three-ring curved thin stent.

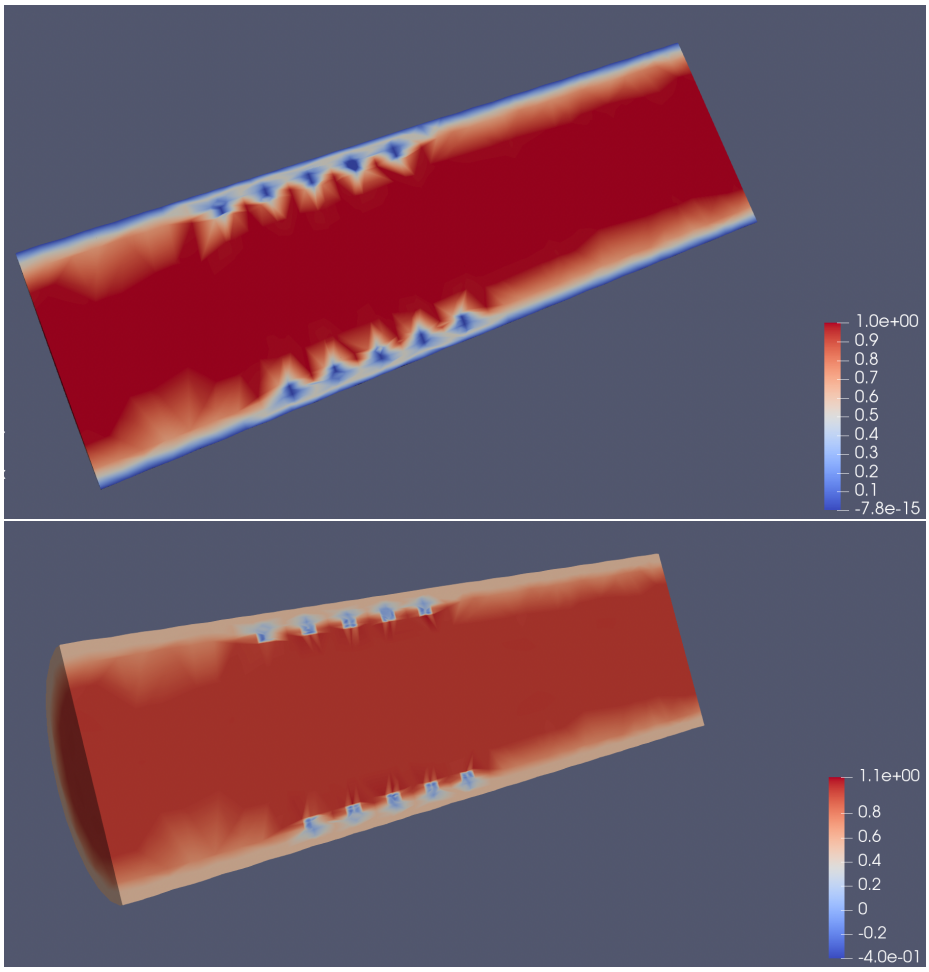

Figure 2.8: Upper: Solute concentration in five-ring stent with different wall diffusivity from lumen after one iteration. Bottom: Solute concentration in five-ring stent with different wall diffusivity from lumen after five iteration.

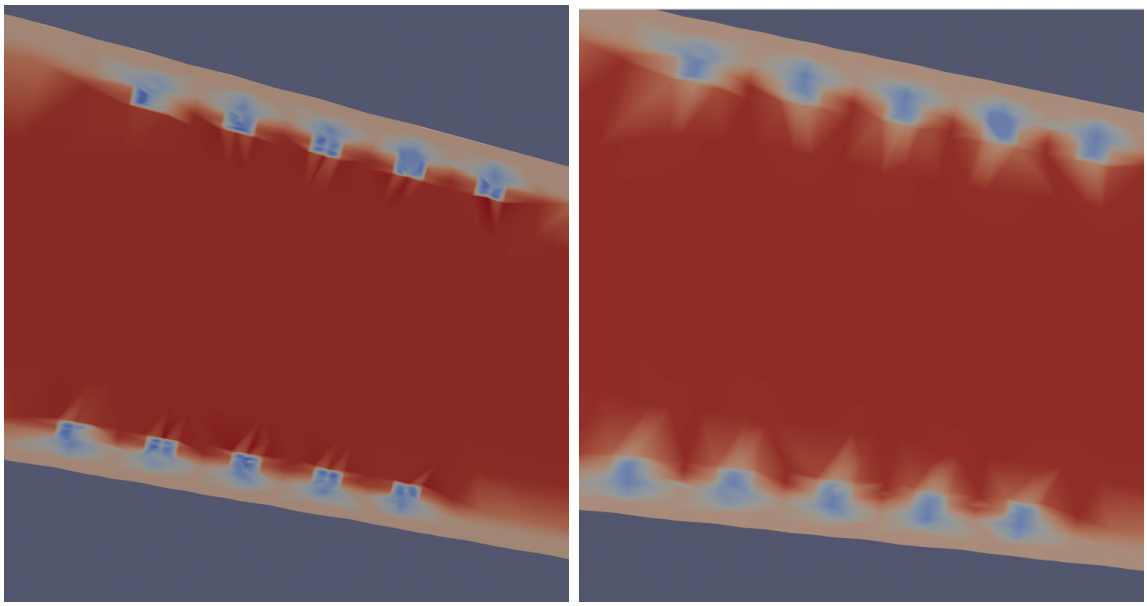

Figure 2.9: Left: Solute concentration in five-ring stent with low diffusivity in the struts. Right: Solute concentration in five-ring stent with high diffusivity in the struts

Chapter 3

Mathematical modeling of drug dynamics in the stent

3.1 Drug in stent motivation

Due to the foreign nature of the stent, the artery is prone to hard coagulation and scarring tissue resulting in the condition of in-stent restenosis, a narrowing of a stented artery lesion, after six months on average from stent placement in the case of bare metal stents (BMS) and after twelve months with drug eluting stents (DES). [37] To prevent this undesirable coagulation around the stent, these were coated with drug, such as heparin, to help the artery heal. It is of interest to model the dynamics of drug around the stent to have a realistic picture of the complete stent transformation. In the past, modeling the drug movement has been achieved in the wall-stent and stent-lumen settings, respectively, but not altogether.[59] In this chapter, we implement techniques of the multi-domain decomposition methodology derived in the previous chapter to achieve drug modeling. It is important to notice that the drug coated stent acts as the source of the solute to be dissolved into the lumen and the wall. The intent of this work is to model a complete drug eluting stent, which has a layer of drug coating that dissipates across the artery system over time. Clinically and experimentally, there have been trials aiming to estimate the timing of drug release, ranging from 15 days to 90 days, as well as their physiological consequence, hoping to discern which is more beneficial in the long term.[25] Different stents customized in terms of shape and drug type have been studied extensively to elucidate on optimal behavior.[3] [58] Moreover, while most stents have the basic metallic strut with a drug

coating, some of them have an additional topcoat layer, with the end of slowing down the drug release and minimizing drug bursts to the artery.[14] In many instances, thrombosis was a derived consequence of DES implantation, with factors such as stent length, underexpansion and residual stenosis being highly correlated to it.[43] In all of these cases, it is still not clear what is the optimal release rate to prevent thrombosis and other stent-related conditions. To provide such insight, we develop the groundwork for the mathematical modeling and simulation of DESs.

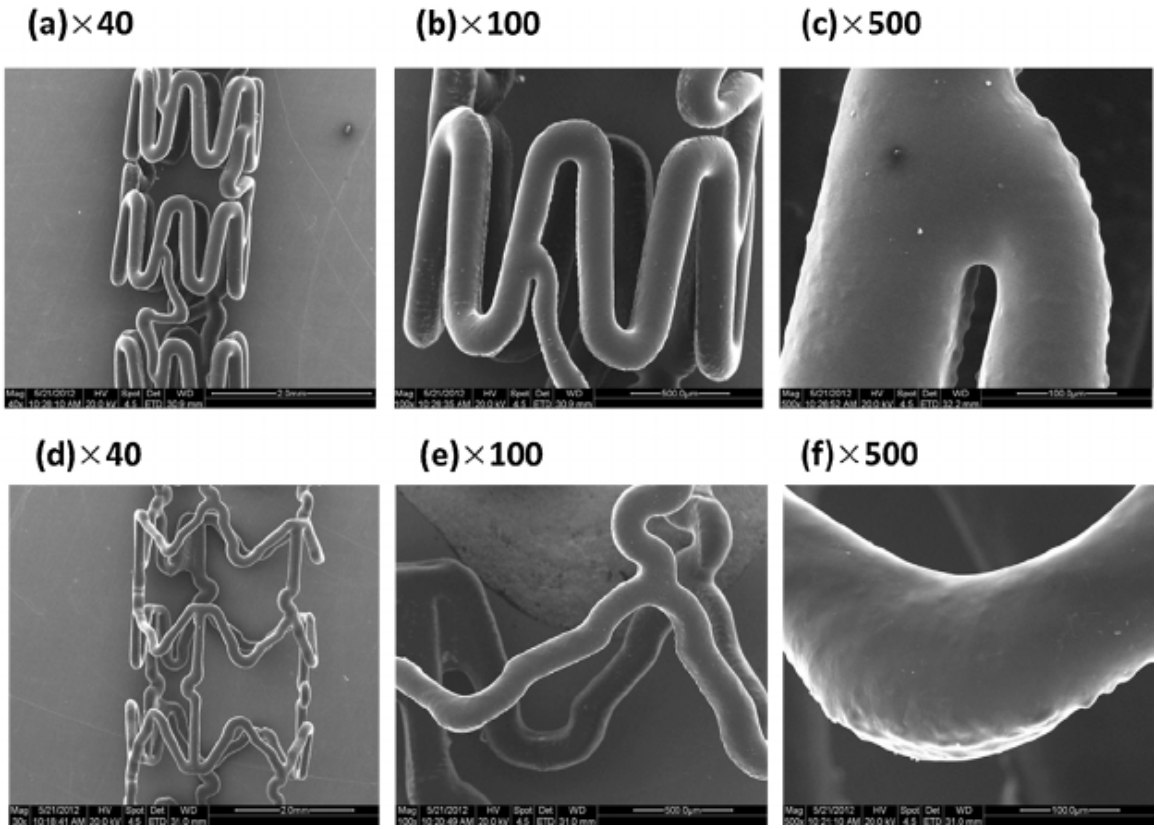

Figure 3.1: Different types of drug eluting stents.[61]

3.2 Geometrical description

For the case of DES, it is necessary that we elaborate a coating layer in the context of our previous geometry. The domain changes in time also for bioresorbable stents (BRS), but shorter time scales could be required for the progression of the erosion. For now, we focus on DES, whose domains will be shaped over time, so we describe their evolution. We let $\Omega_s(t)$, $\Omega_w(t)$, and $\Omega_l(t)$ be domains defined over some time

interval $[0,T]$ for some $T \in \mathbb{R}^+$. In the case of $t = 0$, we let $\Omega_l(0)$, $\Omega_w(0)$, $\Omega_s(0)$, $\Gamma_{lw}(0)$, $\Gamma_{ws}(0)$, and $\Gamma_{sl}(0)$ be the same domains and interfaces from the previous chapter.

3.2.1 Initial Drug Coating

We assume that the coating is initially uniform as is expected in a real stent. And to prevent ambiguity in cusps, such as corners, from the definitions that follow, we initially assume that the boundary $\partial\Omega_s$ is composed of sufficiently smooth manifolds, at least of the C^1 kind, basing on the continuous and differentiable fluid structure of the drug coating (see Figure 3.1).[61] We start to describe the coating by considering a non-negative real constant δ_0, to later determine the inward radial thickness. Then we define

$$\text{dist}_{\partial\Omega_s(0)}(\mathbf{x}) = \min_{\mathbf{y}\in\partial\Omega_s(0)} \|\mathbf{x}-\mathbf{y}\|$$

for $\mathbf{x} \in \Omega_s(0)\backslash\partial\Omega_s(0)$. Fixing $\mathbf{x} \in \Omega_s\backslash\partial\Omega_s(0)$, we obtain the projection on the boundary of $\Omega_s(0)$

$$V_{\mathbf{x}} = \{\mathbf{y} \in \partial\Omega_s(0) : \|\mathbf{x}-\mathbf{y}\| = \text{dist}_{\partial\Omega_s(0)}(\mathbf{x})\}$$

for $\mathbf{x} \in \Omega_s(0)\backslash(\Gamma_{sl}(0) \cup \Gamma_{ws}(0))$. For each $\mathbf{x} \in \Omega_s(0)\backslash\partial\Omega_s(0)$ and each $\mathbf{y} \in V_{\mathbf{x}}$ in its corresponding projection, let $L_{\mathbf{x},\mathbf{y}} \subset \Omega_s(0)$ be the segment given by

$$L_{\mathbf{x},\mathbf{y}} = \{\mathbf{y} + s(\mathbf{x}-\mathbf{y}) : s \in (0,1)\}.$$

Finally, for $t = 0$, we let $C_{\mathbf{x},\mathbf{y},\sigma_0}$ be the region

$$C_{\mathbf{x},\mathbf{y},\sigma_0} = \{\mathbf{z} \in L_{\mathbf{x},\mathbf{y}} : \|\mathbf{z}-\mathbf{y}\| < \delta_0\}.$$

Therefore, we define

$$\Omega_c(0) = \bigcup_{\mathbf{x}\in\Omega_s(0)\backslash\partial\Omega_s(0)} \bigcup_{\mathbf{y}\in V_{\mathbf{x}}} C_{\mathbf{x},\mathbf{y},\sigma_0}$$

to be the coating of the stent. The structure can be observed in Figure 3.2.

Remark: In general, we will be alluding to the non-drug portion of the stent

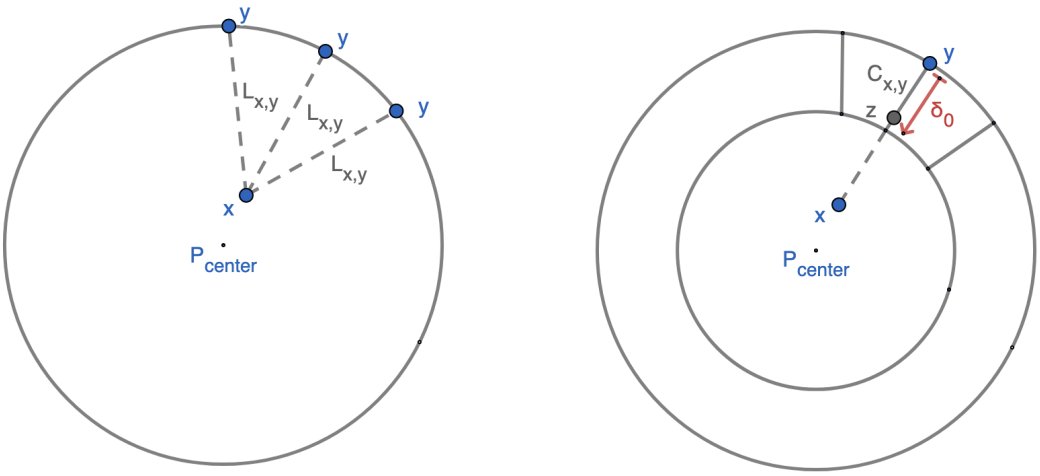

Figure 3.2: Cross-sections of drug coating representation

(i.e. the metal base) from time to time; so for notation ease, we shall refer to it by $\Omega_m = \Omega_s(0) \backslash \Omega_c(0)$, which is constant in time.

3.2.2 Drug Coating Evolution

We denote by I the time interval $(0, T]$. For each $t \in I$, consider the differentiable mapping $\Phi(\mathbf{y}, t) : \partial\Omega_s(0) \times I \to \Omega_c(0)$. The behavior of $\Phi(\mathbf{y}, t)$ depends on the coating's hemodynamic corrosion and arterial drug absorption. In the context of time evolution, for $t \in I$ we define

$$C_{\mathbf{x},\mathbf{y}}(t) = \{\mathbf{z} \in L_{\mathbf{x},\mathbf{y}} : \|\Phi(\mathbf{y}, t) - \mathbf{y}\| \leq \|\mathbf{z} - \mathbf{y}\| \leq \delta_0\}.$$

Thus, for $t \in I$ the drug coating over time becomes

$$\Omega_c(t) = \bigcup_{\mathbf{x} \in \Omega_s(0) \backslash \partial\Omega_s(0)} \bigcup_{\mathbf{y} \in V_{\mathbf{x}}} C_{\mathbf{x},\mathbf{y}}(t).$$

As such, the stent domain is

$$\Omega_s(t) = \Omega_m \cup \Omega_c(t)$$

for $t \in I$. This is shown in Figure 3.3

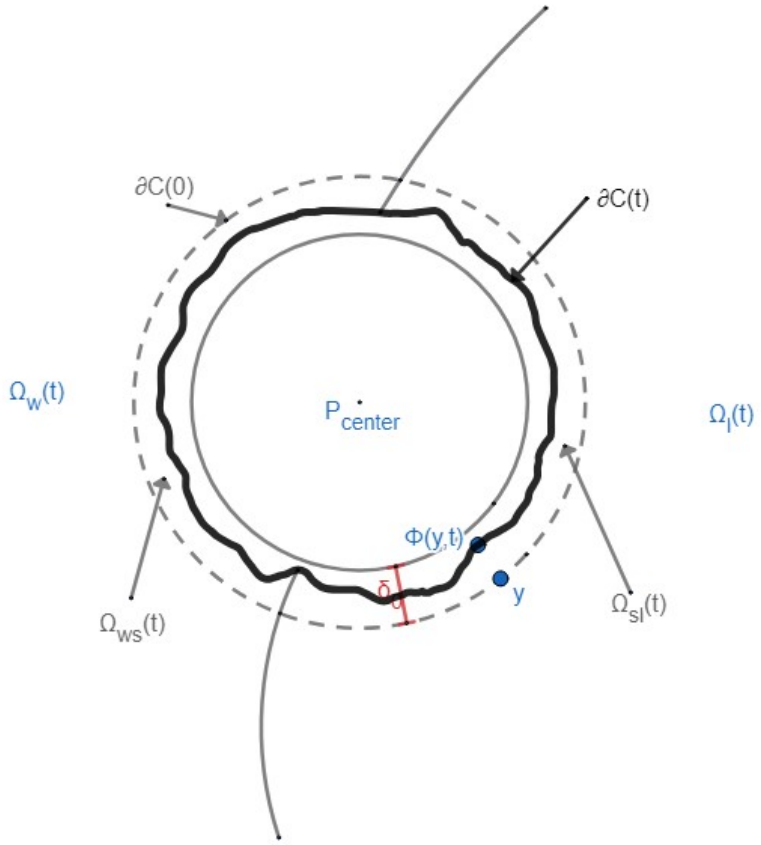

Figure 3.3: Representation of drug as a time-evolving domain. Compare with right-side of Figure 3.2. Notice that now $\Omega_w(t)$ and $\Omega_l(t)$ acquired the domain where the eluded drug used to be; we denote these added regions by $\Omega_{ws}(t)$ and $\Omega_{sl}(t)$. P_{center} represents the metallic core Ω_m.

To update the remaining regions and interface, we need to define the projection of $\Phi(\mathbf{y}, t)$ onto the interfaces $\Gamma_{sl}(0)$ and $\Gamma_{ws}(0)$. For $t \in I$, we let

$$\Phi_{\Gamma_{sl}}(\mathbf{y}, t) := \Phi(\mathbf{y}, t)\Big|_{\Gamma_{sl}(0)}$$

to be the projection of $\Phi(\mathbf{y}, t)$ to $\Gamma_{sl}(0)$. Now for every $\mathbf{y} \in \Gamma_{sl}(0)$ and $\hat{\mathbf{y}} = \Phi_{\Gamma_{sl}}(\mathbf{y}, t)$, we define $\Gamma_{sl}(t)$ to be such that for $\hat{\mathbf{y}} \in \Gamma_{sl}(t)$. In this manner, $\Phi_{\Gamma_{sl}}(\mathbf{y}, t)$ behaves like

a map from $\Gamma_{sl}(0)$ to $\Gamma_{sl}(t)$. Then we define

$$O_{\mathbf{x},\mathbf{y},\Gamma_{sl}}(t) := \{\mathbf{z} \in L_{\mathbf{x},\mathbf{y}} : \|\mathbf{z}-\mathbf{y}\| \leq \|\mathbf{y} - \Phi_{\Gamma_{sl}}(\mathbf{y},t)\|\}$$

so that we can have

$$\Omega_{sl}(t) := \bigcup_{\mathbf{x}\in\Omega_s(0)\setminus\partial\Omega_s(0)} \bigcup_{\mathbf{y}\in V_{\mathbf{x}}} O_{\mathbf{x},\mathbf{y},\Gamma_{sl}}(t)$$

We do the same for the $\Gamma_{ws}(t)$ interface: we allow for $t \in I$

$$\Phi_{\Gamma_{ws}}(\mathbf{y},t) := \Phi(\mathbf{y},t)\Big|_{\Gamma_{ws}(0)}$$

to be the projection of $\Phi(\mathbf{y},t)$ to $\Gamma_{ws}(0)$; and for every $\mathbf{y} \in \Gamma_{ws}(0)$ and $\hat{\mathbf{y}} = \Phi_{\Gamma_{ws}}(\mathbf{y},t)$, we define $\Gamma_{ws}(t)$ to be such that for $\hat{\mathbf{y}} \in \Gamma_{ws}(t)$. Then we let

$$O_{\mathbf{x},\mathbf{y},\Gamma_{ws}}(t) := \{\mathbf{z} \in L_{\mathbf{x},\mathbf{y}} : \|\mathbf{z}-\mathbf{y}\| \leq \|\mathbf{y} - \Phi_{\Gamma_{ws}}(\mathbf{y},t)\|\}$$

so that we can have

$$\Omega_{ws}(t) := \bigcup_{\mathbf{x}\in\Omega_s(0)\setminus\partial\Omega_s(0)} \bigcup_{\mathbf{y}\in V_{\mathbf{x}}} O_{\mathbf{x},\mathbf{y},\Gamma_{ws}}(t)$$

Now, for $t \in I$, we can update Ω_l and Ω_w as follows

$$\begin{aligned}\Omega_l(t) &:= \Omega_l(0) \cup \Omega_{ls}(t)\\ \Omega_w(t) &:= \Omega_w(0) \cup \Omega_{ws}(t).\end{aligned}$$

As such, we do the same for Γ_{lw}:

$$\Gamma_{lw}(t) := \Omega_l(t) \cap \Omega_w(t).$$

3.3 Mathematical modeling

We first explore the distinct possible mechanisms for drug release and then observe drug movement in different domains. There are several forces and factors coming into play for the drug dissolution across distinct regions, not necessarily exclusive. For

instance, diffusion is active in both the lumen and the wall at different rates while the Navier-Stokes convective component from the blood velocity affects only the lumen, exactly as in Chapter 2; however, blood provides the pressure acting on the wall working as an advection agent within it. Moreover, even though the artery wall is composed of several complex layers (e.g. intima, externa) with varied structures, the minuscule reactions occurring throughout them are negligible in the context of the overall drug transport within the wall. [18]. Hence, we may focus principally on the media layer, corresponding to $\Omega_w(t)$ in our model, and on the endothelial layer, being the connective tissue between the lumen and the wall and referred to by $\Gamma_{lw}(t)$ and $\Gamma_{ws}(t)$ in our analysis. In this regard of simplifying the model, we can assume a simple artery wall behaving like a homogeneously and isotropic porous medium [59]. Throughout the later sections, we will be defining by $C_s(\mathbf{x}, t)$ the concentration of dissolved drug in the coating.

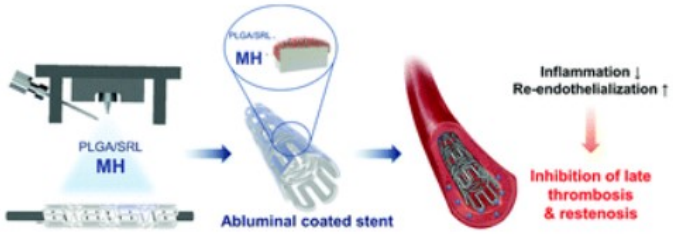

Figure 3.4: Picture overview of DES coated with poly(lactic-co-glycolic acid)(PLGA), sirolimus(SRL), and magnesium hydroxide ($Mg(OH)_2$.[33]

3.3.1 Drug Release

Clinical Considerations

Under certain applicable physical considerations, the distribution of drug to the lumen and the wall can be explained through the Higuchi model [28]. The first requirement is for the medicament to be composed of particles whose diameter is smaller than the apertures in the thickness of the absorbing layer. This is consistent with the comparitive measurements of artery wall and stent coating drugs [48]. In the case of the lumen, most of the drug is carried away by the convective abrasion of the blood movement, so that the absorption is rather instantaneous. Plus, the persistent

scramble of blood platelets results in varying momentaneous and sufficiently larger spacings, in coherence with the necessary condition [5]. The second stipulation concerns that homogeneous mixtures, resulting for example in a thick ointment, do not be formed when in contact with the drug. The wall tissue is efficiently receptive of drug material without creating new substances at the interface, but the coating is prone to platelet adhesion when interacting with blood, provoking stent thrombosis. While this constitutes roughly 2% of cases since most benefit from anti-platelet therapy, the mortality of this percentage of patients is significant [22]. However, given its minor fraction in patients with DES, stent thrombosis will not be encompassed here and should be treated as a separate case. Thus, if we disregard platelet adhesion, the second condition is fulfilled for the stent and lumen interface.

Geometrical Configurations

To properly implement the Higuchi model, we rely on a differential geometry approach, similar to the one developed in [59]. To this end, we let $\mathbf{x}_t$ be a family of mappings, such that for each $t \in [0, T]$ we associate a point (ξ_1, ξ_2) in a region $\omega \subset \mathbb{R}^2$ to a point $\mathbf{x}_t(\xi_1, \xi_2)$ in the current interface $\partial\Omega_s(t) \subset \mathbb{R}^3$:

$$\mathbf{x}_t : \omega \to \partial\Omega_s(t), \quad \mathbf{x}_t = \mathbf{x}_t(\xi_1, \xi_2) \quad \forall (\xi_1, \xi_2) \in \omega.$$

This naturally results in a system of curvilinear coordinates, with covariant vectors

$$\mathbf{a}_1 = \frac{\partial \mathbf{x}_t}{\partial \xi_1}, \quad \mathbf{a}_2 = \frac{\partial \mathbf{x}_t}{\partial \xi_2}, \quad \mathbf{a}_3 = \frac{\mathbf{a}_1 \times \mathbf{a}_2}{|\mathbf{a}_1 \times \mathbf{a}_2|}.$$

The vectors $\mathbf{a}_1$ and $\mathbf{a}_2$ span a tangent plane to $\partial\Omega_s(t)$ at $\mathbf{x}_t(\xi_1, \xi_2)$, with $\mathbf{a}_3$ being its unit normal vector to the plane. For any $\mathbf{x}_t \in \partial\Omega_s(t)$, we define the tangent surface through the span of $\mathbf{a}_1$ and $\mathbf{a}_2$:

$$d\sigma = (x - dx^1\mathbf{a}_1 - dx^2\mathbf{a}_2, x + dx^1\mathbf{a}_1 + dx^2\mathbf{a}_2).$$

To establish a measure of volume, we consider the aforementioned mapping $\Phi(\mathbf{y}, t)$ that we used to describe the evolution of the coating over time. Since we are separately referring to the entire boundary $\partial\Omega_s(t)$ by $\mathbf{x}_t$ and $\Phi(\mathbf{y}, t)$, there is a point $\mathbf{y} \in \partial\Omega_s(0)$ such that $\Phi(\mathbf{y}, t) = \mathbf{x}_t(\xi_1, \xi_2)$. We may consider the current drug thickness to be the length between the boundary of the stent and the metallic core, denoted by Ω_m.

Hence, we let $l(\mathbf{y}, t)$ be the function

$$l(\mathbf{y}, t) = \delta_0 - \|\mathbf{y} - \Phi(\mathbf{y}, t)\|,$$

remembering that δ_0 is the initial thickness of the coating and $\|\mathbf{y} - \Phi(\mathbf{y}, t)\|$ is the length of the drug already vanished by time t. We are now in a position to define the volume $dV = d\sigma \times l(y, t)$. Finally, we attach to dV the drug concentration function $C_s(t, z; \mathbf{x})$, with $z \in (0, l)$ being the axial variable in the direction of the normal $\mathbf{a}_3$. and $\mathbf{x}$ ranging over dV.

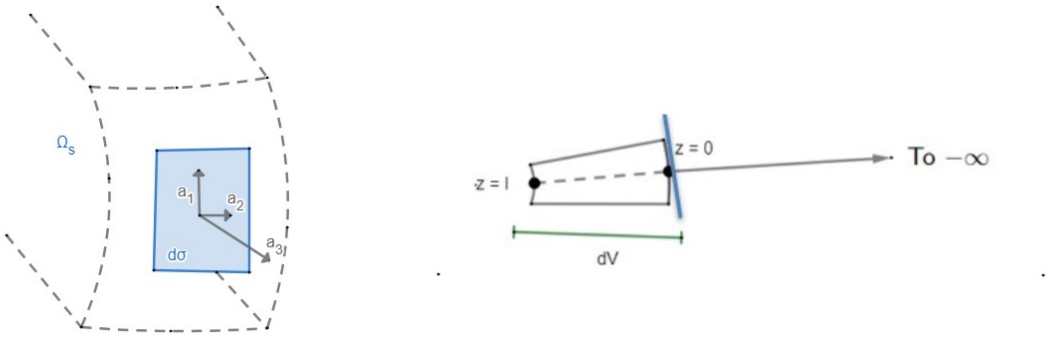

Figure 3.5: Diagram representing an infinitesimal tangent plane on the boundary of Ω_s, acting as a planar slab for external media.

Higuchi Formula

Having laid out proper preliminaries and geometrical considerations, we expound the principles of the Higuchi model to obtain an explicit formula for the drug release. For infinitesimal quantities, we may treat the surface $d\sigma$ on the external media as a semi-indefinite and planar slab, behaving like a perfect sink for the drug diffused through. In this regard, the drug dispersion problem is analogous to the heat conduction problem, enabling us to make use of corresponding partial differential equations. We keep in mind that the equation parameters of the drug tangent surface facing the wall differ from those of the plane in contact with the lumen, so we consider separate systems of PDEs for each instance. We will use the point $\mathbf{x}_t(\xi_1, \xi_2)$ as the reference origin point for $z = 0$, so that positive axial values describe the drug coating (i.e. $z = l$ would indicate the boundary of the metallic base) and negative ones are associated to the external media. Let C_0 be the initial charge concentration in the coating.

For the lumen and stent we have

$$\begin{cases} \frac{\partial C_s}{\partial t} = D_{sl}\Delta C_s \quad z \in (-\infty, 0), \quad t \in [0,T] \\ \nabla C_s \cdot \mathbf{n}_{sl} = 0 \quad \mathbf{x} \in \partial dV, \quad t \in [0,T] \\ C_s = C_0 \quad z \in (0,l), \quad t \in [0,T] \\ C_s = 0 \quad z = l, \quad t \in [0,T], \end{cases}$$

where D_{sl} denotes the conduction factor and $\mathbf{n}_{sl}$ the normal to the boundary of dV. Similarly, for the interface between the wall and the stent, we get

$$\begin{cases} \frac{\partial C_s}{\partial t} = D_{ws}\Delta C_s \quad z \in (-\infty, 0), \quad t \in [0,T] \\ \nabla C_s \cdot \mathbf{n}_{ws} = 0 \quad \mathbf{x} \in \partial dV, \quad t \in [0,T] \\ C_s = C_0 \quad z \in (0,l), \quad t \in [0,T] \\ C_s = 0 \quad z = l, \quad t \in [0,T], \end{cases}$$

with D_{ws} being the proper diffusive coefficient and $\mathbf{n}_{ws}$ the normal to the boundary of dV. Solving explicitly with standard techniques and relying on the heat equation fundamental solution, respectively, we obtain the solutions

$$C_s(t,z;\mathbf{x}_t) = C_0\left(1 - \text{erf}\left(\frac{z}{\sqrt{4D_{sl}t}}\right)\right), \quad z \in (-\infty,0), \quad t \in (0,T], \quad \mathbf{x}_t \in \Gamma_{sl}(t)$$
$$C_s(t,z;\mathbf{x}_t) = C_0\left(1 - \text{erf}\left(\frac{z}{\sqrt{4D_{ws}t}}\right)\right), \quad z \in (-\infty,0), \quad t \in (0,T], \quad \mathbf{x}_t \in \Gamma_{ws}(t),$$

where

$$\text{erf})(z) := \frac{2}{\sqrt{\pi}}\int_0^z e^{-t^2}dt.$$

From Fick's law of diffusion, we can calculate the flux J_{sl} of the drug at the surface of lumen and stent at time t by obtaining the gradient in the axial direction of C_s:

$$J_{sl}(\mathbf{x}_t,t) = -D_{sl}\frac{\partial C_s}{\partial z}\bigg|_{z=0} = \sqrt{\frac{D_{sl}C_0^2}{\pi t}}, \quad t \in (0,T], \quad \mathbf{x}_t \in \Gamma_{sl}(t).$$

Likewise, on the boundary of wall and stent we obtain the flux J_{ws} of the drug

$$J_{ws}(\mathbf{x}_t, t) = -D_{ws}\frac{\partial C_s}{\partial z}\bigg|_{z=0} = \sqrt{\frac{D_{ws}C_0^2}{\pi t}}, \quad t \in (0, T], \quad \mathbf{x}_t \in \Gamma_{ws}(t).$$

We note that the fluxes are independent of $\mathbf{x}_t$, hence being only variables of t. These are the drug release equations we can tangentially use in our study of drug dynamics in different domains.

3.3.2 Drug Dynamics

We are now ready to discuss the movement of drug across $\Omega_w(t)$, $\Omega_l(t)$, and $\Omega_s(t)$ and develop a system of differential equations in light of the principles of the domain decomposition methodology described in Chapter 2. All of these display diffusion activity, but the wall and lumen regions are additionally subject to more constraints. For the wall, we consider several factors at play such as Darcy's law and the extracellular matrix, and in the lumen, the primary force is driven by the convection of blood velocity. Keeping the notation from earlier chapters, we denote the drug concentrations of the wall and the lumen by $C_w(\mathbf{x}, t)$ and $C_l(\mathbf{x}, t)$, respectively.

3.3.3 Drug Dynamics in the Artery Wall

We take into consideration the following phenomena to construct equations for the drug dynamics in the wall.

- Darcy's law: Regional convection in the form of plasma filtration pressure due to Darcy's law. We write this term by $\mathbf{u}_p(\mathbf{x}, t)$, which is related to the pressure p obtained from Navier-Stokes at the interface Γ_{lw}.

- Extracellular matrix: The artery wall is composed of complex tissue resulting in drug being stored, without active transportation, in portions of it. We refer to the density of these free binding sites as $b(\mathbf{x}, t)$, with b_0 the initial density before containing drug. The amount of space where drug can be stored is always non-negative, so $b \geq 0$.

- Endothelial layer absorption: We let P_{lw} be the permeability factor between the wall and the lumen.

Darcy's Law

Darcy's law in filtration is analogous to Fick's law for diffusion. It accounts for the plasma filtration through the artery wall:

$$\mathbf{u}_p = -\frac{k_b}{\mu_b}\nabla p_w, \quad \nabla \cdot \mathbf{u}_p = 0 \quad \text{in} \quad \Omega_w(t),$$

where k_b is the hydraulic permeability and μ_b is the viscosity of the blood plasma. We let the pressure in the wall be given by p_w and realize that it decreases as the plasma reaches the outer channels of the artery. On the other hand, plasma does not infiltrate the stent coating, and its behavior across different ends of the wall, outside of the stent region, is periodic and symmetrical; so that the $\nabla \mathbf{u}_p \cdot \mathbf{n} = 0$ boundary condition applies. We also assume that filtration is initially blocked from $\Gamma_w s$ since the strut is absorbing all of the pressure. Thus, the equations governing the filtration velocity are

$$\begin{cases} \mathbf{u}_p + \frac{k_b}{\mu_b}\nabla p_w = 0 \quad \text{in} \quad \Omega_w(t) \\ \nabla \cdot \mathbf{u}_p = 0 \quad \text{in} \quad \Omega_w(t) \\ p_w = 0 \quad \text{on} \quad \Gamma_{ws} \cup \partial\Omega_{w,\text{outer}}(t) \\ p_w = p \quad \text{on} \quad \Gamma_{lw}(t) \\ \nabla p_w \cdot \mathbf{n}_{ws} = 0 \quad \text{on} \quad \Gamma_{ws}(t) \\ \nabla p_w \cdot \mathbf{n}_{lw} = 0 \quad \text{on} \quad \partial\Omega_{w,\text{outflow}}(t) \cup \partial\Omega_{w,\text{inflow}}(t). \end{cases}$$

Extracellular Matrix (ECM)

Artery walls have intricately complex structures and layers. In particular, the extracellular matrix (ECM) is a stronghold of proteins and molecules providing support and mechanical profile to the tissue.[60] To fully account for the detailed components of the ECM, a laborious geometrical construction would be required. However, for practical purposes, incorporating every minute fragment is deemed unnecessary for the most part because their impact on drug logistics on our model is extremely minuscule given their relative scale. Hence, we implement a simplified model by assessing just free-binding sites, the most relevant aspects of ECM in terms of drug movement, in our analysis. [42]

These free-binding sites prevent a uniform permeability all throughout since some

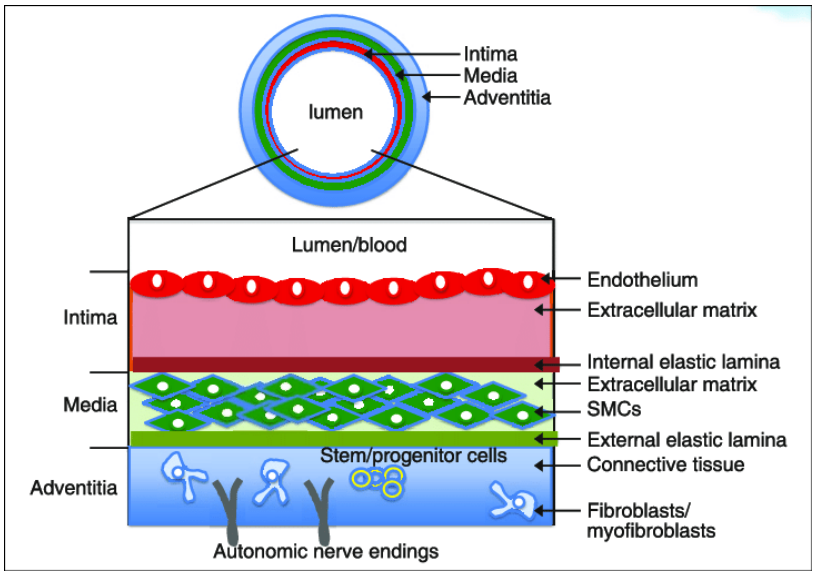

Figure 3.6: Extracellular matrix and artery wall composition diagram [36].

of the dissolved drug will be attached to certain sites of the layer. They can be seen as storage deposits where drug will attach itself, with its movement being thwarted across the wall. We denote $b(\mathbf{x}, t) \in L^2(0, T, \Omega_w)$ be the density of free-binding sites in the tissue and $C_b(\mathbf{x}, t)$ the concentration of drug present in the ECM. At time $t = 0$, we assume that no drug is attached to the free-binding sites, so that we denote the initial density by $b(\mathbf{x}, 0) = b_0(\mathbf{x})$. Of course, as drug starts to fill in these cavities, the initial space will be reduced, so that we have

$$C_b(\mathbf{x}, t) = b_0(\mathbf{x}) - b(\mathbf{x}, t) \quad \text{for some } \mathbf{x} \in \Omega_w, \quad t \geq 0, .$$

We assume that while the drug is attached to the ECM, it cannot be transported by plasma, so it is not subject to convective forces. On the other hand, we keep letting $C_w(\mathbf{x}, t)$ be the concentration value of the drug in the wall whenever drug enters or leaves the free-binding sites. The reaction motions for the dissolution or combination of the drug in the free-binding sites can be summarized by

$$C_w + b \xrightarrow{k_1} C_b, \quad C_b \xrightarrow{k_2} C_w + b$$

where k_1 and k_2 are the association and dissociation constants, respectively. As such, by conservation, in the context of the dynamics of the drug in the artery wall, we

have the behavior Thus, we model the reaction as follows

$$k_1 C_w b + k_2(b - b_0) \quad \text{in} \quad \Omega_w(t).$$

Lastly, we make the observation that $0 \leq b(t) \leq b_0$ for all $t \geq 0$ since the volume in the free-binding sites is a nonnegative limited entity.

Endothelial Layer

The considerations regarding the endothelial layer shall be the same as in Chapter 2, since this is the interface between the wall and the lumen. The transmission of the drug is similar to the solutes, only with different parameters given their difference in thickness and diffusion. The only difference in the treatment of the mechanics from that of solutes is that drug is not mostly crossing the endothelial layer when sufficiently far away from stented regions, as it is mostly driven away by the convective field of the blood to other locations in the body. We let the permebeality constant be given by P_{lw} for the transfer taking place in $\Gamma_{lw}(t)$. We assume suitable continuity of concentration as well as in the flux, according to Fick's law. Therefore, the boundary condition in this surface is

$$-D_w \nabla C_w \cdot \mathbf{n_w} - P_{lw}(C_w - C_l) = 0 \quad \text{on } \Gamma_{lw}(t).$$

3.3.4 Drug Dynamics in the Stent

While we have established the drug release at the boundary of the stent, we also need to account for the drug behavior inside the stent. The structure of the stent is rather simpler than the wall, being prone to diffusivity only. In the core Ω_m, there is no drug concentration, so we set it to zero. The following are the equations governing the drug dynamics in the stent

$$\begin{cases} \frac{\partial C_s}{\partial t} - D_s \Delta C_s = 0 \quad \mathbf{x} \in \Omega_c(t), \quad t \in [0,T] \\ C_s = 0 \quad \mathbf{x} \in \Omega_m, \quad t \in [0,T] \\ \nabla C_s \cdot \mathbf{n}_{sl} - J_{sl} = 0 \quad \mathbf{x} \in \Gamma_{sl}(t), \quad t \in [0,T] \\ \nabla C_s \cdot \mathbf{n}_{ws} - J_{ws} = 0 \quad \mathbf{x} \in \Gamma_{ws}(t), \quad t \in [0,T]. \end{cases}$$

3.3.5 Drug Dynamics in the Lumen

Finally, we consider that some drug is carried away to the lumen but its permanence in the channel is short-lived. The more pressing and interesting aspect is the rate by which the stent's drug coating is affected by the continuous friction with blood velocity. In general, the drug dynamics are given by the convective and diffusive elements in the lumen; the boundary conditions have already been established by the other domains.

3.3.6 General Drug Dynamics

We now put everything together with the purpose of solving for C_l, C_w, and C_s just like it was done previous through domain decomposition. For $t \in [0, T]$, the drug dynamics across all domains and boundaries are given by

$$
\begin{cases}
\frac{\partial C_l}{\partial t} + \nabla \cdot (-\mu_l \nabla C_l + \mathbf{u} C_l) = 0 \quad \text{in} \quad \Omega_l(t) \\
\frac{\partial C_w}{\partial t} + \mathbf{u}_p \cdot \nabla C_w - \mu_w \Delta C_w + k_1 C_w b + k_2(b - b_0) = 0 \quad \text{in} \quad \Omega_w(t) \\
\frac{\partial b}{\partial t} + k_1 C_w b + k_2(b - b_0) = 0 \quad \text{in} \quad \Omega_w(t) \\
\frac{\partial C_s}{\partial t} - \mu_s \Delta C_s = 0 \quad \text{in} \quad \Omega_c(t) \\
C_s = 0 \quad \text{in} \quad \Omega_m \\
-\mu_w \nabla C_w \cdot \mathbf{n}_{lw} - P_{lw}(C_w - C_l) = 0 \quad \text{on} \quad \Gamma_{lw}(t) \\
\mu_w \nabla C_w \cdot \mathbf{n}_{ws} + J_{ws} = 0 \quad \text{on} \quad \Gamma_{ws}(t) \\
\mu_l \nabla C_l \cdot \mathbf{n}_{sl} + J_{sl} = 0 \quad \text{on} \quad \Gamma_{sl}(t) \\
\mu_s \nabla C_l \cdot \mathbf{n}_{lw} + \mu_w \nabla C_w \cdot \mathbf{n}_{lw} = 0 \quad \text{on} \quad \Gamma_{lw}(t) \\
\mu_s \nabla C_s \cdot \mathbf{n}_{ws} + \mu_w \nabla C_w \cdot \mathbf{n}_{ws} = 0 \quad \text{on} \quad \Gamma_{ws}(t) \\
\mu_s \nabla C_s \cdot \mathbf{n}_{sl} + \mu_l \nabla C_l \cdot \mathbf{n}_{sl} = 0 \quad \text{on} \quad \Gamma_{sl}(t) \\
\nabla C_w \cdot \mathbf{n}_w = 0 \quad \text{on} \quad \partial\Omega_w(t) \backslash (\Gamma_{lw}(t) \cup \Gamma_{ws}(t)) \\
\nabla C_s \cdot \mathbf{n}_s = 0 \quad \text{on} \quad \partial\Omega_c(t) \backslash (\Gamma_{ws}(t) \cup \Gamma_{sl}(t)) \\
\nabla C_l \cdot \mathbf{n}_l = 0 \quad \text{on} \quad \partial\Omega_{l,outflow}(t) \\
C_l = 0 \quad \text{on} \quad \partial\Omega_{l,inflow}(t) \\
C_w = 0 \quad \text{on} \quad \partial\Omega_{w,inflow}(t),
\end{cases}
\tag{3.1}
$$

with initial conditions

$$C_l(\mathbf{x},\mathbf{0}) = 0, \quad \mathbf{x} \in \Omega_l, \quad C_w(\mathbf{x},\mathbf{0}) = 0, \quad \mathbf{x} \in \Omega_w, \quad C_s(\mathbf{x},\mathbf{0}) = C_0, \quad \mathbf{x} \in \Omega_s,$$

where $b \in L^2(0,T)$ and $b_0 \in L^2(0,T)$ are nonnegative functions and $\mu_l,\ \mu_w,\ \mu_s,\ k_1,$ and k_2 are nonnegative constants.

3.3.7 Weak Formulation of the Problem

With our assumptions, we rely on some results and theory derived by Vergara and Zunino in [59]. The functions $\mathbf{u}$, $\mathbf{u_p}$, and b are all self-contained within their respective domains, so they can be assumed to have been solved before C_l, C_w, and C_s. While C_w and b are coupled, we can first solve for b and then use this value to linearize equation 3.1(b). For each $t \in [0,T]$, we consider the family of Sobolev spaces $H^1(t)(\Omega_l(t))$, $H^1(\Omega_w(t))$, and $H^1(\Omega_s(t))$, where a different Sobolev space corresponds to each domain change in time. With that in mind, for functions $v_l \in L^2(0,T;H^1(\Omega_l(t)))$, $v_w \in L^2(0,T;H^1(\Omega_w(t)))$, and $v_s \in L^2(0,T;H^1(\Omega_s(t)))$ we define the following bilinear forms

$$\begin{aligned}
a_l(C_l, v_l) &:= \mu_l \int_{\Omega_l(t)} \nabla C_l \nabla v_l d\omega + \int_{\Omega_l(t)} (\mathbf{u}\cdot\nabla) C_l v_l d\omega \\
a_w(C_w, v_w) &:= \mu_w \int_{\Omega_w(t)} \nabla C_w \nabla v_w d\omega + \int_{\Omega_w(t)} \mathbf{u_p}\cdot\nabla C_w v_w d\omega + k_1 \int_{\Omega_w(t)} b C_w v_w d\omega \\
a_w(C_s, v_s) &:= \mu_s \int_{\Omega_s(t)} \nabla C_s \nabla v_s d\omega.
\end{aligned}$$

Similarly to chapter two, a_l, a_w, and a_s are all continuous and coercive assuming that μ_l, μ_w, and μ_s are all bounded, so we prove it in the next lemma.

Lemma 5. The bilinear forms a_l, a_w, and a_s are well-defined, continuous, and coercive with coercivity constants α_l, α_w, and α_s, respectively.

Proof. Since a_l and a_s have the same structure as in Lemma 1 with coercivity constants α_l and α_w, respectively, we just need to prove the continuity and coercivity of

a_w. Let $u_w, v_w \in H^1_{\Gamma_{lw}(t)\cup\Gamma_{ws}(t)}(\Omega_w(t))$, so that

(3.2)
$$|a_w(u_l, v_l)| = \left|\mu_w \int_{\Omega_w(t)} \nabla u_w \nabla v_w d\omega + \int_{\Omega_w(t)} \mathbf{u}_p \cdot \nabla u_w v_w d\omega + k_1 \int_{\Omega_w(t)} b u_w v_w d\omega\right|$$

(3.3)
$$\leq |\mu_w| \int_{\Omega_w(t)} |\nabla u_w \nabla v_w| d\omega + \int_{\Omega_w(t)} |\mathbf{u}_p \cdot \nabla u_w v_w| d\omega + k_1 \int_{\Omega_w(t)} |b u_w v_w| d\omega$$

For the first term on the right side of equation (3.3), we implement Holder's inequality to get

$$\begin{aligned}\int_{\Omega_w} |\nabla u_w \nabla v_w| d\omega &\leq \|\nabla u_w\|_{L^2(\Omega_w(t))} \|\nabla v_w\|_{L^2(\Omega_w(t))} \\ &\leq \|u_w\|_{H^1_{\Gamma_{lw}(t)\cup\Gamma_{ws}(t)}(\Omega_w(t))} \|v_w\|_{H^1_{\Gamma_{lw}(t)\cup\Gamma_{ws}(t)}(\Omega_w(t))}.\end{aligned}$$

For the second term in equation (3.3), we derive an identity that will also be useful for the coercivity portion:

$$\begin{aligned}\int_{\Omega_w(t)} \mathbf{u}_p \cdot \nabla v_w v_w d\omega &= \sum_i \int_{\Omega_w(t)} \mathbf{u}_{p,i} \frac{\partial v_w}{\partial x_i} v_w d\omega \\ &= \sum_i \left(- \int_{\Omega_w(t)} v_w \frac{\partial}{\partial x_i} (\mathbf{u}_{p,i} v_w) d\omega + \int_{\partial\Omega_w(t)} (\mathbf{u}_{p,i} \mathbf{n}_i) v_w^2 d\omega \right)\end{aligned}$$

Since v_w is a test function vanishing in every boundary except Γ_{ws} and Γ_{lw} and $\mathbf{u}_p = 0$ at Γ_{ws}, we have

$$\begin{aligned}\int_{\Omega_w(t)} \mathbf{u}_p \cdot \nabla v_w v_w d\omega &= \sum_i \left(- \int_{\Omega_w(t)} v_w^2 \frac{\partial \mathbf{u}_p}{\partial x_i} d\omega - \int_{\Omega_w(t)} v_w \mathbf{u}_{p,i} \frac{\partial v_w}{\partial x_i} d\omega + \int_{\Gamma_{lw}(t)} v_w^2 (\mathbf{u}_{p,i} \mathbf{n}_i) d\omega \right) \\ &= - \int_{\Omega_w(t)} (\nabla \cdot \mathbf{u_p}) v_w^2 d\omega - \int_{\Omega_w(t)} \mathbf{u}_p \cdot \nabla v_w v_w d\omega + \sum_i \int_{\Gamma_{lw}} v_w^2 (\mathbf{u}_{p,i} \mathbf{n}_i) d\omega\end{aligned}$$

We note that $\mathbf{u}_p$ is divergence-free and the second term is the same as the one on the left side; thus, we obtain

(3.4)
$$\int_{\Omega_w(t)} \mathbf{u}_p \cdot \nabla v_w v_w d\omega = \frac{1}{2} \int_{\Gamma_{lw}} v_w^2 (\mathbf{u}_p \cdot \mathbf{n}) d\omega$$

We want to show that equation (3.4) is bounded:

$$\begin{aligned}
\left|\int_{\Omega_w(t)} \mathbf{u}_p \cdot \nabla v_w v_w d\omega\right| &= \frac{1}{2}\left|\sum_i \int_{\Gamma_{lw}(t)} v_w^2(\mathbf{u}_{p,i}\mathbf{n}_i)d\omega\right| \\
&\leq \frac{1}{2}\sum_i \left(\left(\int_{\Gamma_{lw}(t)} (\mathbf{u}_{p,i}\mathbf{n}_i)^2 d\omega\right)^{1/2}\left(\int_{\Gamma_{lw}(t)} (v_w^2)^2 d\omega\right)^{1/2}\right) \\
&\qquad\qquad \text{[By Hölder's inequality]} \\
&= \frac{1}{2}\sum_i \left(\|\mathbf{u}_{p,i}\mathbf{n}_i\|_{L^2(\Gamma_{lw})}\|v_w\|^2_{L^4(\Gamma_{lw})}\right) \\
&\leq \frac{3}{2}\left(\|\mathbf{u}_p\|_{L^2(\Gamma_{lw})}\|v_w\|^2_{H^1(\Gamma_{lw}(t))}\right) \\
&\qquad\qquad \text{[By Sobolev Embedding Theorem]} \\
&\leq \frac{3}{2}\left(C_p\|\mathbf{u}_p\|_{L^2(\Gamma_{lw})}\|v_w\|^2_{H^1_{\Gamma_{lw}(t)\cup\Gamma_{ws}(t)}(\Omega_w(t))}\right) \\
&\qquad\qquad \text{[By Trace Theorem with constant } C_p > 0\text{]} \\
&\leq \left(\frac{3}{2}C_p\|\mathbf{u}_p\|_{L^2(\Gamma_{lw})}\right)\|u_w\|^2_{H^1_{\Gamma_{lw}(t)\cup\Gamma_{ws}(t)}(\Omega_w(t))}\|v_w\|^2_{H^1_{\Gamma_{lw}(t)\cup\Gamma_{ws}(t)}(\Omega_w(t))},
\end{aligned}$$

where we multiplied by $\|u_w\|^2_{H^1_{\Gamma_{lw}(t)\cup\Gamma_{ws}(t)}(\Omega_w(t))}$ on the last line and treated $\|\mathbf{u}_p\|_{L^2(\Gamma_{lw})}$ as a bounded constant. We now prove the boundedness of the last term in equation (3.3) by using Hölder's inequality twice and then Sobolev embedding theorem:

$$\begin{aligned}
\left|k_1\int_{\Omega_w(t)} b u_w v_w d\omega\right| &\leq |k_1|\|b\|_{L^2(\Omega_w(t)}\|u_w v_w\|_{L^2(\Omega_w(t))} \\
&\leq |k_1|\|b\|_{L^2(\Omega_w(t))}\|u_w\|_{L^4(\Omega_w(t))}\|v_w\|_{L^4(\Omega_w(t))} \\
&\leq |k_1|\|b\|_{L^2(\Omega_w(t))}\|u_w\|^2_{H^1_{\Gamma_{lw}(t)\cup\Gamma_{ws}(t)}(\Omega_w(t))}\|v_w\|^2_{H^1_{\Gamma_{lw}(t)\cup\Gamma_{ws}(t)}(\Omega_w(t))}
\end{aligned}$$

Putting everything together, we get

$$|a_w(u_l, v_l)| \leq \left(1 + \frac{3}{2}C_p\|\mathbf{u}_p\|_{L^2(\Gamma_{lw})} + |k_1|\|b\|_{L^2(\Omega_w(t))}\right)\|u_w\|^2_{H^1_{\Gamma_{lw}(t)\cup\Gamma_{ws}(t)}(\Omega_w(t))}\|v_w\|^2_{H^1_{\Gamma_{lw}(t)\cup\Gamma_{ws}(t)}(\Omega_w(t))},$$

establishing that a_w is continuous.

We now move on to showing coercivity:

$$\begin{aligned} a_w(v_w, v_w) &= \mu_w \int_{\Omega_w(t)} \nabla v_w \nabla v_w d\omega + \int_{\Omega_w(t)} \mathbf{u}_p \cdot \nabla v_w v_w d\omega + k_1 \int_{\Omega_w(t)} b v_w v_w d\omega \\ &= \mu_w \|\nabla v_w\|^2_{L^2(\Omega_w(t))} + \frac{1}{2} \int_{\Gamma_{lw}(t)} v_w^2 (\mathbf{u}_p \cdot \mathbf{n}) d\omega + k_1 \int_{\Omega(t)} b v_w^2 d\omega, \end{aligned}$$

where we employed the identity from equation (3.4) for the second term on the right-hand side. We use Poincare's inequality with constant $C_p > 0$

$$C_p \|\nabla v_w\|_{L^2(\Omega_w(t)} \geq \|v_w\|_{L^2(\Omega_w(t))}$$

to have

$$a_w(v_w, v_w) \geq \frac{\mu_w}{C_p} \|v_w\|^2_{L^2(\Omega_w(t))} + \frac{1}{2} \int_{\Gamma_{lw}(t)} v_w^2 (\mathbf{u}_p \cdot \mathbf{n}) d\omega + k_1 \int_{\Omega(t)} b v_w^2 d\omega.$$

We make the observation that $\mathbf{u}_p \cdot \mathbf{n}$ is non-negative on Γ_{lw} since pressure is decreasing and $\mathbf{n}$ is in the contrary direction to the filtration velocity and also that b and k_1 are always non-negative always. Thus, we derive

$$\begin{aligned} \left(1 + \frac{1}{C_p}\right) a_w(v_w, v_w) &\geq \frac{\mu_w}{C_p} (\|v_w\|^2_{L^2(\Omega_w(t)} + \|\nabla v_w\|^2_{L^2(\Omega_w(t)}) \\ &\quad + \left(\frac{1}{2} + \frac{1}{2C_p}\right) \int_{\Gamma_{lw}(t)} v_w^2 (\mathbf{u}_p \cdot \mathbf{n}) d\omega + \left(k_1 + \frac{k_1}{2C_p}\right) \int_{\Omega(t)} b v_w^2 d\omega \\ &\geq \frac{\mu_w}{C_p} \|v_w\|_{H^1_{\Gamma_{lw}(t) \cup \Gamma_{ws}(t)}(\Omega_w(t))} \end{aligned}$$

so that

$$a_w(v_w, v_w) \geq \frac{\mu_w}{1 + C_p} \|v_w\|_{H^1_{\Gamma_{lw}(t) \cup \Gamma_{ws}(t)}(\Omega_w(t))},$$

proving that a_w is coercive with coercivity constant $\alpha_w = \mu_w/(1 + C_p)$. □

For the lumen, for any test function $\phi_l \in H^1(\Omega_l(t))$, we derive the weak formula-

tion:

$$\int_{\Omega_l(t)} \frac{\partial C_l}{\partial t}\phi_l d\omega + \int_{\Omega_l(t)} (\mathbf{u}\cdot\nabla) C_l\phi_l d\omega$$
$$+ \mu_l \int_{\Omega_l(t)} \nabla C_l \nabla\phi_l d\omega - \mu_l \int_{\partial\Omega_l(t)} (\nabla C_l\cdot \mathbf{n}_l)\phi_l d\gamma = \int_{\Omega_l(t)} f_l\phi_l d\omega$$
$$\int_{\Omega_l(t)} \frac{\partial C_l}{\partial t}\phi_l d\omega + \int_{\Omega_l(t)} (\mathbf{u}\cdot\nabla) C_l\phi_l d\omega + \mu_l \int_{\Omega_l(t)} \nabla C_l \nabla\phi_l d\omega$$
$$- \mu_l \int_{\Gamma_{lw}(t)} (\nabla C_l\cdot \mathbf{n}_{lw})\phi_l d\gamma - \mu_l \int_{\Gamma_{sl}(t)} (\nabla C_l\cdot \mathbf{n}_{sl})\phi_l d\gamma = \int_{\Omega_l(t)} f_l\phi_l d\omega$$
$$\int_{\Omega_l(t)} \frac{\partial C_l}{\partial t}\phi_l d\omega + \int_{\Omega_l(t)} (\mathbf{u}\cdot\nabla) C_l\phi_l d\omega + \mu_l \int_{\Omega_l(t)} \nabla C_l \nabla\phi_l d\omega$$
$$- \mu_l \int_{\Gamma_{lw}(t)} P_{lw}(C_l - C_w)\phi_l d\gamma = \int_{\Omega_l(t)} f_l\phi_l d\omega + \mu_l \int_{\Gamma_{sl}(t)} J_{sl}\phi_l d\gamma,$$

where we used the boundary conditions in the last equation for the normal derivatives. Similarly, for the wall, the weak formulation for any $\phi_w \in H^1_{\Gamma_{lw}(t)\cup\Gamma_{ws}(t)}(\Omega_w(t))$ is

$$\int_{\Omega_w(t)} \frac{\partial C_w}{\partial t}\phi_w d\omega + \int_{\Omega_w(t)} (\mathbf{u}_p\cdot\nabla) C_w\phi_w d\omega + \mu_w \int_{\Omega_w(t)} \nabla C_w \nabla\phi_w d\omega + k_1 \int_{\Omega_w(t)} C_w b\phi_w d\omega$$
$$- \mu_w \int_{\partial\Omega_w(t)} (\nabla C_w\cdot \mathbf{n}_w)\phi_w d\gamma + k_2 \int_{\Omega_w(t)} (b - b_0)\phi_w d\omega = \int_{\Omega_w(t)} f_w\phi_w d\omega$$
$$\int_{\Omega_w(t)} \frac{\partial C_w}{\partial t}\phi_w d\omega + \int_{\Omega_w(t)} (\mathbf{u}_p\cdot\nabla) C_w\phi_w d\omega + \mu_w \int_{\Omega_w(t)} \nabla C_w \nabla\phi_w d\omega + k_1 \int_{\Omega_w(t)} C_w b\phi_w d\omega$$
$$- \mu_w \int_{\Gamma_{lw}} (\nabla C_w\cdot \mathbf{n}_{lw})\phi_w d\gamma - \mu_w \int_{\Gamma_{ws}} (\nabla C_w\cdot \mathbf{n}_{ws})\phi_w d\gamma + k_2 \int_{\Omega_w(t)} (b - b_0)\phi_w d\omega = \int_{\Omega_w(t)} f_w\phi_w d\omega$$

.

Implementing boundary and interface conditions, we get

$$\int_{\Omega_w(t)} \frac{\partial C_w}{\partial t}\phi_w d\omega + \int_{\Omega_w(t)} (\mathbf{u}_p\cdot\nabla) C_w\phi_w d\omega + \mu_w \int_{\Omega_w(t)} \nabla C_w \nabla\phi_w d\omega + k_1 \int_{\Omega_w(t)} C_w b\phi_w d\omega$$
$$= \int_{\Omega_w(t)} f_w\phi_w d\omega + \mu_w \int_{\Gamma_{lw}} P_{lw}(C_w - C_l)\phi_w d\gamma - \mu_w \int_{\Gamma_{ws}} J_{ws}\phi_w d\gamma + k_2 \int_{\Omega_w(t)} (b - b_0)\phi_w d\omega$$

Finally, for the stent, the weak formulation for $\phi_s \in H^1_{\Gamma_{ws}(t)\cup\Gamma_{sl}(t)}(\Omega_s(t))$ is

$$\int_{\Omega_s(t)} \frac{\partial C_s}{\partial t}\phi_s d\omega + \mu_s \int_{\Omega_s(t)} \nabla C_s \nabla \phi_s d\omega - \mu_s \int_{\partial\Omega_s(t)} (\nabla C_s \cdot \mathbf{n}_s)\phi_s d\gamma = \int_{\Omega_s(t)} f_s \phi_s d\omega$$

$$\int_{\Omega_s(t)} \frac{\partial C_s}{\partial t}\phi_s d\omega + \mu_s \int_{\Omega_s(t)} \nabla C_s \nabla \phi_s d\omega$$
$$- \mu_s \int_{\Gamma_{ws}(t)} (\nabla C_s \cdot \mathbf{n}_{ws})\phi_s d\gamma - \mu_s \int_{\Gamma_{sl}(t)} (\nabla C_s \cdot \mathbf{n}_{sl})\phi_s d\gamma = \int_{\Omega_s(t)} f_s \phi_s d\omega$$

$$\int_{\Omega_s(t)} \frac{\partial C_s}{\partial t}\phi_s d\omega + \mu_s \int_{\Omega_s(t)} \nabla C_s \nabla \phi_s d\omega$$
$$= \int_{\Omega_s(t)} f_s \phi_s d\omega - \mu_s \int_{\Gamma_{ws}(t)} (J_{ws})\phi_s d\gamma - \mu_s \int_{\Gamma_{sl}(t)} (J_{sl})\phi_s d\gamma,$$

where again we relied on the boundary conditions for the products of the gradients with the normal. To adapt the system to our previous methodology, we allow $\zeta_{lw} = P_{lw}$. For ease of notation, we set $V_{D,l} = H^1_{\Gamma_{lw}(t)\cup\Gamma_{sl}(t)}(\Omega_l(t))$, $V_{D,w} = H^1_{\Gamma_{lw}(t)\cup\Gamma_{ws}(t)}(\Omega_w(t))$, and $V_{D,s} = H^1_{\Gamma_{sl}(t)\cup\Gamma_{ws}(t)}(\Omega_s(t))$. We can now redefine the problem in terms of weak derivatives:

Problem 5. *Given the initial conditions*

$$C_l(t=0,\mathbf{x}) = 0, \quad C_w(t=0,\mathbf{x}, \quad C_s(t=0,\mathbf{x}) = C_0$$

and positive function $\zeta_{lw} \in L^\infty$, find $C_l \in L^2(0,T,V_{D,l})$, $C_w \in L^2(0,T,V_{D,w})$, and $C_s \in L^2(0,T,V_{D,s})$ such that for all $\phi_l \in V_{D,l}$, $\phi_w \in V_{D,w}$, $\phi_s \in V_{D,s}$, the following system holds

$$\begin{cases} \left(\frac{\partial C_l}{\partial t}, \phi_l\right) + a_l(C_l,\phi_l) + (C_l - C_w, \phi_l)_{\zeta_{lw}} = (s_l,\phi_l) + (J_{sl},\phi_l)_{sl} \\ \left(\frac{\partial C_w}{\partial t}, \phi_w\right) + a_w(C_w,\phi_w) + (C_w - C_l, \phi_w)_{\zeta_{lw}} = (s_w,\phi_w) + (J_{ws},\phi_w)_{ws} \\ \left(\frac{\partial C_s}{\partial t}, \phi_s\right) + a_s(C_s,\phi_s) = (s_s,\phi_s) - (J_{ws},\phi_s)_{ws} - (J_{sl},\phi_s)_{sl}. \end{cases}$$

Theorem 3.3.1. For $\mathbf{u} \in L^\infty(0,T;L^2(\Omega_l)) \cap L^2(0,T;H^1(\Omega_l)$ with $\mathbf{u}\cdot\mathbf{n} > 0$ on $\Gamma_{l,\text{out}}$, $\mathbf{u}_p \in L^\infty(0,T;L^2(\Omega_w)) \cap L^2(0,T;H^1(\Omega_w)$ with $\mathbf{u}_p \cdot \mathbf{n} > 0$ on Γ_{lw}, and nonnegative function $b \in L^\infty(0,T;L^2(\Omega_w)) \cap L^2(0,T;H^1(\Omega_w)$, Problem 5 admits a unique solution depending continuously on the data.

Proof. We first notice that

$$(C_l - C_w, \phi_l) + (C_w - C_l, \phi_w) = (C_l - C_w, \phi_l - \phi_w).$$

We define

$$\begin{aligned}
&\mathbf{C} = [C_l, C_w, C_s]^T, \quad \mathbf{\Phi} = [\phi_l, \phi_w, \phi_s]^T, \quad \mathbf{S} = [s_l, s_w, s_s]^T, \\
&\mathbf{J}_{sl} = [J_{sl}, 0, J_{sl}], \quad \mathbf{J}_{ws} = [0, J_{ws}, J_{ws}], \quad \text{and} \\
&\mathcal{A}(\mathbf{C}, \mathbf{\Phi}) = a_l(C_l, \phi_l) + a_w(C_w, \phi_w) + a_s(C_s, \phi_s) + (C_l - C_w, \phi_l - \phi_w)_{\zeta_{lw}}.
\end{aligned}$$

Adding up all the equations in Problem 5, we get the system

$$\left(\frac{\partial \mathbf{C}}{\partial t}, \mathbf{\Phi}\right) + \mathcal{A}(\mathbf{C}, \mathbf{\Phi}) = (\mathbf{S}, \mathbf{\Phi}) + (\mathbf{J}_{sl}, \mathbf{\Phi}) + (\mathbf{J}_{ws}, \mathbf{\Phi}). \tag{3.5}$$

From Lemma 5, we know that $\mathcal{A}(\cdot, \cdot)$ is continuous and weakly coercive with $\alpha := \min(\alpha_l, \alpha_w, \alpha_s)$. Given that the right-hand side of (3.5) is a linear and continuous functional in $V_{D,l} \times V_{D,w} \times V_{D,s}$ and through the Faedo-Galerkin method, Problem 5 is well-posed. □

3.3.8 Numerical Approximation

Time semi-discretization

We start discretizing Problem 5 in time by allowing the time interval $[0, T]$ be split into N subintervals of uniform length Δt such that $t^n = n\Delta t$ for $n = 0, 1, ..., N$. We consider backward Euler discretization and set $\chi = \frac{1}{\Delta t}$ to define

$$\begin{aligned}
&\hat{a}_l(C_l, v_l) = \chi(C_l, v_l) + a_l(C_l, v_l) \quad \forall v_l \in V_{D,l} \\
&\hat{a}_w(C_w, v_w) = \chi(C_w, v_w) + a_w(C_w, v_w) \quad \forall v_w \in V_{D,w} \\
&\hat{a}_s(C_s, v_s) = \chi(C_s, v_s) + a_s(C_s, v_s) \quad \forall v_s \in V_{D,s}
\end{aligned}$$

The addition of the extra term in each bilinear form still maintains their coercivity.

Problem 6. *Given C_l^0, C_w^0, and C_s^0 for every $n = 0, 1, ...N - 1$ find*

$$C_l^{n+1} \in V_{D,l}, \quad C_w^{n+1} \in V_{D,w}, \quad C_s^{n+1} \in V_{D,s}$$

such that for all $\phi_l \in V_{D,l}$, $\phi_w \in V_{D,w}$, *and* $\phi_s \in V_{D,s}$ *solve*

$$\begin{cases} \hat{a}_l(C_l^{n+1}, \phi_l) + (C_l^{n+1}, \phi_l)_{\zeta_{lw}} - (C_w^{n+1}, \phi_l)_{\zeta_{lw}} = \chi(C_l^n, \phi_l) + (s_l^{n+1}, \phi_l) + (J_{sl}^{n+1}, \phi_l)_{sl} \\ \hat{a}_w(C_w^{n+1}, \phi_w) + (C_w^{n+1}, \phi_w)_{\zeta_{lw}} - (C_l^{n+1}, \phi_w)_{\zeta_{lw}} = \chi(C_w^n, \phi_w) + (s_w^{n+1}, \phi_w) + (J_{ws}^{n+1}, \phi_w)_{ws} \\ \hat{a}_s(C_s^{n+1}, \phi_s) = \chi(C_s^n, \phi_s) + (s_s^{n+1}, \phi_s) - (J_{ws}^{n+1}, \phi_s)_{ws} - (J_{sl}^{n+1}, \phi_s)_{sl}, \end{cases}$$

where $s_l^{n+1} = s_l(t^{n+1})$, $s_w^{n+1} = s_w(t^{n+1})$, $s_s^{n+1} = s_s(t^{n+1})$, $J_{sl}^{n+1}) = J_{sl}(t^{n+1})$, *and* $J_{ws}^{n+1} = J_{ws}(t^{n+1})$.

Space discretization

Lastly, we fulfill the entire discretization by incorporating the finite element method. We assume that domains Ω_l(t), $\Omega_w(t)$, and $\Omega_s(t)$ can be approximated geometrically through conformal meshes $\mathcal{T}_{h,l}(t)$, $\mathcal{T}_{h,w}(t)$, and $\mathcal{T}_{h,s}(t)$, respectively. To that end, we consider the finite-dimensional subspaces $V_{h,l} \subset V_{D,l}$, $V_{h,w} \subset V_{D,w}$, and $V_{h,s} \subset V_{D,s}$ of piecewise polynomial functions. We state the weak formulation of the fully discrete problem

Problem 7. *Given* $C_{h,l}^0$, $C_{h,w}^0$, *and* $C_{h,s}^0$ *for every* $n = 0, 1, ...N-1$ *find*

$$C_{h,l}^{n+1} \in V_{h,l}, \quad C_{h,w}^{n+1} \in V_{h,w}, \quad C_{h,s}^{n+1} \in V_{h,s}$$

such that for all $\phi_{h,l} \in V_{h,l}$, $\phi_{h,w} \in V_{h,w}$, *and* $\phi_{h,s} \in V_{h,s}$ *solve*

$$\begin{cases} \hat{a}_l(C_{h,l}^{n+1}, \phi_{h,l}) + (C_{h,l}^{n+1}, \phi_{h,l})_{\zeta_{lw}} - (C_{h,w}^{n+1}, \phi_{h,l})_{\zeta_{lw}} \\ \qquad\qquad = \chi(C_{h,l}^n, \phi_{h,l}) + (s_{h,l}^{n+1}, \phi_{h,l}) + (J_{h,sl}^{n+1}, \phi_{h,l})_{sl} \\ \hat{a}_w(C_{h,w}^{n+1}, \phi_{h,w}) + (C_{h,w}^{n+1}, \phi_{h,w})_{\zeta_{lw}} - (C_{h,l}^{n+1}, \phi_{h,w})_{\zeta_{lw}} \\ \qquad\qquad = \chi(C_{h,w}^n, \phi_{h,w}) + (s_{h,w}^{n+1}, \phi_{h,w}) + (J_{h,ws}^{n+1}, \phi_{h,w})_{ws} \\ \hat{a}_s(C_{h,s}^{n+1}, \phi_{h,s}) = \chi(C_s^n, \phi_{h,s}) + (s_{h,s}^{n+1}, \phi_{h,s}) - (J_{h,ws}^{n+1}, \phi_{h,s})_{ws} - (J_{h,sl}^{n+1}, \phi_{h,s})_{sl}, \end{cases}$$

where $s_{h,l}^{n+1} = s_{h,l}(t^{n+1})$, $s_{h,w}^{n+1} = s_{h,w}(t^{n+1})$, $s_{h,s}^{n+1} = s_{h,s}(t^{n+1})$, $J_{h,sl}^{n+1}) = J_{h,sl}(t^{n+1})$, *and* $J_{h,ws}^{n+1} = J_{h,ws}(t^{n+1})$.

The well-posedness can be proved similarly to Problem 5. Also, given the exact structure and limited nature of drug concentration, the arguments of convergence analysis of the iterative methods previously explored in chapter two can also be

replicated for this problem.

Domain Decomposition

In chapter two, for the problem of solutes, we wanted to solve for unknowns C_l, C_w, and C_s in interfaces Γ_{lw}, Γ_{ws}, and Γ_{sl}. In the case of drug elution, the drug in the stent coating acts as a source; therefore, we know the value of concentration C_s at the interfaces Γ_{sl} and Γ_{ws}. This means that the concentration value in the interface remains unknown in Γ_{lw}. This reduces the problem of finding $\rho_{lw} \in \Lambda_{lw}$ to the one solved in [52][53]. Let's assume that we are solving for time $t = (n+1)\Delta t$ so that we can temporarily drop the index and instead use k for the substructuring iterations. Assuming initial guesses $C_l^{(0)}$ and $C_w^{(0)}$ and given $C_s^{(0)}$, we decompose into three problems by domain:

1. **Lumen Problem (Strong):** Solve

$$\begin{aligned}
&\chi C_l^{(k+1)} - \mu_l \Delta C_l^{(k+1)} + \mathbf{u} \cdot C_l^{(k+1)} = f_l \quad \text{in} \quad \Omega_l \\
&\mu_l \frac{\partial C_l^{(k+1)}}{\partial \mathbf{n}_l} + \zeta_{lw}(C_l^{(k+1)} - C_w^{(k)}) = 0 \quad \text{on} \quad \Gamma_{lw} \\
&\mu_l \frac{\partial C_l^{(k+1)}}{\partial \mathbf{n}_l} - J_{sl} = 0 \quad \text{on} \quad \Gamma_{sl}
\end{aligned}$$

   (Weak): Find $C_l^{(k+1)} \in V_{D,l}$ such that

$$\hat{a}_l(C_l^{(k+1),\phi_l} + (C_l^{(k+1)} - C_w^{(k+1)}, \phi_l)_{lw} = (f_l, \phi_l) + (J_{sl}, \phi_l)_{sl}$$

   for all $\phi_l \in V_{D,l}$.

2. **Wall Problem (Strong):** Solve

$$\begin{aligned}
&\chi C_w^{(k+1)} - \mu_w \Delta C_w^{(k+1)} + \mathbf{u}_p \cdot \nabla C_w^{(k+1)} + k_1 b C_w = f_w - k_2(b - b_0) \quad \text{in} \quad \Omega_w \\
&\mu_w \frac{\partial C_w^{(k+1)}}{\partial \mathbf{n}_w} + \zeta_{lw}(C_w^{(k+1)} - C_l^{(k)}) = 0 \quad \text{on} \quad \Gamma_{lw} \\
&\mu_w \frac{\partial C_w^{(k+1)}}{\partial \mathbf{n}_w} - J_{ws} = 0 \quad \text{on} \quad \Gamma_{ws}
\end{aligned}$$

(Weak): Find $C_w^{(k+1)} \in V_{D,w}$ such that

$$\hat{a}_w(C_w^{(k+1),\phi_w} + (C_w^{(k+1)} - C_l^{(k+1)}, \phi_w)_{lw} = (f_w, \phi_w) + (J_{ws}, \phi_w)_{ws}$$

for all $\phi_w \in V_{D,w}$.

3. **Stent Problem (Strong):** Solve

$$\begin{aligned}
&\chi C_s^{(k+1)} - \mu_s \Delta C_s^{(k+1)} = f_s \quad \text{in} \quad \Omega_s \\
&\mu_s \frac{\partial C_s^{(k+1)}}{\partial \mathbf{n}_s} + J_{ws} = 0 \quad \text{on} \quad \Gamma_{ws} \\
&\mu_s \frac{\partial C_s^{(k+1)}}{\partial \mathbf{n}_s} + J_{sl} = 0 \quad \text{on} \quad \Gamma_{sl}
\end{aligned}$$

(Weak): Find $C_s^{(k+1)} \in V_{D,s}$ such that

$$\hat{a}_s(C_s^{(k+1),\phi_s} = (f_s, \phi_s) - (J_{ws}, \phi_s)_{ws} - (J_{sl}, \phi_s)_{sl}$$

for all $\phi_s \in V_{D,s}$.

The convergence analysis is similar to the one carried out in chapter two. It is more convenient to start solving for the strut problem first in the sequence since drug is stemming from the stent coating to the other domains.

Steklov-Poincaré Implementation

Given that we can solve for the traces of Γ_{ws} and Γ_{sl} when updating $C_s^{(k+1)}$, we only need to consider the Steklov-Poincaré problem in the context of Γ_{lw}. Therefore, given the functions $\mathbf{u}$, $\mathbf{u_p}$, b, and $C_s^{(k+1)}$, it only suffices to consider a two-domain Steklov-Poincaré domain decomposition between the lumen and the wall, with $\rho_{lw} \in \Lambda_{lw}$ the unknown we want to seek.

For the lumen side, we let the operator $\mathcal{H}_l : \Lambda_{lw} \to H^1_{\partial\Omega_l \backslash \Gamma_{lw}}$ be such that for a given function $\rho_{lw} \in \mathcal{H}_l \rho_{lw}$, $C_l = \mathcal{H}_l \rho_{lw}$ solves

$$\begin{cases}
\chi C_l - \mu_l \Delta C_l + \mathbf{u} \cdot \nabla C_l = 0 \quad \text{in} \quad \Omega_l \\
C_l = 0 \quad \text{on} \quad \partial\Omega_l \backslash \Gamma_{lw}, \quad \mu_l \frac{\partial C_l}{\partial \mathbf{n}_l} + \zeta_{lw} C_l = \zeta_{lw} \rho_{lw} \quad \text{on} \quad \Gamma_{lw}.
\end{cases}$$

For the heteregenous part, we define $\mathcal{G}_l : L^2(\Omega_l) \to H^1_{\partial\Omega_l \backslash \Gamma_{lw}}$ such that for $r_l \in L^2(\Omega_l)$, $g_l = \mathcal{G}_l r_l$ satisfies

$$\begin{cases} \chi g_l - \mu_l \Delta g_l + \mathbf{u} \cdot \nabla g_l = r_l \quad \text{in} \quad \Omega_l \\ g_l = 0 \quad \text{on} \quad \partial\Omega_l \backslash \Gamma_{lw}, \quad \mu_l \frac{\partial g_l}{\partial \mathbf{n}_l} + \zeta_{lw} g_l = 0 \quad \text{on} \quad \Gamma_{lw}. \end{cases}$$

On the wall domain, we define similarly by allowing $\mathcal{H}_w : \Lambda_{lw} \to H^1_{\partial\Omega_w \backslash \Gamma_{lw}}$ be such that for $\rho_{lw} \in \mathcal{H}_w \rho_{lw}$, $C_w = \mathcal{H}_w \rho_{lw}$ fulfills

$$\begin{cases} \chi C_w - \mu_w \Delta C_w + \mathbf{u}_p \cdot \nabla C_w + k_1 b C_w = 0 \quad \text{in} \quad \Omega_w \\ C_w = 0 \quad \text{on} \quad \partial\Omega_w \backslash \Gamma_{lw}, \quad C_w = \rho_{lw} \quad \text{on} \quad \Gamma_{lw}. \end{cases}$$

Complementing, we let $\mathcal{G}_w : L^2(\Omega_w) \to H^1_{\partial\Omega_w \backslash \Gamma_{lw}}$ such that for $r_w \in L^2(\Omega_w)$, $g_w = \mathcal{G}_w r_w$ satisfies

$$\begin{cases} \chi g_w - \mu_w \Delta g_w + \mathbf{u}_p \cdot \nabla g_w + k_1 b g_w = r_w \quad \text{in} \quad \Omega_w \\ g_w = 0 \quad \text{on} \quad \partial\Omega_w. \end{cases}$$

Then, for $\rho_{lw} \in \Lambda_{lw}$, we set

$$\begin{aligned} &\mathcal{S}_l : \Lambda_{lw} \to \Lambda_{lw}^{'} \quad \text{such that} \quad \mathcal{S}_l \rho_{lw} = -\zeta_{lw}(\gamma_l \mathcal{H}_l \rho_{lw}) \\ &\mathcal{S}_w : \Lambda_{lw} \to \Lambda_{lw}^{'} \quad \text{such that} \quad \mathcal{S}_w \rho_{lw} = \mu_w \frac{\partial \mathcal{H}_w \rho_{lw}}{\partial \mathbf{n}_w} + \zeta_{lw} \rho_{lw} \end{aligned}$$

so that it makes sense to define

$$\mathcal{S} = \mathcal{S}_l + \mathcal{S}_w \quad \text{and} \quad \eta = -\left(\mu_l \frac{\partial \mathcal{G}_l r_l}{\partial \mathbf{n}_l} + \mu_w \frac{\partial \mathcal{G}_w r_w}{\partial \mathbf{n}_w} \right).$$

Thus, we only need to solve for ρ_{lw} at each time step:

$$\mathcal{S} \rho_{lw} = \eta.$$

Having set up the system between the lumen and the wall, the convergence analysis and equivalence to Problem 5 is identical to [53].

3.4 Numerical Results (Before meshing reassignment)

By changing the diffusivity parameters and initial conditions, it is possible with our domain decomposition from Chapter 2 and the analysis of this chapter to model different behaviors and types of stents. For instance, we remark that by letting $C_{s,0}$ and μ_s be negligibly small we can essentially mimic a BMS, as we have shown in previous simulations. However, by letting instead $C_{l,0}$ and $C_{w,0}$ be zero with $C_{s,0} = 1$ and a relatively higher diffusivity, the simulation becomes one of drug elution such as expected in DES.

In general, we implement the full scale model for the drug eluting stents by considering similar notions to the model in Chapter 2 as well as fitting parameters. For instance, we let the diffusion parameters be $D_s = 5.0 \times 10^{-12}$, $D_l = 0.2$, and $D_w = 7.7 \times 10^{-6}$. For the initial free-binding value, we have $b_0 = 0.5$, and the association and dissociation reaction constants are $k_1 = 1$ and $k_2 = 0.02$, respectively. The permeability constant is $P_{lw} = 2.0 \times 10^{-7}$. For this section, we consider results only before remeshing, when the drug volume is still relatively high.

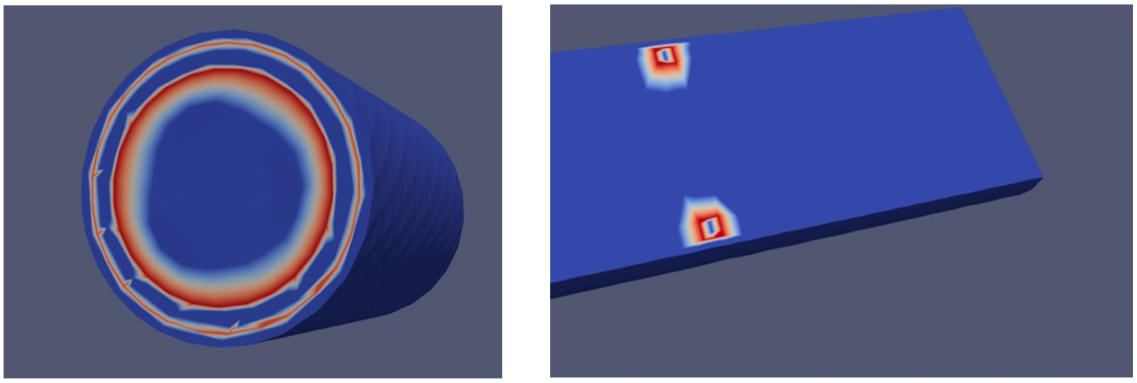

Figure 3.7: Cylindrical (left) and longitudinal (right) cross-sections of the initial drug simulation.

We consider small time steps of $\Delta t = 0.1$ seconds, up until we reach 6 seconds. There is a slight but nonetheless present evolution in the distribution of the drug shown by Figure 3.8.

These simulations were performed on a simple stent with 1 ring strut. We also attempted to simulate on a more complex geometry having a more net-like structure

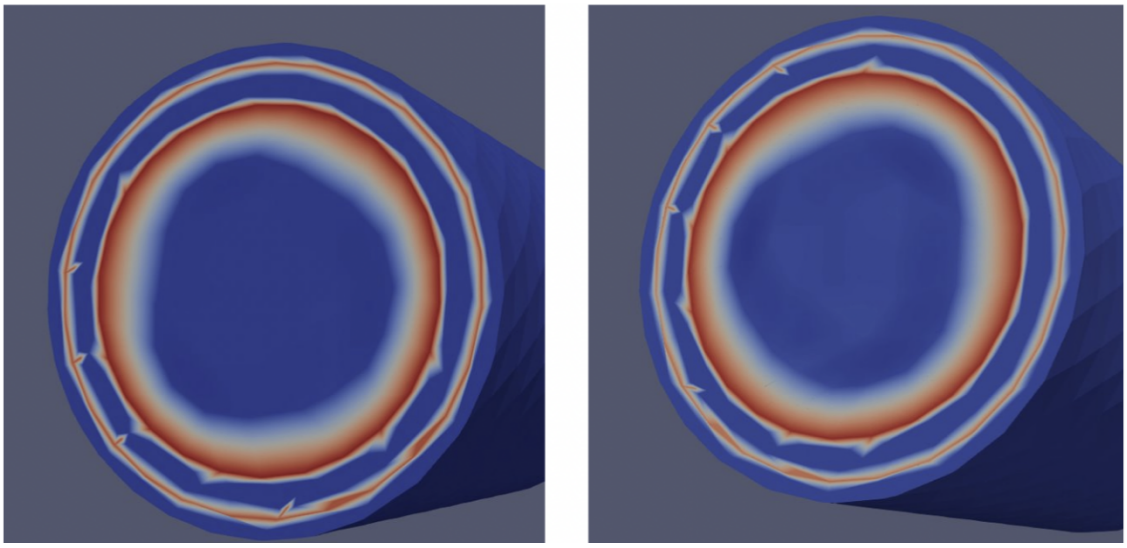

Figure 3.8: Initial drug simulation (left) vs six seconds after (right)

of a more realistic stent. We refer to the next chapter for the construction of this geometry but provide sample simulations before remeshing.

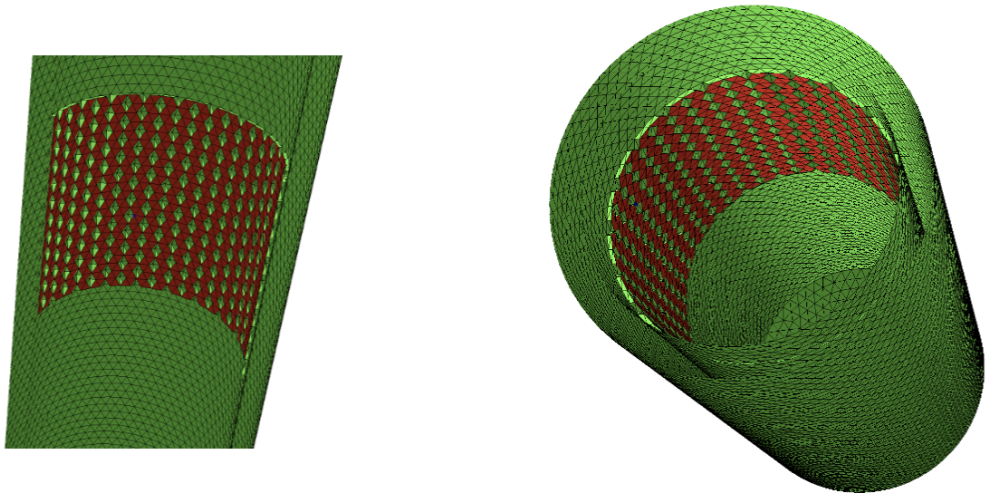

Figure 3.9: More complex stent geometry shell for simulation

We keep the same parameters in our model and illustrate only the initial and short-term values, deferring the long-term time scale simulation and analysis for future work. We showcase the lumen and the wall separately by thresholding the concentration levels.

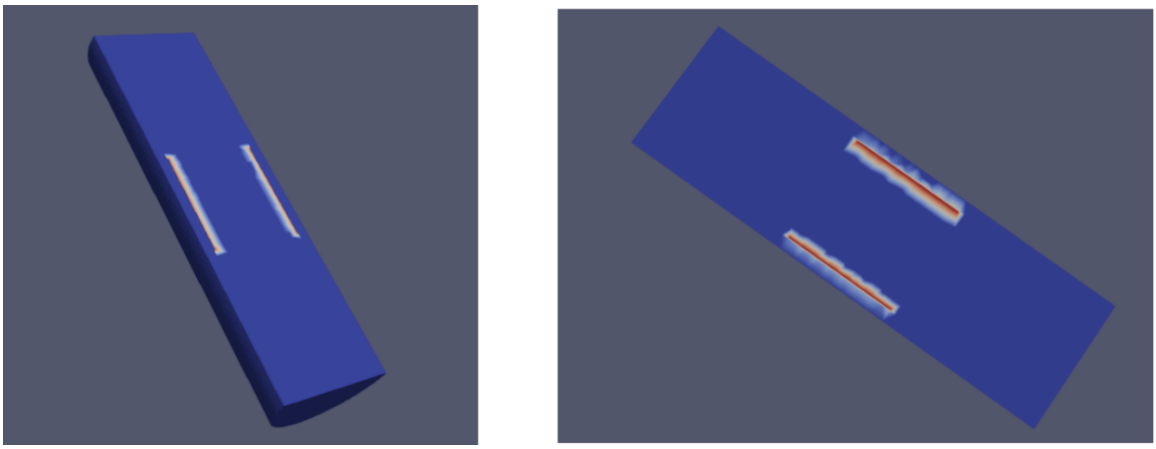

Figure 3.10: Cross-section of drug simulation in more complex geometry before (left) and after six seconds (right).

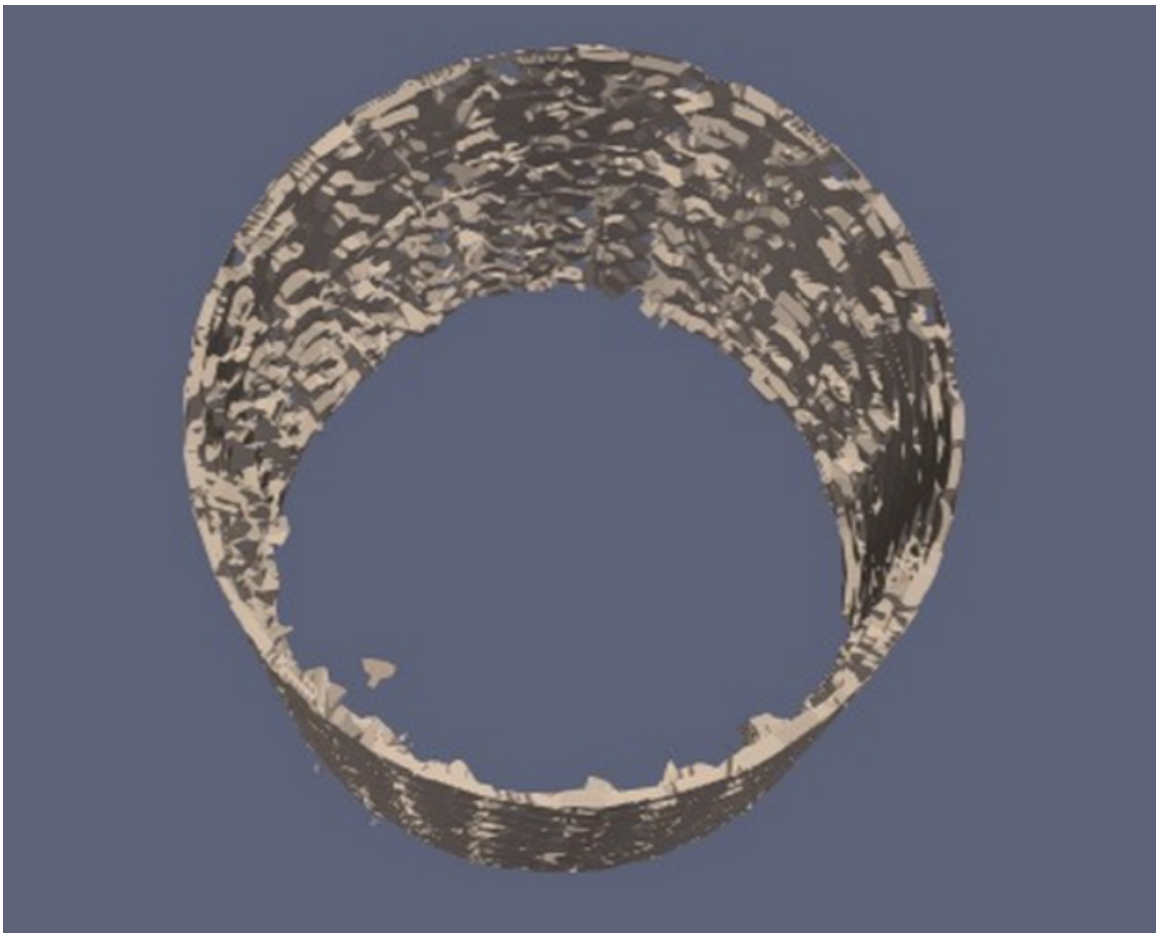

Figure 3.11: Drug simulation in lumen after six seconds.

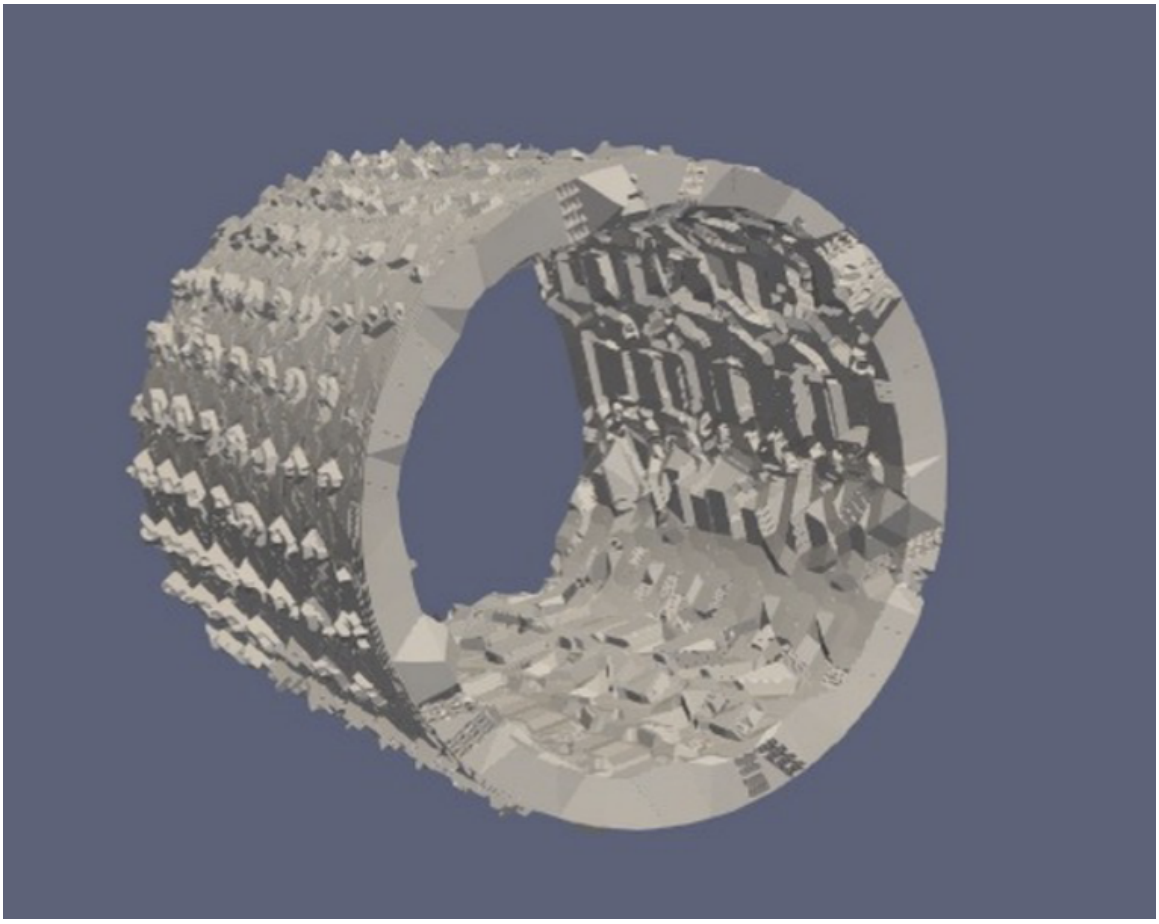

Figure 3.12: Drug simulation in wall after six seconds.

3.5 Discussion

Overall, the domain decomposition methodology elaborated in Chapter 2 proved to be exceedingly useful in modeling the drug behavior. By invoking the Higuchi model on DES, the geometry-independent drug flux remarkably reduced the model without compromising accuracy or having to resort to long-term flux movement, when certain conditions are met. The time-evolving domain and drug elution will be necessary to approach a more realistic model behind the evolution of the drug mechanism in the long term, but currently this is out of this work. Finally, the preliminary results show that the drug absorption by the wall and its fast dissipation by the lumen are in concordance with the clinical expectations.

Chapter 4

Remeshing-free sculpting algorithms via reassignment for multidomain geometry modification

4.1 Motivation

One of the most significant hurdles when modeling stents is accounting for their geometrical changes over time. In our case, we are considering long stretches such as spans of weeks or months. Time-dependent domains are ubiquitous, so there are many numerical techniques to manage them, including adaptive moving meshes [30], mesh-deforming methods like ALE [11], and mesh fracture and relabeling. [45] [16]. For our problem, we explore remeshing-free techniques. In fact, in our problems a mesh can be fixed over time with only elements and boundaries changing the overall geometry. More precisely, erosion induces elements of the interface between two physical subdomains to move from one domain to the other. In this chapter, we describe two methods to modify geometries by using an initial uniform mesh, without requiring any remeshing. Since the objective and research motivation is to reach the construction and modeling of drug eluting stents, the simplified stented artery seen in the previous chapters will be the guidance example upon which to implement the algorithmic principles just laid out. Although the discussion will encompass a general framework for distinct geometries with multiple domains, the implementation of the

algorithms will ultimately be particular pertaining to the geometries considered so far; minimal algorithmic modification for other applications might be needed, but the essence behind the execution stays the same. Finally, the ideas posed in this chapter should extend to software and programming languages with the capacity to handle uniform meshes, multidomain labels of volume materials and boundaries, dictionaries of nodes and edges, and graph-based simple features. For practical purposes and having familiarity with the solver, here we shall be using STL and VOL files through NETGEN and NGSolve.

4.2 Background

To describe a mesh for a moving domain problem, it is necessary to establish spatial coordinates, denoted by $\mathbf{x}$ and also called Eulerian coordinates. Accordingly, the material or Lagrangian coordinates are denoted by $\mathbf{X}$. Each material point is uniquely associated to a spatial coordinate at an initial time $t = 0$, usually so that $\mathbf{X} = \mathbf{x}$. The main difference between these two descriptions is that with Lagrangian coordinates, the coordinates associated to the material will move along with it while the Eulerian coordinates are not necessarily injective to the material points.

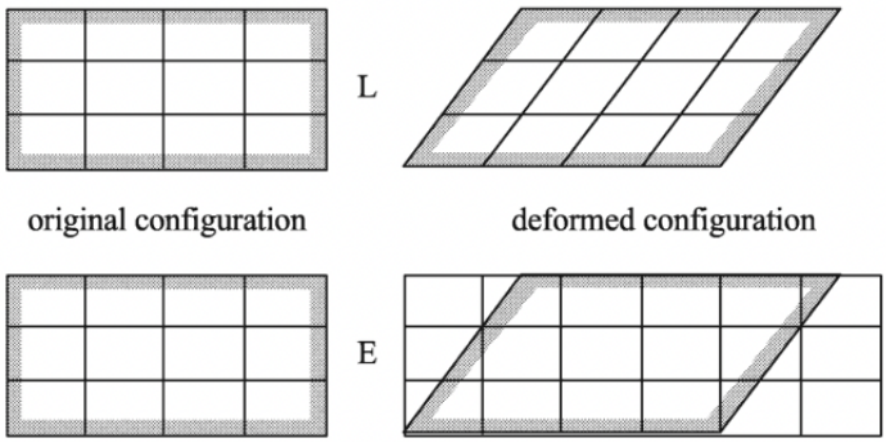

Figure 4.1: The upper part of the diagram shows a Lagrangian transformation of themesh while the bottom one displays an Eulerian representation.[4]

Most of the existing literature deals with Lagrangian or hybrid Lagrangian-Eulerian mesh techniques to account for material displacement and transformations; that is, the mesh will move according to the material. Here, we introduce methods based on

Eulerian meshes with transformed materials.

4.3 Multidomain sculpting transformations on uniform Eulerian meshes

4.3.1 Tetrahedral element reassignment

Suppose that we are given a solid geometry having initial uniform mesh $\mathcal{T}$ composed only of tetrahedral elements. Let $\mathcal{T}$ be divided into m domains and n surface boundaries, each of which is to be labelled accordingly with an additional "zero domain" consisting of the region external to $\mathcal{T}$. Here $\mathcal{T}$ will serve the role of a fixed Eulerian mesh, where only domain labels will move across it. The virtual sculpting method relies on existing mesh points and already established elements. Having a configuration of tetrahedral arrangement and domain labels of elements and surfaces, we can re-assign them within the existing layout. Say that a tetrahedron is initially assigned to domain $m_i \in \{1, ..., m\}$ and one of its faces to surface boundary $n_i \in \{1, ..., n\}$, with the other faces not pertaining to any surface boundaries. Then by editing the file directly, it is possible to change the domain of the tetrahedral element (or even create a new one) as well as to eliminate or change the existing surface boundary n_i and to make any of the other three faces a surface boundary. The example in Figure 4.3 displays the result of such a reassignment. Notwithstanding, to avoid corruption in the mesh and file, the following conditions should be implemented.

1. Without refinement, vertices must only form a new surface boundary from a face that already exists in a tetrahedron. That is, any three vertices should not form a new face if it is not originally attached to an existing single tetrahedron. Figure 4.2 illustrates this notion. While it could be possible to define a new face entirely in the file, it creates complications in finite element methods when accessing boundaries not conforming to tetrahedra.

2. The material of a domain can be from a previous one or new; however, new materials should be defined.

3. The encoded information of the surface boundaries should appropriately account for belongingness to volume elements with updated domains.

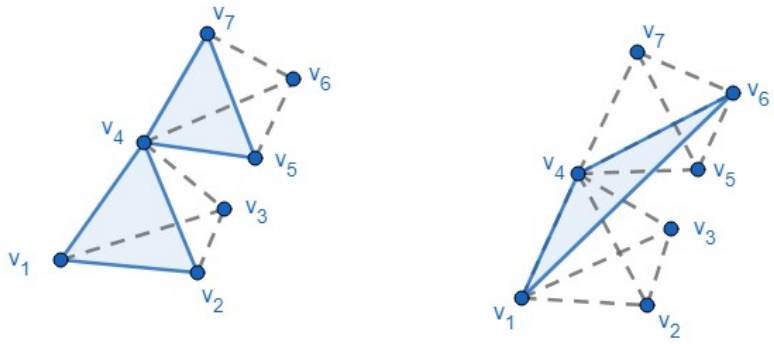

Figure 4.2: On the left we have two given tetrahedra with valid surface boundaries (shaded). The figure on the right represents an invalid surface definition since $v_1v_4v_6$ is not attached to an existing single tetrahedron.

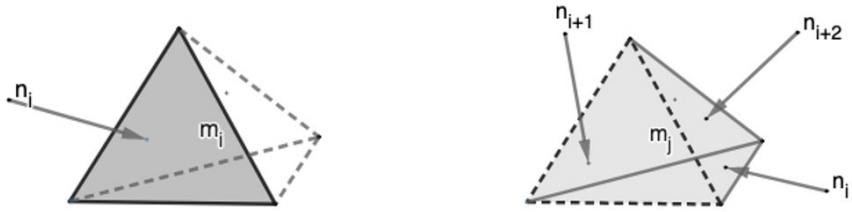

Figure 4.3: The left side shows a tetrahedral element with domain m_i and one surface boundary n_i (displayed by the solid lines and shaded region). On the other hand, with proper modifications, the same element is now reassigned to domain m_j and contains three different surface boundaries n_i, n_{i+1}, n_{i+2}. Notice that the label n_i is different in both instances.[4]

Since this is based on an Eulerian mesh setting, any elements can be relabeled without need to remesh. The complexity lies in finding which elements and boundaries to modify and properly keeping track of such changes.

4.3.2 Pathfinding

Since we have a lattice of vertices and edges, we wish to find paths (i.e. pathfinding) along already found edges and vertices to have control over the search of elements we plan on manipulating; this can be analogous to a hiker tying a rope to himself and going inside an unexplored cave, then coming back with new information and paths along the cave. Having initial information about domains and boundaries in the mesh is useful to generate pathfinding algorithms. Constructing one to target

specific pieces depends on the type of geometry and user's needs. The algorithmic process begins through boundary elements and then finding volume elements by digging deeper into the mesh domains. A uniform mesh is extremely convenient to locate elements throughout the graph. By uniform, we mean that the volume elements are practically identical, so that in our cases any two neighboring tetrahedra have similar structure. Although this requirement can be circumvented, predicting where certain elements are can become considerably more complicated. This is due to the fact that whenever the packing of tetrahedra is not uniform, guessing the shape and neighbors of unexplored tetrahedra becomes uncertain. We provide a general lattice-based framework, with considerations, and then attempt to illustrate through specific examples.

Since the mesh is uniform and composed of tetrahedra, we can infer that the surface elements are mostly equilateral triangles and that the lattice is rather substructured by repetitive layers, permitting pattern control. For simplicity, the surface boundaries are essentially approximations of local manifolds of the geometry, so that unwanted overlapping never occurs (i.e. a surface triangle is never assigned two boundaries simultaneously). Let $G_0 = (V, E)$ be the overall graph defined by the initial mesh, where V and E are collections of vertices and edges, respectively. From this multidomain mesh, we can have subgraphs composed of vertices and edges pertaining to each domain and surface boundaries; as such, we write M_i to denote the subgraph of G_0 corresponding to a domain m_i and N_r to be the subgraph associated with surface boundary n_r.

4.3.3 Algorithms for mesh transformation

We will consider two unrelated uniform tetrahedral meshes, but slight variations of each method can be adapted without much effort. The first is a generic geometry to elucidate the main ideas of the sculpting algorithm, and the latter will be specifically tailored to form a working stent from a cylindrical mesh. We begin by constructing an algorithm for a meshed cube and then proceed with the creation of another algorithm for the second geometry.

Generic mesh algorithm

Uniform mesh considerations: To have a consistent arrangement of packing by layers, we enclose the elements in hexahedra, more specifically a cube, and then split into tetrahedra, so that each one contains five of them as seen in Figure 4.5.

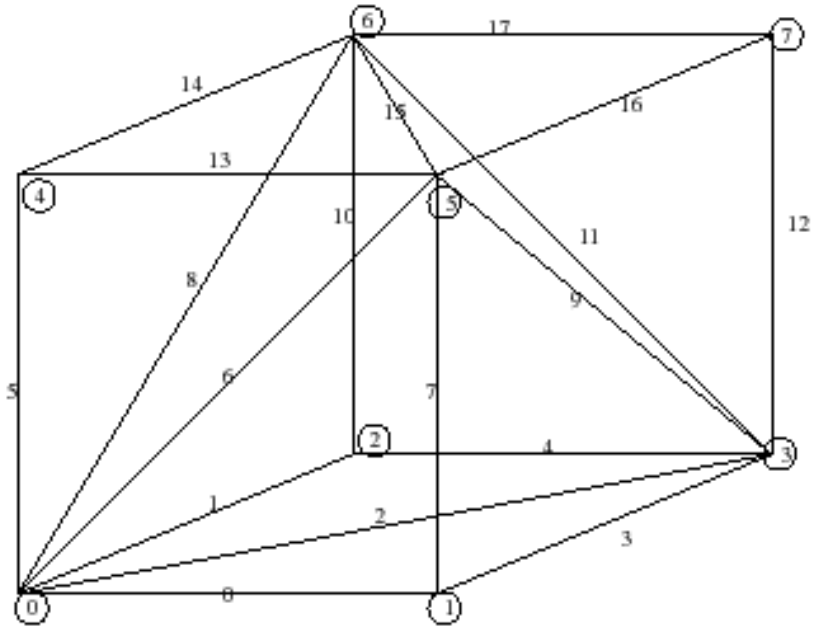

Figure 4.4: Hexahedron decomposition into five tetrahedra. [44]

Then, we assort them by levels, so we can implement a geometry transformation algorithm. For this transformation, the plan is to remove one of the hexahedra in the corner from the geometry. The boundaries are the six faces of the original cube, so we have six external boundaries.

Part 1: Locating intersection of boundaries

1. We first track elements containing edges lying on intersections of physically adjacent boundaries (e.g. two different faces of the cube) and notice that surface elements are triangles. Without loss of generality, consider adjacent boundaries n_r and n_s. Then we search all surface elements in boundary n_r and store the edges from corresponding subgraph N_r in a list E_r; we do the same for n_s, storing the edges from N_s in a different list E_s; and we take the intersection of both sets of edges and call it $E_{r,s}$. We set $k = 0$ and $j = 2$

2. We now select an edge $e \in E_{r,s}$ with vertices v_1 and v_2. We store e in an array

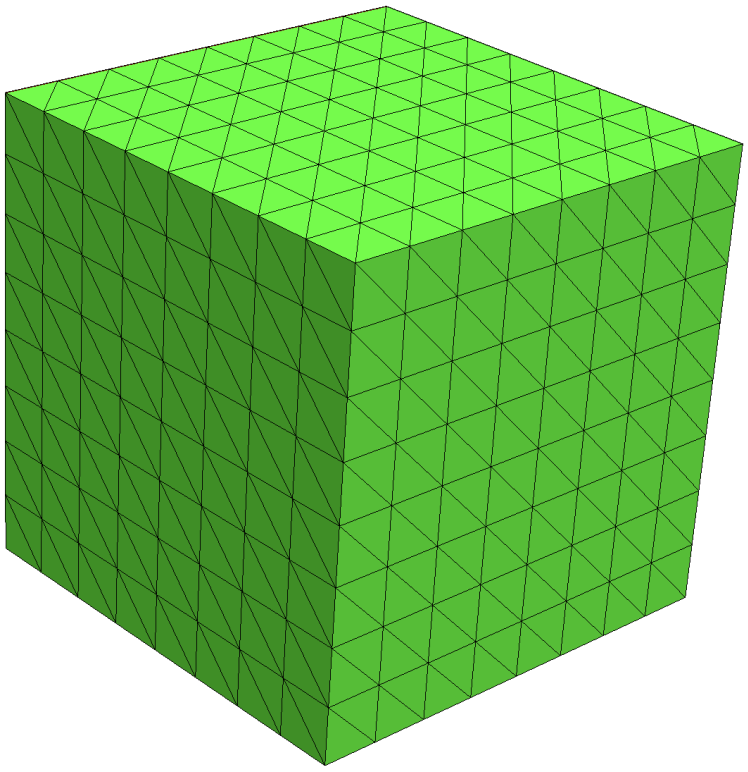

Figure 4.5: Uniform meshing of a cube. Notice that this is essentially a packing of many smaller hexahedra of the form seen in Figure 4.5.

called *selected_edges*. If we want to be specific about which initial edge to choose among the members in the $E_{r,s}$, the coordinates of its vertices can be consulted. Because e is in an intersection, it belongs to both a triangle in N_r and in N_s. We select a triangle in N_s, so that the third vertex v_3, conforming a triangle with v_1 and v_2, is contained entirely within it. We set $k = 1$

Part 2: Obtaining faces and volume elements of layer k

1. We store the vertices we use in a vertex array called $vertex\_layer_k$ and set $j = j + 1$. We also create $volume\_layer_k$, $old\_Ns\_boundary_k$, $new\_Ns\_boundary_k$, $old\_Nr\_boundary_k$, $new\_Nr\_boundary_k$, $other\_boundary_k$, and $last\_level$. Also, by levels we indicate the number of hexahedral stacked vertically (in the N_r direction) from the original N_s floor. In essence, N_s will be our relative base floor, N_r the relative height, and other boundary refers to different boundaries than N_r and N_s. The name "$old\_Face\_boundary$" indicates the structure as seen before any modifications, while "$new\_Face\_boundary$" indicates that this

will be the updated boundary. For example, the ceiling of a hexahedral of the first level will become the floor of the hexahedral of the second level.

2. Now edges $v_{j-1}v_j$ and $v_{j-2}v_j$ determine different adjacent triangles to $v_{j-2}v_{j-1}v_j$, as shown in Figure 4.6.

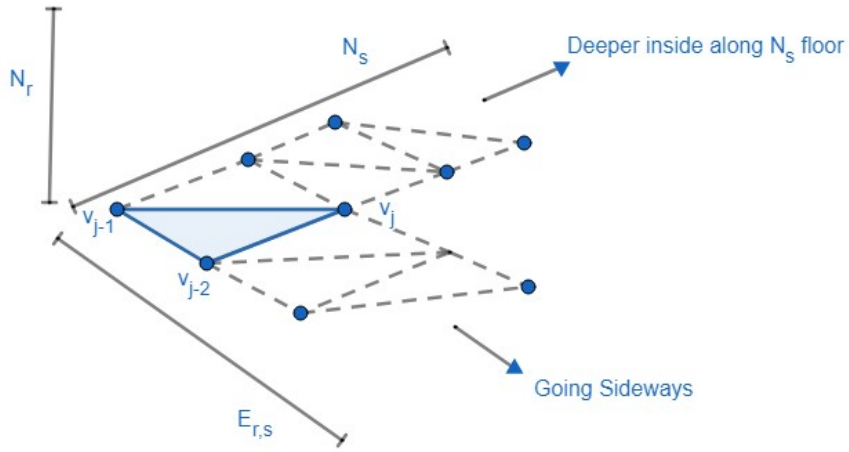

Figure 4.6: Overview of N_s floor. After having triangle $v_jv_{j-1}v_{j-2}$ (shaded), vertices v_jv_{j-1} and v_jv_{j-2} could determine new triangles in different directions. In our example, we choose to go deeper inside and away from $E_{r,s}$. Here N_r is not pictured but represents the relative mesh altitude from the floor N_s.

Instead of going sideways, it is desirable to go deeper away from the boundary in the most straight manner possible, so that we can explore the mesh in parallel by selecting another pair of adjacent vertices from $E_{r,s}$. From v_jv_{j-1} and v_jv_{j-2} and conforming to the diagonal of the hexahedron face, we select the edge having greater magnitude, say it is v_jv_{j-1}. This edge is attached to exactly two triangles in the surface. To avoid repeating triangle $v_{j-2}v_{j-1}v_j$, we avoid triangles whose vertices are all contained in $floor\_layer_k$. Then we will have triangle $v_{j-1}v_jv_{j+1}$ and we store vertex v_{j+1} in $floor\_layer_k$.

3. Having vertices v_{j-2}, v_{j-1}, v_j, and v_{j+1} consecutively, these conform the face of a hexahedron. We explore the other vertices of the hexahedral sub-geometry. We have faces $v_{j-2}v_{j-1}v_j$ and $v_{j-1}v_jv_{j+1}$, which are each attached to one or two volume elements. If each face corresponds to only one tetrahedra, we simply go through all elements of the corresponding domain, say M_i, until we find one containing all the vertices in the triangle, then we store that volume element

in a volume array called $volume\_layer_k$. Otherwise, if one or both of them are between two tetrahedra, then we search only within the domain to be modified and store the correct tetrahedra in $volume\_layer_k$. For either instance, we add the new vertices u_1 and u_2 to $upper\_layer_k$. Since v_{j-1} and v_j lie on the diagonal of $v_{j-2}v_{j-1}v_jv_{j+1}$, these form the faces with u_1u_2 and tetrahedron $v_{j-1}v_ju_1u_2$, which we add to $volume\_layer_k$. We find the remaining vertices u_3 and u_4 by searching for volume elements that are not $v_{j-1}v_ju_1u_2$ within M_i and contain the faces $v_ju_1u_2$ and $v_{j-1}u_1u_2$. The overall step is illustrated in the first part of the diagram of Figure 4.7. We add the newly found vertices and tetrahedra to $upper\_layer_k$ and $volume\_layer_k$, respectively.

4. If we are satisfied with $volume\_layer_k$ and do not wish to go further(e.g. for geometry customization purposes), we add $v_jv_{j+1}u_2$ and $v_ju_2u_4$ to $new\_Nr\_boundary$; or if v_jv_{j+1} belongs to a boundary different than N_s or N_r, say to another face N_t, we add $v_jv_{j+1}u_2$ and $v_ju_2u_4$ to $other\_boundary_k$ if we wish to replace the boundary.

5. We store faces $v_{j-2}v_{j-1}v_j$ and $v_{j-1}v_jv_{j+1}$ in $old\_Ns\_Boundary_k$. Similarly, if there are members of $upper\_layer_k$ that do not belong to either N_r, N_s, or N_t, we add faces $u_1u_2u_3$ and $u_1u_2u_4$ in $old\_Ns\_Boundary_k$. Otherwise, we add them to $last\_level$. If $j = 3$, we add faces $v_{j-2}v_{j-1}u_1$ and $v_{j-1}u_1u_3$ to $old\_Nr\_boundary_k$ and set $e = u_1u_3$.

6. If neither of the previous conditions of Step 4 are met, we set $j = j+1$. We find a new vertex v_{j+1}, through a new triangle (i.e. not found in $old\_Ns\_Boundary$) having $v_{j-1}v_j$ as a side, and store it in $floor\_layer_k$. We set $j = j+1$ and repeat the once more to find another vertex v_{j+1} and store it $floor\_layer_k$. Updated nodes v_{j-2}, v_{j-1}, v_j, and v_{j+1} correspond to the face of a new hexahedron.

7. We repeat steps 3-6 until we wish to stop (i.e. we are content with not exploring further per the user's desired modifications) or cannot longer continue, in which case we ran out of levels and faces.

Part 3: Rewriting labels and reassigning tetrahedra of layer k in the mesh file

This part focuses on modifying information directly from the initial mesh file by finding lines to pre-existing faces and volume elements. We then alter or delete them,

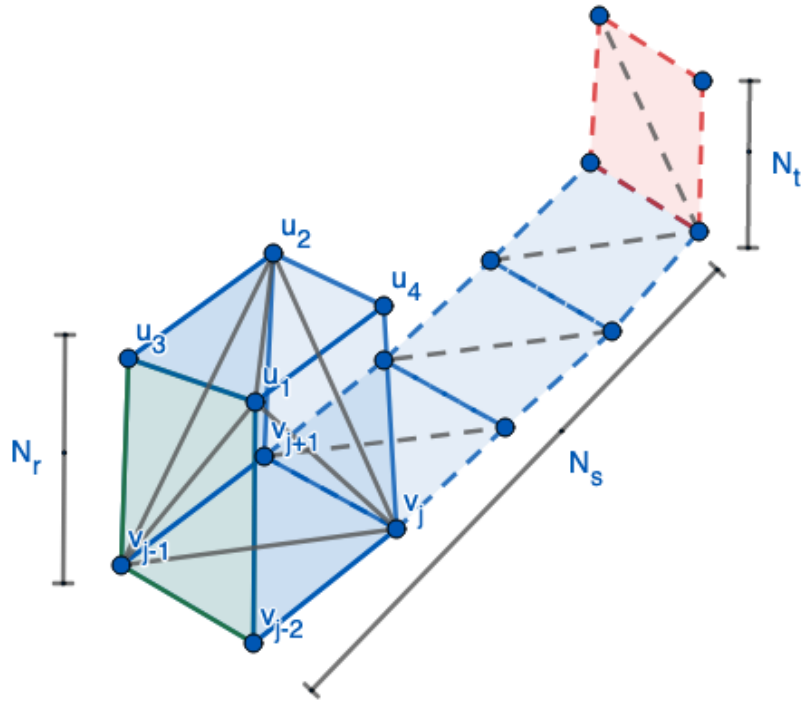

Figure 4.7: Element finding algorithm for one hexahedron at a time. The dashed faces belong to hexahedra not shown for clarity.

and we add newly created lines corresponding to new faces. The format could vary by software/mesher; for this research, we used VOL files, the standard Netgen mesh file format.

1. *Tetrahedra alteration.* To simplify search in the file, for each member in $volume\_layer_k$, we get the correct order of vertices. We write two strings: one indicating the current domain of each element in the file and another with the new domain instead. We then replace the original string with the replacement one.

2. *N_r-boundary replacement.* Similar to the previous step, we appropriately update $old\_Nr\_boundary_k$ in terms of node order in file. We write strings from $old\_Nr\_boundary_k$ in the format of the file. We locate these lines in the file and delete them. Now, if $new\_Nr\_boundary_k$ is not empty, we write in the file the same strings we deleted but with the new information; otherwise if $other\_boundary_k$ is not empty, we instead write strings to replace the boundary or erase it.

3. *N_s-boundary replacement.* Finally, if *last_level* is empty, we once again update

the vertex order in $old\_Ns\_boundary_k$. We write strings from $old\_Ns\_boundary_k$ in the format of the file. Then, we find these lines in the file and erase them. We replace the deleted information with strings from $new\_Ns\_boundary_k$.

Part 4: Application of Parts 2 and 3 in subsequent layers

1. If *last_level* is nonempty and we seek to replace or erase this part of the different boundary, call it N_l, we find correct vertex order from $new\_Ns\_boundary_k$ and write one or two sets of lines: one corresponding to original information in file and another one with new boundary information. If we seek to erase, we only use the former; but if we want to replace, we also add the second set.

2. Otherwise, if *last_level* is empty, we set $k = k + 1$ and implement Parts 2 and 3 starting with e.

3. We repeat steps 1 and 2 until we no longer can do so or wish to stop.

Part 5: Selecting different edges in $E_{r,s}$

1. We pick a different edge $e \in E_{r,s}$ not in *selected_edges* and implement Parts 2-4.

2. We repeat step 1 until we no longer wish to continue or cannot do so.

Part 6: Choosing different adjacent boundaries

We can apply Parts 1-5 on two different sets of boundaries until we wish to stop.

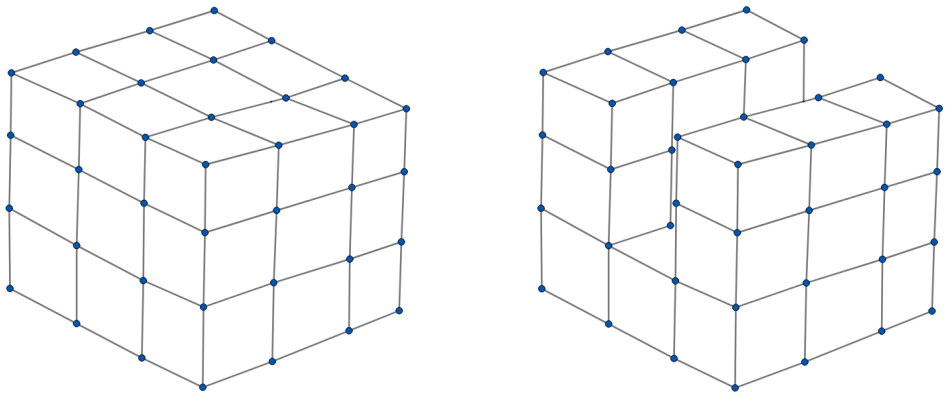

Figure 4.8: Cube representation after implementing the algorithm (diagonal edges are not shown for illustration purposes).

Stent cylindrical mesh algorithm

Different types of geometries and objectives require adaptations of the aforementioned approach. For instance, the end goal behind the development of this meshing algorithm is to be able to form a more realistic stent geometry with the purpose of emulating any type of stent through FEM. In this case, the algorithmic process is similar to the previous one, we merely adjust the main ideas in a different context. It is important to note that the applications and ideas are not limited to just stents, so careful tailoring of a sculpting algorithm is encouraged. The geometry was generated with a matlab file and meshed in Netgen. We also note that the node labels that follow are artificial to illustrate the algorithm; so that vertex algorithm label is not necessarily the same as the vertex ID found in the mesh.

Uniform mesh considerations

We consider three cylindrical shells, embedded in successive order. Each one of these represents a different domain corresponding to significant layers of a coronary artery. They are wall, lumen, and stent. We seek to mainly alter the stent layer for sculpting purposes, to make it more complex. The mesh layout varies by boundary; so while the radial width of the stent cylindrical shell has a similar composition to a face of the cubic mesh and benefits from the previous algorithm, we need to consider a different pathfinding pattern along the cylinder's height given its more hexagonal arrangement. The mesh in the stent is structed by levels, so that the composition repeats by layers.

Overview

We will go into detail shortly but first state a general overview of the main ideas and structure of the algorithm. As seen in the upper portion of Figure 4.10, the given labels for the boundary faces of the stent mesh are the reference **cylinder height** N_s, the starting **floor base** N_r, the other cylinder height N_t, and the top face N_m. The lower part of Figure 4.10 represents the enclosure of a sub-packing of the stent that we are going to refer as a **level**; the area selected by the yellow lines is comprised of tetrahedra, and it repeats uniformly upwardly. In that example of the yellow enclosure of the first level, there are four levels in the stent mesh, which we can see if we raise the yellow box by one triangle in altitude at a time.

We assume we have a design in mind before exploring the volume and surface elements we want to reassign. The plan is to start at an edge e of the boundary intersection $E_{r,s}$ of N_r and N_s and then locate all the tetrahedra in the section of the

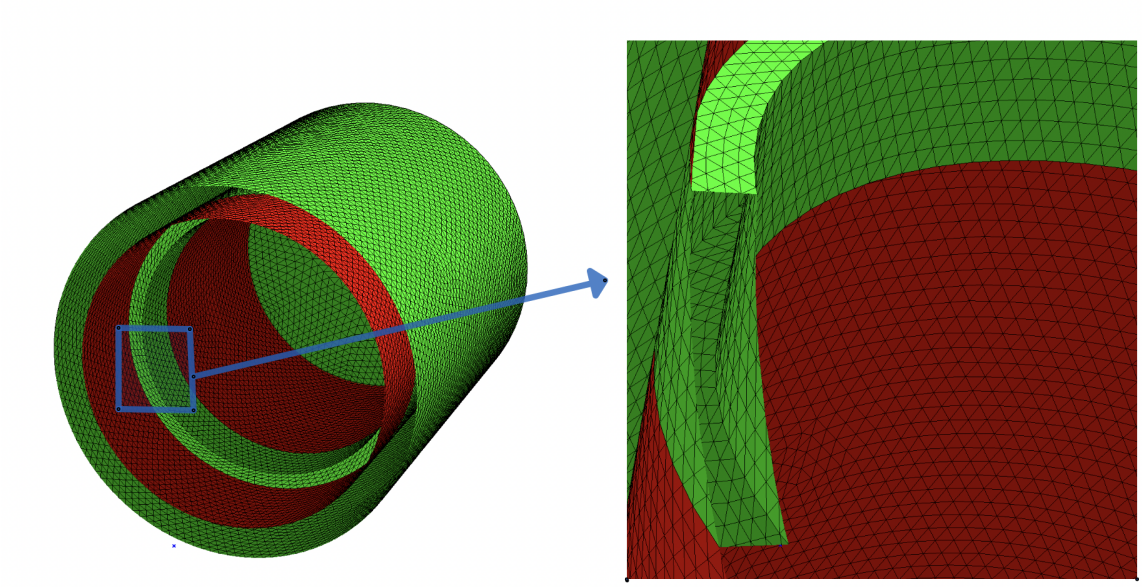

Figure 4.9: Snapshot of the initial stent before implementing modification.

first level starting from the edge e deeper in the direction of N_t until reaching it. By **upside tetrahedra** we mean those tetrahedra having one of their faces in the floor boundary N_r; we keep track of the nodes in the **floor layer**, that is, those nodes belonging to N_r. Similarly, the **ceiling layer** of the same level will be those nodes not lying on the floor N_r; combinations of these ceiling nodes will result in the faces of tetrahedra whose faces are not part of the floor N_r and we will refer to these as **upside-down tetrahedra**.

After identifying the tetrahedra of the first level, the geometry can be modified and we move up with one level within the same section; we are still not going sideways, but vertically along N_s. The ceiling of the previous level becomes the floor of the new level, so that N_r has shifted up by one level. We keep doing the aforementioned this until we reach the top level N_m. Having cleared one small section vertically, we can now start moving sideways and pick a different edge in $E_{r,s}$ and tackled a new section deeply into N_t and then vertically, and so on. Lastly, whenever we indicate in the text that "we repeat until we cannot longer continue or wish to stop", we refer to either being unable to find more levels upwardly or new edges in $E_{r,s}$, or that we are satisfied with the geometry modification we seek to implement. We now describe carefully the mechanics of the algorithm.

Part 1: Locating intersection of boundaries

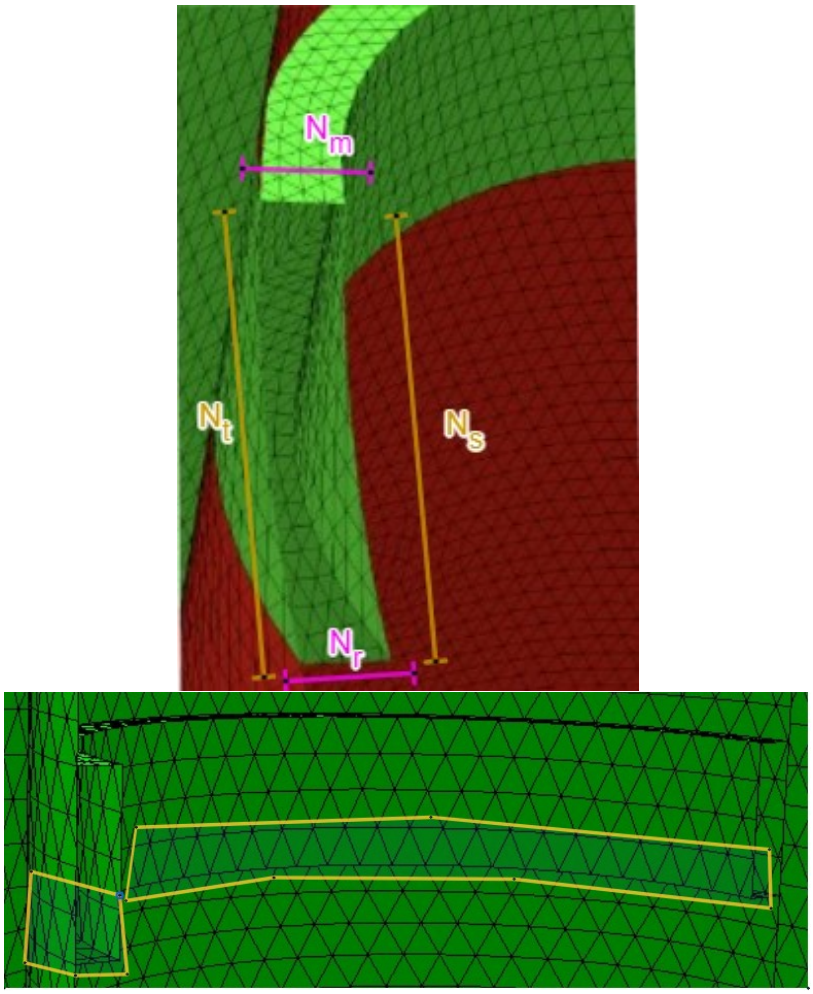

Figure 4.10: The upper figure displays the labels of faces in our reassignment algorithm, while the bottom one shows a level enclosure marked by the yellow lines.

1. We first track elements containing edges lying on intersections of adjacent boundaries and notice that surface elements are triangles. Without loss of generality, consider adjacent boundaries n_r and n_s, that is, two different labeled faces next to each other in the mesh. Then we search all surface elements from boundary n_r and store the edges from its corresponding subgraph N_r; we do the same for n_s, storing the edges from N_s; and we take the intersection of both sets of edges and call it $E_{r,s}$. In this case, N_s will be the relative floor and N_r will be the cylindrical height as seen on Figure 4.11.

2. We now select an edge $e \in E_{r,s}$ with vertices v_1 and v_2. If we want to be specific about which initial edge to choose among the members in the "ring" $E_{r,s}$, the coordinates of its vertices can be consulted. Set $k = 1$ and $j = 2$.

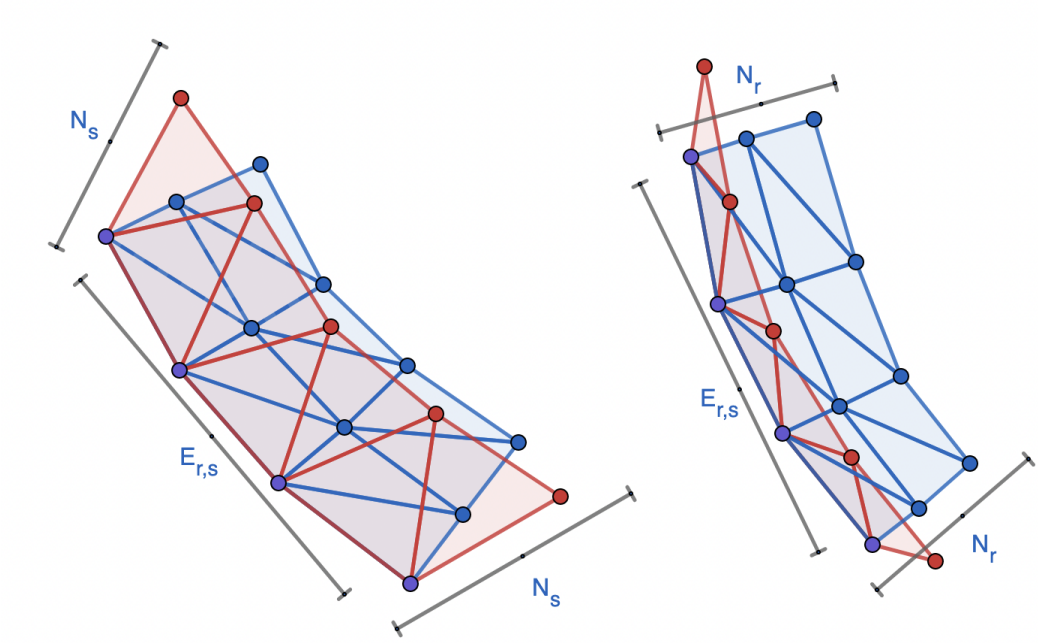

Figure 4.11: Boundary intersection of N_r and N_s showing two different kinds of surface element configuration.

Part 2: Exploring and obtaining boundary face of cylinder height

1. We initialize array *selected_edges* and add e to it. Because e is in an intersection, it belongs to both a triangle in N_r and in N_s. We store the vertices we use in a vertex array called $floor\_layer_k$. We also create array *last_level*. Then, we set $k = k + 1$ and select a triangle in the height boundary N_s, so that the third vertex v_3, conforming a triangle with v_1 and v_2, is contained entirely within it. We store v_3 in the new initialized array $floor\_layer_k$.

2. Now edges $v_{j-1}v_j$ and $v_{j-2}v_j$ determine different adjacent triangles to $v_{j-2}v_{j-1}v_j$. Depending on the symmetry of the arrangement, they could result in similar paths and volumes but different directions. Without loss of generality, pick either edge, say $v_{j-1}v_j$. This edge is attached to exactly two triangles in the surface. To avoid repeating triangle $v_{j-2}v_{j-1}v_j$, we avoid triangles whose vertices are all contained in $floor\_layer_{k-1}$. Then we will have triangle $v_{j-1}v_jv_{j+1}$ and we store vertex v_{j+1} in $floor\_layer_k$. If we are satisfied, we stop searching; otherwise, we set $j = j + 1$ and $k = k + 1$ (by now v_j corresponds to v_4 and $k = 3$) and initialize $floor\_layer_k$. This is shown in Figure 4.12.

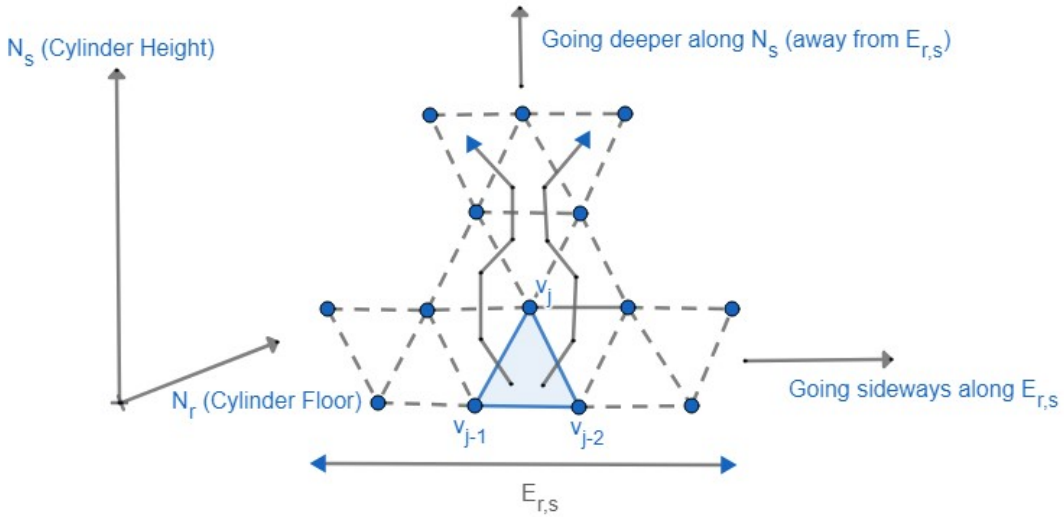

Figure 4.12: The paths show how surface triangles can be explored along the cylinder height N_s.

3. Again, edges $v_{j-1}v_j$ and $v_{j-2}v_j$ are attached to different triangles. However, if we choose $v_{j-2}v_j$ as the next edge to find the new vertex, we will have vertex v_b which is on the boundary, and we start moving sideways along it. Instead, it is desirable to go deeper away from the boundary in the most straight manner possible, so that we can explore the mesh in parallel by selecting another pair of adjacent vertices from $E_{r,s}$. Given the triangular structure of the lattice, this path would most likely resemble a zigzag. Thus, we select edge $v_{j-1}v_j$ to find v_{j+1} and store it in $floor\_layer_k$. If we are satisfied, we stop searching; otherwise, we set $j = j + 1$.

4. We have that j is an odd integer since we have now explored an odd number of triangles, starting with the two vertices of edge e. Triangle $v_{j-2}v_{j-1}v_j$ is sufficiently away from vertices in $E_{i,j}$ and is adjacent to two surface triangles whose vertices are not all in $floor\_layer_{k-1}$. To prevent the triangular path from deviating too much to the sides and maintain the zigzag height, we search the new vertex through the unexplored triangle corresponding to edge $v_{j-2}v_j$ (notice that both are odd). We store v_{j+1} in $floor\_layer_k$. If we are satisfied, we stop searching; otherwise, we set $j = j + 1$ and $k = k + 1$ and initialize $floor\_layer_k$, .

5. We observe that j is an even integer and that the current triangle is $v_{j-3}v_{j-1}v_j$.

Like before, we search the new vertex through the triangle attached to edge $v_{j-1}v_j$ (notice that both are consecutive). We store v_{j+1} in $floor\_layer_k$. If we are satisfied or if both v_{j-1} and v_j belong to a different boundary N_m (in which case we add them to $last\_level$) we stop searching; otherwise, we set $j = j + 1$.

6. We implement steps 5 and 6 in alternating sequence to obtain a proper zigzag path until we decide to stop or cannot longer continue.

This will be our desired transformation height with level wise vertex arrays. For the next part, we set $k = 1$ and $j = 2$.

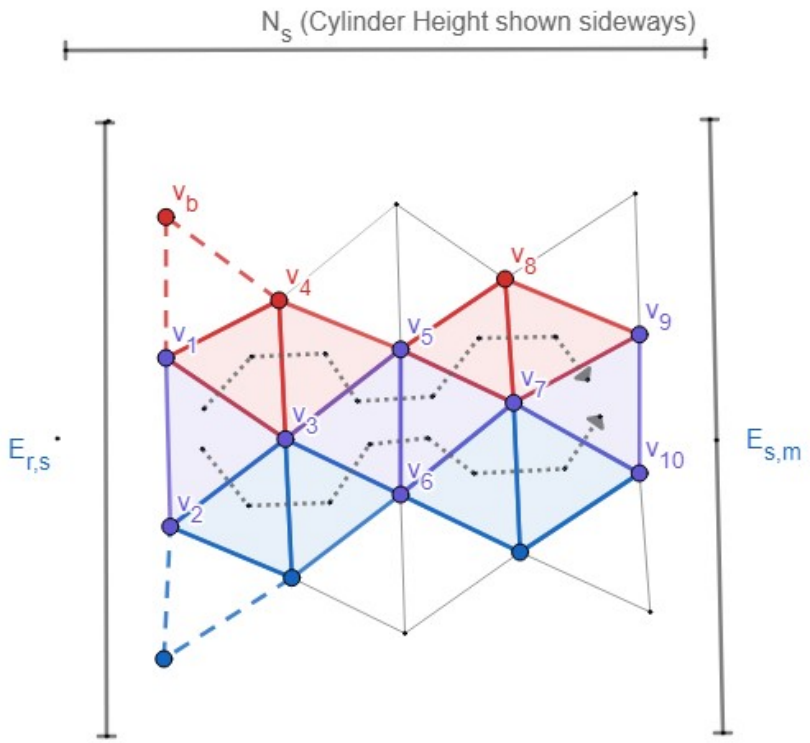

Figure 4.13: The figure illustrates the zigzag pathfinding process to obtain surface elements in the cylinder's height. Here N_s is the boundary from which triangles are obtained, and N_r and N_m are the other faces in the cylinder, with $E_{r,s}$ and $E_{s,m}$ are marking the edges belonging to $N_r \cap N_s$ and $N_s \cap N_m$, respectively.

Part 3a: Getting boundary floor of layer k

This part is similar to Part 2 of the Generic mesh algorithm; however, the main discrepancy consists of the distinct packing arrangements of volume elements. For

this part, we work on N_r, the other adjacent boundary to $E_{r,s}$ corresponding to the base of the stent cylindrical shell.

1. Similarly to the previous cube algorithm, we refer to $floor\_layer_k$ and create $volume\_layer_k$, $old\_Nr\_boundary_k$, $old\_Ns\_boundary_k$, otherboundary$_k$, and $ceiling\_vertex_k$. We let v_{2k-1} and v_{2k} from $floor\_layer_k$ and set $w_{j-1} = v_{2k-1}$ and $w_j = v_{2k}$. We add the face $v_{2k-1}v_{2k}v_{2k+1}$ to $old\_Ns\_boundary_k$, where v_{2k+1} is obtained from $volume\_layer_{k+1}$.

2. In part 2, we explored that w_{j-1} and w_j belong to a triangle N_s. But we also know that they are in N_r so we select the triangle $w_{j-1}w_jw_{j+1}$, noting that there is only one available option. We add w_{j+1} to $floor\_layer_k$ and $w_{j-1}w_jw_{j+1}$ to $old\_Nr\_boundary$. Searching within the proper domain, we obtain the tetrahedron attached to face $w_{j-1}w_jw_{j+1}j$ and add it to $volume\_layer_k$. We keep track of the additional vertex u_j from the tetrahedron and add it to $ceiling\_vertex_k$. We set $j = j + 1$.

3. Edges $w_{j-1}w_j$ and $w_{j-2}w_j$ determine different adjacent triangles to $w_{j-2}w_{j-1}w_j$. From w_jw_{j-1} and w_jw_{j-2} and conforming to the diagonal, we select the edge having greater magnitude, say it is w_jw_{j-1}. This edge is attached to exactly two triangles in the surface. To avoid repeating triangle $w_{j-2}w_{j-1}w_j$, we avoid triangles whose vertices are all contained in $floor\_layer_k$. Then we will have triangle $w_{j-1}w_jw_{j+1}$ and we store vertex w_{j+1} in $floor\_layer_k$ and $w_{j-1}w_jw_{j+1}$ to $old\_Nr\_boundary$. We search for the tetrahedron corresponding to face $w_{j-1}w_jw_{j+1}$ in the desired domain, add it to $volume\_layer_k$, and put its other vertex u_j in $ceiling\_layer_k$.

4. If we are satisfied with $volume\_layer_k$, we add $w_jw_{j+1}u_j$ to $new\_Ns\_boundary$; or if w_jw_{j+1} belongs to a boundary different than N_r or N_s, say to N_t, we search for the triangle in N_t containing w_jw_{j+1}, add the final ceiling vertex u_{j+1} to $ceiling\_layer_k$, and include the face $w_jw_{j+1}u_{j+1}$ to $other\_boundary_k$ if we wish to replace the boundary.

5. If neither of the previous conditions of Step 4 are met, we set $j = j+1$. We find a new vertex w_{j+1}, through a new triangle (i.e. not found in $old\_Nr\_Boundary$) having $w_{j-1}w_j$ as a side and store it in $floor\_layer_k$. We also add $w_{j-1}w_jw_{j+1}$ to $old\_Nr\_boundary$. We find the correct domain tetrahedron attached to

$w_{j-1}w_jw_{j+1}$, add it to $volume\_layer_k$, and let the new vertex u_j be part of $ceiling\_layer_k$. We set $j = j + 1$ and repeat the once more to find another vertex w_{j+1}, tetrahedron $w_{j-1}w_jw_{j+1}u_j$, and vertex u_j and store them $floor\_layer_k$, $volume\_layer_k$, and $ceiling\_layer_k$, respectively.

6. We continuously implement Step 4, to check for continuation requirements, and step 5 until we cannot or no longer want do so.

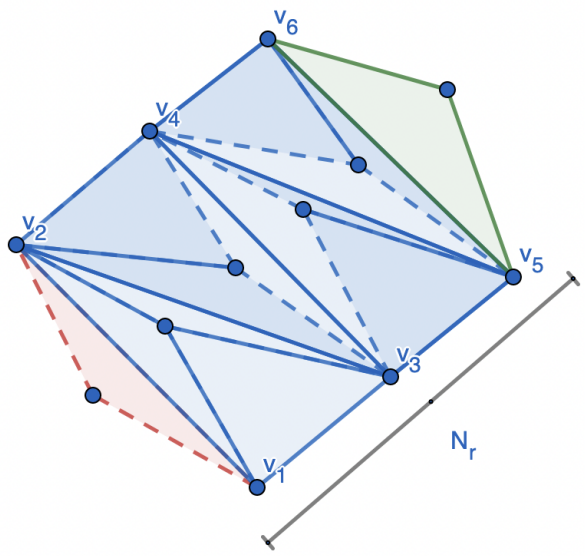

Figure 4.14: Part 3a: The figure illustrates the pathfinding process to obtain surface elements in the cylinder's base.

Part 3b: Getting adjacent points in layer k

To obtain a proper ceiling, it is necessary to consider points that are found in layer $k + 1$ parallel to $ceiling\_layer_k$. These can be found repeating a similar process to Part 3a when considering the edge $e_a \in E_{r,s}$ adjacent to e. We can guarantee the existence of e_a in either direction to e in $E_{r,s}$ since these are edges that approximate a circular contour. Thus, we implement Part 3a starting from e_a and store in the proper sets.

Part 4: Getting ceiling faces, upside-down tetrahedra of layer k, and side boundaries

So far, we have only obtained tetrahedra in $volume\_layer_k$ pointing upside from the boundary floor. To get the entire volume from layer k, we wish to obtain the tetrahedra pointing upside down. Although the packing of volume elements depends

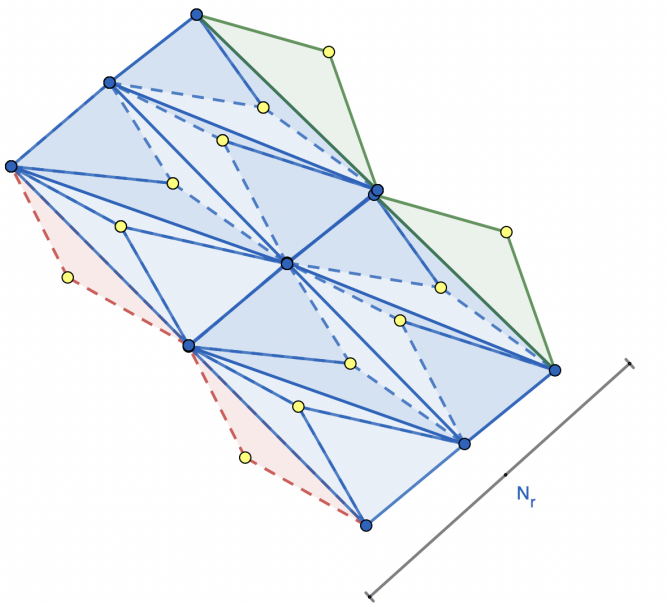

Figure 4.15: Part 3b: The figure illustrates the pathfinding process to fully obtain ceiling nodes, shown as yellow.

on the mesh and could vary slightly, the assumption of uniform mesh allows us to consider a predictable arrangement. For this step, we require the sets $upper\_vertex_k$ and $floor\_layer_k$ from Parts 3a and 3b.

1. We form combinations of four points among the points in $floor\_layer_k$ and $ceiling\_layer_k$. Then, we search among the tetrahedra in the corresponding domain and store the matching results in $volume\_layer_k$.

2. We initialize the array $ceiling\_faces_k$. To find ceiling faces, we generate combinations of three points from $ceiling\_layer_k$. We seek if any of these three-point sets are proper subsets of tetrahedra in the desired domain and add them to $ceiling\_faces_k$.

3. We create array $side\_faces_k$. To have boundaries connecting the floor and ceiling of $layer_k$, we get combinations of three points among either two points from $floor\_layer_k$ and one from $ceiling\_layer_k$ and viceversa. Then, we explore whether any of these are found in existing tetrahedra and, if so, add them to $side\_faces_k$. This step requires carefulness with arrangement and split of $floor\_layer_k$ and $ceiling\_layer_k$ to have correct desired alignment. Otherwise, we could end up forming faces illegally cutting the tetrahedra and not conforming to the existing tetrahedral layout.

Part 5: Rewriting labels and reassigning tetrahedra of layer k

We modify information directly from the file similarly to Part 3 in the Generic mesh algorithm

1. *Tetrahedra alteration.* For each member in $volume\_layer_k$, we get the correct order of nodes, write a string for current domain of each element on file and another with new domain information. We then replace the original string with the replacement one.

2. *N_s-boundary replacement.* We obtain correct order of each item $old\_Nsboundary_k$ as they appear on file. We write strings for $old\_Nsboundary_k$ in the proper format, then locate these lines and delete them. If $new\_Ns\_boundary_k$ is not empty, we write the same strings deleted with new information; otherwise, if $other\_boundary_k$ is nonempty, we write strings to replace the boundary of erase it.

3. *N_r-boundary replacement.* Finally, if *last_level* does not contain vertices in $ceiling\_layer_k$, we update vertex order in $old\_Nr\_boundary_k$. We write strings from $old\_Ns\_boundary_k$ in the correct format as found in the file and delete the lines. We then replace the deleted information with strings from $new\_Ns\_boundary_k$.

Part 6: Applications of Parts 3-5 in subsequent layers

1. If *last_level* has vertices that also appear in $ceiling\_layer_k$ and we want to either replace or erase this part of the boundary N_m, we find correct vertex order from *new_Nr_boundary* and write one or two sets of lines: one corresponding to original information and another with new information. If we only want to erase, we just use the former; but if we want to replace, we use the second set of strings as well.

2. Otherwise, if conditions for Step 1 are not met, we set $k = k + 1$, $j = 2$, and $e = w_{j-1}w_j$, where $w_{j-1} = v_{2k-1}$ and $w_j = v_{2k}$ from vertexlayer$_k$. We then implement Parts 3-5 with starting with e.

   We repeat steps 1 and 2 until we no longer can do so or wish to stop.

Remark: Instead of searching all the nodes again in boundary floors, we could rely on previous knowledge about ceiling nodes and faces and employ a dynamic programming approach by setting $floor\_layer_k = ceiling\_layer_{k-1}$.

Part 7: Selecting different edges in $E_{r,s}$

1. We pick a different edge $e \in E_{r,s}$ and implement Parts 2-6.

2. We repeat step 1 until we no longer wish to continue or cannot do so.

4.4 Computational Results

We provide some results regarding the implementation of the aforementioned algorithms. In all of these cases, the number of volume elements remains unchanged; some of them just get reassigned to a different domain. On the other hand, the quantity of surface elements could fluctuate. As has been the emphasis of this chapter, we use this example to show the versatility of the algorithm to sculpt and modify geometries rather than to solve for differential equations via FEM; for modeling solutions using geometries obtained through meshing reassignment, we refer to the previous chapter.

4.4.1 Example: Cube

Coarse cube

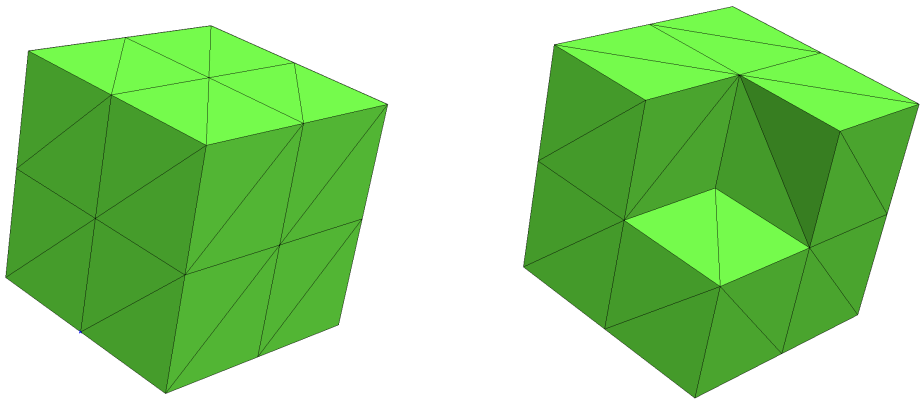

Figure 4.16: The cube on the left shows the original cube without modification while the one on the right shows the visible alterations.

We first consider the simple mesh shown on the left side of Figure 4.16. It is a cube having a coarse mesh with eighty-eight volume elements and forty-eight surface elements. Using a variation of the Generic mesh algorithm, we reassign a quarter of the volume elements to the external (default) zero domain. The total of surface

elements is still the same but now they reflect the proper domains after modification. The right side of the same figure displays the transformation. The initial mesh remains intact, but the labels were changed to obtain a slightly different geometry.

Fine cube

For this instance, we implement a carving algorithm on Figure 4.5. The mesh has 11776 volume elements and 768 boundary faces. We decide to "extract" every single initial surface element by reassigning their corresponding tetrahedra to the external zero domain. We then relabel these faces to the other adjacent ones within the tetrahedra. The result is shown in Figure 4.17 and has 2304 boundary faces, three times more than the original amount. This geometry was not designed with FEM implementation in mind but rather to elucidate what can be done with meshing reassignment.

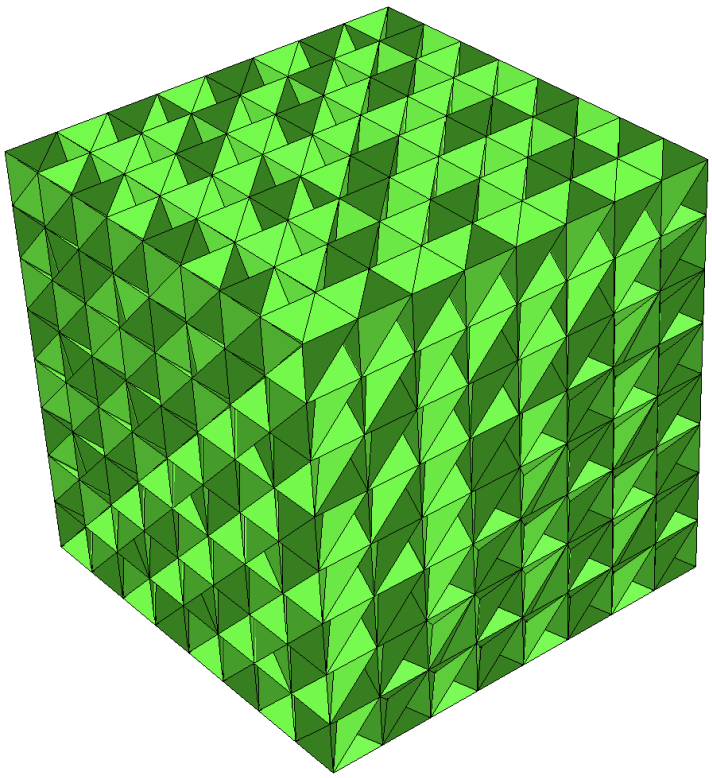

Figure 4.17: Transformation of the mesh in Figure 4.5

4.4.2 Example: Creating a stent

We present a few examples with coarse, medium, and fine meshes based on the same geometry. All of these are composed of three domains and ten boundaries, with the stent domain being surrounded by four. The main geometry was meshed with Netgen, whereby all the pathfinding is done.

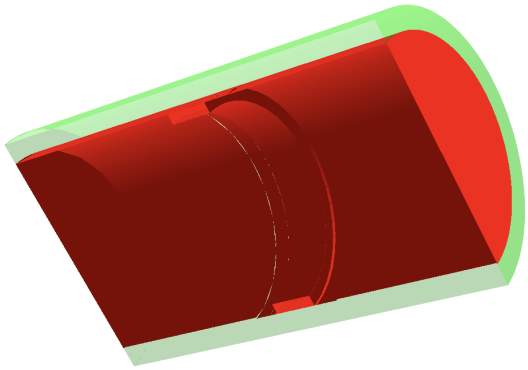

Figure 4.18: Cross-section of the initial stent geometry before meshing (left), after meshing (center), and with reassignment modification (right).

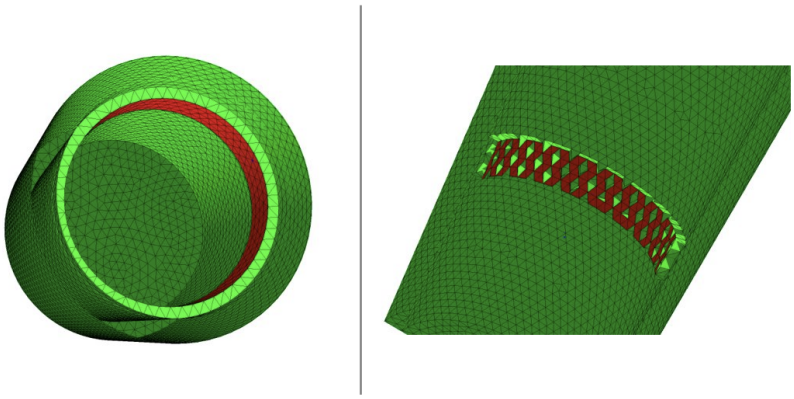

Figure 4.19: Cross-section of some initial stent mesh (left) and after reassignment modification (right).

Coarse stent mesh

As seen on Figure 4.20, the coarse stent mesh has 64822 tetrahedral elements and 13304 surface triangles. We modify the stent by carving in a zigzag manner. After implementing the algorithm, the mesh has 14266 boundary elements and took 18 minutes and 11 seconds for element reassignment.

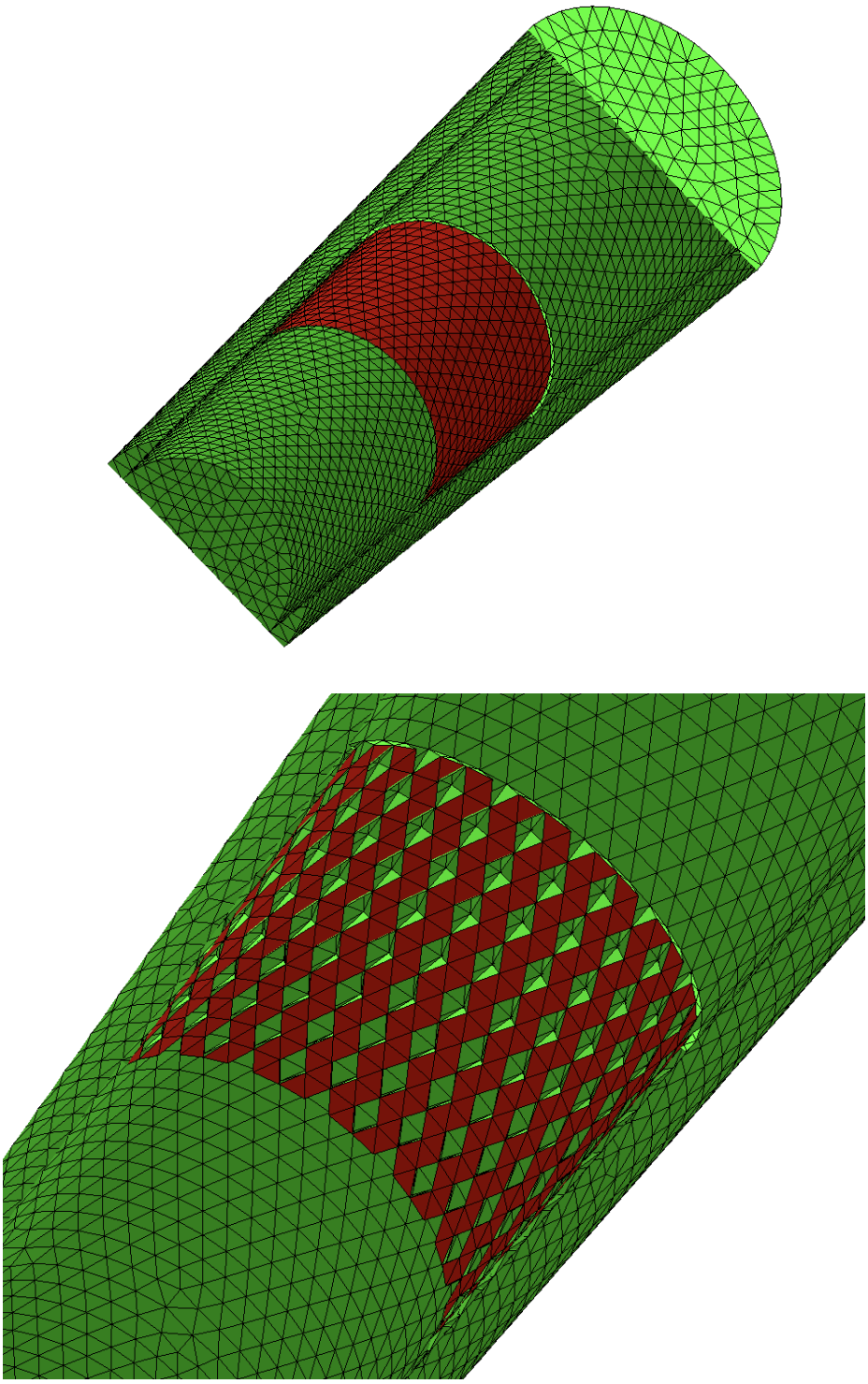

Figure 4.20: Cross-section of the initial coarse stent mesh, before (top) and after (bottom) modifications . The red area corresponds to the stent shell.

Fine stent mesh

Originally, the number of volume elements is 247811 with 30188 surface boundaries.

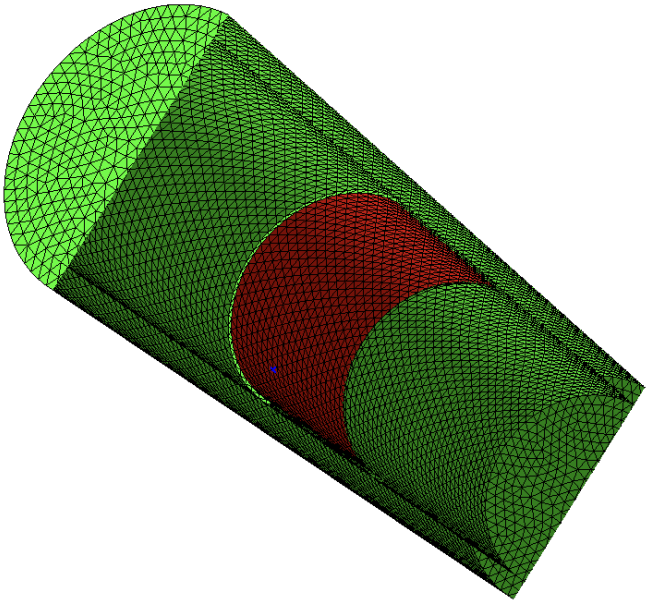

After implementing reassignment algorithm, the number of volume elements remains the same but now there are 32896 surface boundaries. With this finer mesh, the new transformation resembles a stent much more. However, given the increased number of elements, it took 2 hours, 43 minutes, and 20 seconds to complete the overall transformation. Most of the time in the implementation was devoted to searching elements while modifying the file directly was rather quick in the order of a couple seconds.

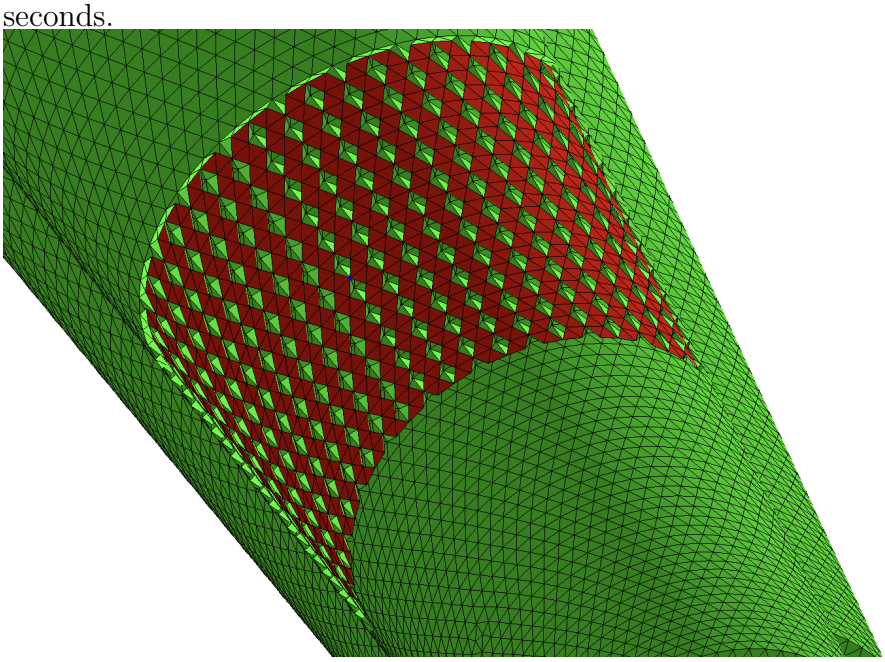

Figure 4.21: Cross-section of the fine stent geometry, before (upper) and after (lower) modifications. The red area corresponds to the stent shell.

4.4.3 Example: Volume-less Stents

Here we present three designs in which the stent volume has been completely reassigned to the lumen domain, but the stent boundaries are visible. However, these are only for design purposes and showing the potential behind meshing reassignment, rather than for an assessment of our domaing decomposition techniques when obtaining FEM solutions.

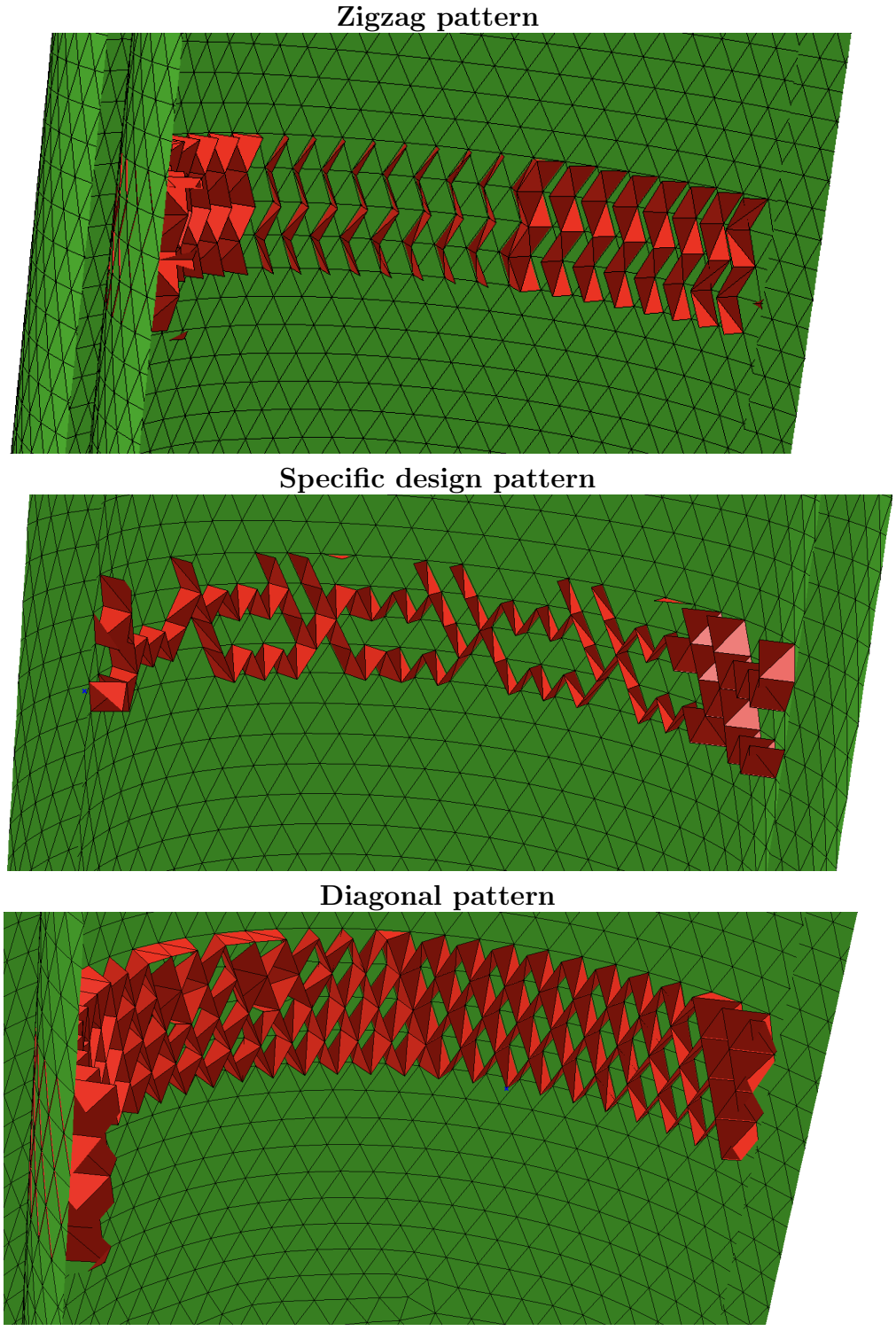

Figure 4.22: Cross-sections of volume-less stent geometries having zigzag pattern.

4.5 Discussion

The results show that element reassignment is possible for geometry reconstruction starting from an initial mesh. And while carving implementations have been explored before in [23], the outward-to-inward approach is rather limiting and monotonous, so that it only removes permanently. With our multidomain technique, we are able to tackle any direction between domains, as was seen with the outward transformations from the inner cylinder. This allows us to preserve outer mesh layers intact while modifying other inner regions. While our method is in early stages, it has potential to become more sophisticated, especially when combined and integrated with other established meshing algorithms and techniques. Indeed, rather than compete with other processes, the reassignment mesh aims to be an additional tool to improve and maximize definition and geometrical precision. For instance, instead of deforming several elements, it might be more helpful to "extricate" them instead by blending them with surrounding domains via mesh reassignment.

Semi-automatic mesh reassignment is easier to implement with coarser meshes, when paths between elements are simpler and time complexities of searches among potential element candidates are smaller. After which, the mesh can be properly refined and other meshing techniques could be employed. One key disadvantage with mesh reassignment occurs with finer meshes, since it takes more time to search through elements. On the other hand, once the initial structure is finished, reassigning elements individually rather than collectively becomes more doable. This is particularly good if we seek to model erosion or buildup (e.g. plaque) and have some mapping to mark certain elements through the solution of the system, then isolated reassignments are straightforward. This is what we deem to be the method's strength: that we can account for changes in geometry without having to remesh, saving computational time and energy in the long term by not drafting new geometries and meshes from scratch over and over.

Chapter 5

Future Work

The ultimate purpose of this project is to have a realistic and thorough understanding of stents through mathematical modeling. In this chapter, we highlight some of the ideas that we expect to provide continuity for in the near future.

5.1 Elution and Erosion via Meshing Reassignment

While a domain decomposition was elaborated to model the fluid mechanics taking into account the current geometry, a methodology to explain vanishing components of concentrations was not fulfilled. In particular, we hope that combining the techniques of Chapter 4 with Chapter 3 and Chapter 2 will enable the elaboration of processes dealing with the natural disappearance and bodily absorption of these fluids.
The meshing reassignment allows consideration for semi-discrete time evolving domains by swapping stent elements, corresponding to dispersed concentration measures, with those nearby such as the wall or lumen domains. The discarding of elements can be potentially determined through element thresholding, in which each element has a measure or charge capacity that is over time decreasing depending on their direct contact with external environments such as blood and plasma filtration. Once this measure reaches zero, we reassign the element without having to create a new geometry. This also could result in modeling malapposition of stents, depending on the core's distance from the wall, as well as the erosion of bioresorbable stents, when the chemical relationships of the polymeric structures are understood.

5.2 Mapping of Time-Evolving Domains

While we introduce (general) mappings from initial domains to domains later in time, their numerical approach was not given. We posit that this can be done by looking at level sets from data to have a better understanding behind the natural transition of these stents.

5.3 Patient-Specific Modeling

Another objective is to be able to eventually create a model working on real-patient data (See Figure 5.3). Currently, there is development of digital reconstructions that explain the deformation of the stent over time. This project has been trying to meet such goal from the other then. We hope in the future to polish our methods and techniques to fully integrate the model.[38]

5.4 Optimization of Stents

Finally, modeling coronary stents can help their improvements. By controlling the initial parameters, geometries, and overall settings of stents, we want to be able to predict the long term behavior of coronary stents. Once we achieve this, we may start thinking about tweaking variables and designs with the goal of providing an optimal stent that works in the majority of cases for the longest time without further medical complications or surgical interventions.

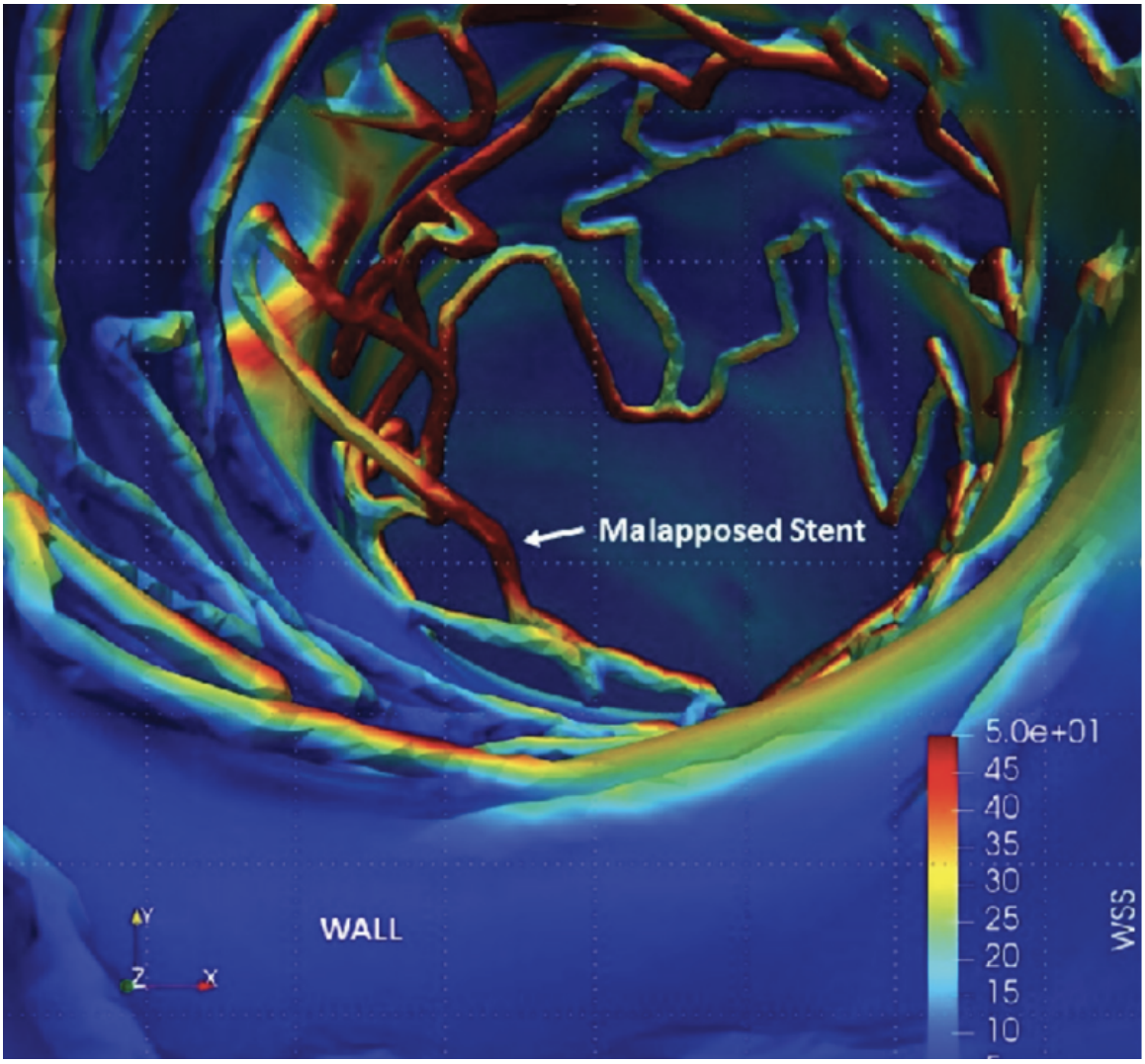

Figure 5.1: Digital reconstruction of stent with real patient data

Appendix A

Summary of the numerical schemes implemented

We refer to the documentation of NGSolve [54] regarding the implementation of numerical schemes to solve some partial differential equations relevant in this project.

A.1 Advection-Diffusion Equations

We consider the following system of advection-diffusion equations in weak form in $\Omega \subset \mathbb{R}^d$: Find $C : [0, T] \to H^1_{0,D}(\Omega))^d$ such that

$$\int_\Omega \frac{\partial C}{\partial t} v d\omega + \int_\Omega \nu \nabla C \nabla v d\omega + \int_\Omega \mathbf{u} \cdot \nabla C v d\omega = \int_\Omega f v d\omega \quad \forall v \in H^1_{0,D}$$
$$C(t = 0) = C_0,$$

where ν is a given viscosity, C_0 is an initial condition, $\mathbf{u}$ is a convective field, and f is a given source function. Let $\mathcal{T}_h$ be a mesh triangulation on Ω, so that a FEM space for C is

$$C \in V = \{v \in H^1(\Omega) : v|_{\mathcal{T}_h} \in \mathcal{P}^k(\mathcal{T}_h)\}^d,$$

with $\mathcal{P}^k$ being the space of polynomials of degree k. We then define bilinear and linear forms as follows for members of $H^1_{0,D}(\Omega)$

$$m_1(C,v) = \int_\Omega Cvd\omega, \qquad m_2(C,v) = \int_\Omega \nu\nabla C\nabla vd\omega,$$
$$k(C,v) = \int_\Omega \mathbf{u}\cdot\nabla Cvd\omega, \qquad F(v) = \int_\Omega fvd\omega.$$

Solving over V, we have the problem:
Find $C \in V$ such that for all $v \in V$

$$m_1\left(\frac{\partial C}{\partial t}, v\right) + m_2(C,v) + k(C,v) = F(v).$$

Starting with time $t = 0$, we discretize $[0,T]$ into N uniform intervals of length Δt and define $t^n = n\Delta t$. We adopt the superscript notation to indicate the solution in time we are employing (i.e. $C^n = C(t^n)$). We implement a Backward Euler implicit scheme so that we use the $n+1$-th step whenever possible, and hence the problem now reads
Find $C^{n+1} \in V$ such that for all $v \in V$

$$\frac{1}{\Delta t}m_1(C^{n+1} - C^n) + m_2(C^{n+1}, v) + k(C^{n+1}, v) = F^{n+1}(v).$$

In matrix form, denoting the matrices of bilinear forms with non-bold upper case letters and vectors of solutions with bold upper case letters, we have

$$M_1\mathbf{C}^{n+1} + \Delta t(M_2\mathbf{C}^{n+1} + K\mathbf{C}^{n+1}) = M_1\mathbf{C}^n + \Delta t\mathbf{F}.$$

We use the incremental form $\mathbf{C}^{n+1} = \mathbf{C}^n + \delta\mathbf{C}^{n+1}$ to have

$$M_1(\mathbf{C}^{n+1} - \mathbf{C}^n) + \Delta t(M_2(\mathbf{C}^{n+1} - \mathbf{C}^n) + K(\mathbf{C}^{n+1} - \mathbf{C}^n)) = \Delta t(-M_2\mathbf{C}^n - K\mathbf{C}^n + \mathbf{F}^{n+1}).$$

Then, through substitution, we get

$$(M_1 + \Delta t(M_2 + K))\delta\mathbf{C}^{n+1} = -\Delta t(M_2\mathbf{C}^n + K\mathbf{C}^n - \mathbf{F}^{n+1})$$

Defining $S = M_1 + \Delta t(M_2 + K)$, we have

$$S\delta\mathbf{C}^{n+1} = -\Delta t(M_2\mathbf{C}^n + K\mathbf{C}^n - \mathbf{F}^{n+1}).$$

Therefore, we can update $C^{n+1} = C^n + \delta C^{n+1}$.

A.2 Navier-Stokes Equations

Consider the following unsteady Navier-Stokes problem in weak form in some region $\Omega \subset \mathbb{R}^d$:
Find $(\mathbf{u}, p) : [0, T] \to (H^1_{0,D}(\Omega))^d \times L^2$ such that

$$\begin{aligned}\int_\Omega \frac{\partial \mathbf{u}}{\partial t} \cdot \mathbf{v} d\omega + \int_\Omega \nu \nabla \mathbf{u} \nabla \mathbf{v} d\omega + \int_\Omega \mathbf{u} \cdot \nabla \mathbf{u} \mathbf{v} d\omega - \int_\Omega \operatorname{div}(\mathbf{v}) p d\omega = \int_\Omega \mathbf{f} \cdot v d\omega \quad \forall \mathbf{v} \in (H^1_{0,D})^d,\\ - \int_\Omega \operatorname{div}(\mathbf{u}) q d\omega = 0 \quad \forall q \in L^2,\\ \mathbf{u}(0) = u_0 \quad \text{on} \quad \partial\Omega_{in},\end{aligned}$$

where ν is a given viscosity, $\mathbf{u}_0$ is an initial boundary condition, and $\mathbf{f}$ is a given source function. We assume a suitable mesh triangulation $\mathcal{T}_h$ on Ω and employ a Taylor-Hood discretization of degree k. This means that the FEM space for $\mathbf{u}$ and p are

$$\begin{aligned}\mathbf{u} \in V &= \{\mathbf{v} \in H^1(\Omega) : \mathbf{v}|_{\mathcal{T}_h} \in \mathcal{P}^k(\mathcal{T}_h)\}^d\\ p \in Q &= \{q \in H^1(\Omega) : q|_{\mathcal{T}_h} \in \mathcal{P}^{k-1}(\mathcal{T}_h)\},\end{aligned}$$

where $\mathcal{P}^k$ is the space of polynomials of degree k. To ease notation and solving, we define following the bilinear and trilinear forms:

$$\begin{aligned}m_1(\mathbf{u}, \mathbf{v}) &:= \int_\Omega \mathbf{u} \cdot \mathbf{v} d\omega, \qquad m_2(\mathbf{u}, \mathbf{v}) := \int_\Omega \nu \nabla \mathbf{u} \nabla \mathbf{v} d\omega,\\ r(\mathbf{u}, p) &:= \int_\Omega \operatorname{div}(\mathbf{u}) p d\omega, \qquad c(\mathbf{w}; \mathbf{u}, \mathbf{v}) := \int_\Omega \mathbf{w} \cdot \nabla \mathbf{u} \mathbf{v} d\omega.\end{aligned}$$

We also let $F(\mathbf{v})$ be the linear form

$$F(\mathbf{v}) := \int_\Omega \mathbf{f} \cdot \mathbf{v} d\omega.$$

Thus, if we consider the space product $X = V \times Q$, we have the problem
Find $(\mathbf{u}, p) \in X$ such that for all $(\mathbf{v}, q) \in X$

$$m_1\left(\frac{\partial \mathbf{u}}{\partial t}, \mathbf{v}\right) + m_2(\mathbf{u}, \mathbf{v}) + c(\mathbf{u}; \mathbf{u}, \mathbf{v}) - r(\mathbf{v}, p) - r(\mathbf{u}, q) = F(\mathbf{v}).$$

For our purposes, we decided to implement an IMEX (Implicit-Explicit) scheme by letting the convective part be partially explicit and everything else implicit. The problem then becomes Find $(\mathbf{u}^{n+1}, p^{n+1}) \in X$ such that for all $(\mathbf{v}, q) \in X$

$$\frac{1}{\Delta t} m_1(\mathbf{u}^{n+1} - \mathbf{u}^n, \mathbf{v}) + m_2(\mathbf{u}^{n+1}, \mathbf{v}) + c(\mathbf{u}^n; \mathbf{u}^n, \mathbf{v}) - r(\mathbf{v}, p^{n+1}) - r(\mathbf{u}^{n+1}, q) = F(\mathbf{v}),$$

with Δt being the time interval. Multiplying by Δt and expressing in matrix form, we have

$$M_1 \mathbf{U}^{n+1} + \Delta t(M_2 \mathbf{U}^{n+1} - R^T \mathbf{P}^{n+1} - R\mathbf{U}^{n+1}) = M_1 \mathbf{U}^n - \Delta t(C\mathbf{U}^n - \mathbf{F}),$$

where we can solve for $\mathbf{U}^{n+1}$ and $\mathbf{P}^{n+1}$.

Bibliography

[1] Arteriosclerosis / atherosclerosis. URL https://www.mayoclinic.org/diseases-conditions/arteriosclerosis-atherosclerosis/symptoms-causes/syc-20350569?utm_source=Google&utm_medium=abstract&utm_content=Atherosclerosis&utm_campaign=Knowledge-panel.

[2] M. Tuveri A. Quarteroni and A. Veneziani. Computational vascular fluid dynamics: Problems, models and methods. *Comput. Visual. Sci.*, 2:pp. 163–197, 2000.

[3] Ghanashyam Acharya and Kinam Park. Mechanisms of controlled drug release from drug-eluting stents. *Advanced drug delivery reviews*, 58(3):387–401, 2006.

[4] Kam Liu W. Moran B. Belytschko, T. and Elkhodary K. *Nonlinear Finite Elements for Continua and Structures, 2nd Edition*. Wiley, 2014. ISBN 978-1-118-63270-3.

[5] Roy Biran and Daniel Pond. Heparin coatings for improving blood compatibility of medical devices. *Advanced drug delivery reviews*, 112:12–23, 2017.

[6] H. Brezis. *Functional Analysis, Sobolev Spaces, and Partial Differential Equations*. Springer, 2010. ISBN 978-0-387-70913-0.

[7] Alexander N Brooks and Thomas JR Hughes. Streamline upwind/petrov-galerkin formulations for convection dominated flows with particular emphasis on the incompressible navier-stokes equations. *Computer methods in applied mechanics and engineering*, 32(1-3):199–259, 1982.

[8] WR Castaneda-Zuniga, Augustln Formanek, Murthy Tadavarthy, Z Vlodaver, JE Edwards, C Zollikofer, and K Amplatz. The mechanism of balloon angioplasty. *Radiology*, 135(3):565–571, 1980.

[9] Mayo Clinic. Coronary angioplasty and stents. URL `https://www.mayoclinic.org/tests-procedures/coronary-angioplasty/about/pac-20384761`.

[10] MJ Davies and N Woolf. Atherosclerosis: what is it and why does it occur? *British heart journal*, 69(1 Suppl):S3, 1993.

[11] Giuliani S. Halleux J. P. Donea, J. An arbitrary lagrangian-eulerian finite element method for transient dynamic fluid-structure interactions. *Computer Methods in Applied Mechanics and Engineering*, 33(1-3):pp. 689–723, 1982. doi: 10.1016/0045-7825(82)90128-1.

[12] L. Evans. *Partial Differential Equations*. 2nd ed. American Mathematical Society, 2010. ISBN 978-0-8218-4974-3.

[13] Erling Falk. Pathogenesis of atherosclerosis. *Journal of the American College of cardiology*, 47(8S):C7–C12, 2006.

[14] Shady Farah. Protective layer development for enhancing stability and drug-delivery capabilities of des surface-crystallized coatings. *ACS applied materials & interfaces*, 10(10):9010–9022, 2018.

[15] Luca Formaggia, Sara Minisini, and Paolo Zunino. Modeling polymeric controlled drug release and transport phenomena in the arterial tissue. *Mathematical models and methods in applied sciences*, 20(10):1759–1786, 2010.

[16] Jones M. D. Frogley, D. Fast relabeling of deformable delaunay tetrahedral meshes using a compact uniform grid. *Journal of Graphics Tools*, 17(1-2):pp. 17–29, 2013. doi: doi:10.1080/2165347x.2013.870057.

[17] Jiri Frohlich and Ahmad Al-Sarraf. Cardiovascular risk and atherosclerosis prevention. *Cardiovascular Pathology*, 22(1):16–18, 2013.

[18] Donald L Fry. Mathematical models of arterial transmural transport. *American Journal of Physiology-Heart and Circulatory Physiology*, 248(2):H240–H263, 1985.

[19] Su Y. Qin Y. X. Zheng Y. Wang Y. Zhu D. Fu, J. Evolution of metallic cardiovascular stent materials: a comparative study among stainless steel, magnesium and zinc. *Biomaterials*, 230, 2020. doi: 119641.

[20] Francesco Giannini, Luciano Candilio, Satoru Mitomo, Neil Ruparelia, Alaide Chieffo, Luca Baldetti, Francesco Ponticelli, Azeem Latib, and Antonio Colombo. A practical approach to the management of complications during percutaneous coronary intervention. *JACC: Cardiovascular Interventions*, 11(18):1797–1810, 2018.

[21] Cindy L Grines, David A Cox, Gregg W Stone, Eulogio Garcia, Luiz A Mattos, Alessandro Giambartolomei, Bruce R Brodie, Olivier Madonna, Marcel Eijgelshoven, Alexandra J Lansky, et al. Coronary angioplasty with or without stent implantation for acute myocardial infarction. *New England Journal of Medicine*, 341(26):1949–1956, 1999.

[22] E Grouve and S Kristensen. Stent thrombosis: definitions, mechanisms and prevention. *E-journal of Cardiology Practice*, 32(5), 2007.

[23] Nate Hagbi and Jihad El-Sana. Carving for topology simplification of polygonal meshes. *Computer-Aided Design*, 42(1):67–75, 2010.

[24] Göran K Hansson and Andreas Hermansson. The immune system in atherosclerosis. *Nature immunology*, 12(3):204–212, 2011.

[25] Jorg Hausleiter, Adnan Kastrati, Rainer Wessely, Alban Dibra, Julinda Mehilli, Thomas Schratzenstaller, Isolde Graf, Magdalena Renke-Gluszko, Boris Behnisch, Josef Dirschinger, et al. Prevention of restenosis by a novel drug-eluting stent system with a dose-adjustable, polymer-free, on-site stent coating. *European heart journal*, 26(15):1475–1481, 2005.

[26] J. Heywood. The navier-stokes equations: On the existence, regularity and decay of solutions. *Indiana Univ. Math. J.*, 29:pp. 639–681, 1980.

[27] J. Heywood and R. Rannacher. Finite element approximation of the nonstationary navier-stokes problem. i.regularity of solutions and second-order error estimates for spatial discretization. *SIAM J. Numer. Anal.*, 19:pp. 275–311, 1982.

[28] Takeru Higuchi. Rate of release of medicaments from ointment bases containing drugs in suspension. *Journal of pharmaceutical sciences*, 50(10):874–875, 1961.

[29] E. Hopf. Uber die aufgangswertaufgabe fur die hydrodynamischen grundliechungen. *Math. Nachr.*, 4:pp. 213–231, 1951.

[30] Russell R. D. Huang, W. *Adaptive Moving Mesh Methods*. Applied Mathematical Sciences. Springer, 2010. ISBN 978-1-4419-7915-5.

[31] Javaid Iqbal, Julian Gunn, and Patrick W Serruys. Coronary stents: historical development, current status and future directions. *British medical bulletin*, 106 (1), 2013.

[32] E. Magenes J.-L. Lions. Problemes aux limites non homoqenes et applications. *Dunod*, 1, 1968a.

[33] Da-Won Jeong, Wooram Park, Tarek M Bedair, Eun Young Kang, Ik Hwan Kim, Dae Sung Park, Doo Sun Sim, Young Joon Hong, Won-Gun Koh, Myung Ho Jeong, et al. Augmented re-endothelialization and anti-inflammation of coronary drug-eluting stent by abluminal coating with magnesium hydroxide. *Biomaterials science*, 7(6):2499–2510, 2019.

[34] Hiroyuki Jinnouchi, Sho Torii, Atsushi Sakamoto, Frank D Kolodgie, Renu Virmani, and Aloke V Finn. Fully bioresorbable vascular scaffolds: lessons learned and future directions. *Nature Reviews Cardiology*, 16(5):286–304, 2019.

[35] Shishir Karthik, Antony D Grayson, Emer E McCarron, D Mark Pullan, and Michael J Desmond. Reexploration for bleeding after coronary artery bypass surgery: risk factors, outcomes, and the effect of time delay. *The Annals of thoracic surgery*, 78(2):527–534, 2004.

[36] Malgorzata Kloc and Rafik M Ghobrial. Chronic allograft rejection: A significant hurdle to transplant success. *Burns & trauma*, 2(1):2321–3868, 2014.

[37] Banka G Lee MS. In-stent restenosis. *Interv Cardio Clin.*, 5:pp. 211–220, 2016. doi: 10.1016/j.iccl.2015.12.006.

[38] Adrien Lefieux, Sara Bridio, David Molony, Marina Piccinelli, Claudio Chiastra, Habib Samady, Francesco Migliavacca, and Alessandro Veneziani. Semi-automatic reconstruction of patient-specific stented coronaries based on data assimilation and computer aided design. *Cardiovascular Engineering and Technology*, pages 1–18, 2022.

[39] J. Leray. Etude de diverses equations int egrales et de quelques probl'emes que pose l'hydro-dynamique. *J. Math. Pures Appl.*, 12:pp. 1–82, 1933.

[40] J. Leray. Essai sur les mouvement d'un liquide visqueux emplissant l'espace. *Acta. Math.*, 63:pp. 193–248, 1934.

[41] J. Leray. Essai sur les mouvements plans d'un liquide visqueux que limitent des parois. *J. Math. Pures Appl.*, 13:pp. 331–418, 1934.

[42] MARK A Lovich and ELAZER R Edelman. Computational simulations of local vascular heparin deposition and distribution. *American Journal of Physiology-Heart and Circulatory Physiology*, 271(5):H2014–H2024, 1996.

[43] Thomas F Luscher, Jan Steffel, Franz R Eberli, Michael Joner, Gaku Nakazawa, Felix C Tanner, and Renu Virmani. Drug-eluting stent and coronary thrombosis: biological mechanisms and clinical implications. *Circulation*, 115(8):1051–1058, 2007.

[44] G. L. Maile. *Three-dimensional analysis of electromagnetic problems by finite element methods*. PhD thesis, University of Cambridge, U.K., 1979.

[45] Chaudhuri P. Mandal, A. and S. Chaudhuri. Remeshing-free graph-based finite element method for fracture simulation. 0 (0), 2022.

[46] Noel L Mills and Charles T Everson. Atherosclerosis of the ascending aorta and coronary artery bypass: pathology, clinical correlates, and operative management. *The Journal of thoracic and cardiovascular surgery*, 102(4):546–553, 1991.

[47] Duk-Woo Park, Seong-Wook Park, Kyoung-Ha Park, Bong-Ki Lee, Young-Hak Kim, Cheol Whan Lee, Myeong-Ki Hong, Jae-Joong Kim, and Seung-Jung Park. Frequency of and risk factors for stent thrombosis after drug-eluting stent implantation during long-term follow-up. *The American journal of cardiology*, 98 (3):352–356, 2006.

[48] Giuseppe Pontrelli and Filippo de Monte. Mass diffusion through two-layer porous media: an application to the drug-eluting stent. *International Journal of Heat and Mass Transfer*, 50(17-18):3658–3669, 2007.

[49] A. Quarteroni and A. Valli. *Numerical Approximation of Partial Differential Equations*. Springer-Verlag, 1994.

[50] A. Quarteroni, A. Valli. Theory and applications of steklov-poincaré operators for boundary-value problems. *Applied and Industrial Mathematics*, pages pp. 179–203, 1991.

[51] Alfio Quarteroni and Alberto Valli. *Domain decomposition methods for partial differential equations*. Number BOOK. Oxford University Press, 1999.

[52] Alfio Quarteroni, Alessandro Veneziani, and Paolo Zunino. A domain decomposition method for advection-diffusion processes with application to blood solutes. *SIAM Journal on Scientific Computing*, 23, 01 2002. doi: 10.1137/S1064827500375722.

[53] Alfio Quarteroni, Alessandro Veneziani, and Paolo Zunino. Mathematical and numerical modeling of solute dynamics in blood flow and arterial walls. *SIAM Journal on Numerical Analysis*, 39, 01 2002. doi: 10.1137/S0036142900369714.

[54] J. Schroebel. Netgen/NGSolve. `https://ngsolve.org/`.

[55] Trevor Simard, Benjamin Hibbert, F Daniel Ramirez, Michael Froeschl, Yong-Xiang Chen, and Edward R O'Brien. The evolution of coronary stents: a brief review. *Canadian Journal of Cardiology*, 30(1):35–45, 2014.

[56] R. Temam. *Navier-Stokes Equations and Nonlinear Functional Analysis*. SIAM, 1983.

[57] R. Temam. *Navier-Stokes Equations: Theory and Numerical Analysis*. North-Holland, 1984.

[58] Subbu Venkatraman and Freddy Boey. Release profiles in drug-eluting stents: issues and uncertainties. *Journal of Controlled Release*, 120(3):149–160, 2007.

[59] Christian Vergara and Paolo Zunino. Multiscale boundary conditions for drug release from cardiovascular stents. *Multiscale Modeling & Simulation*, 7(2):565–588, 2008.

[60] Jessica E Wagenseil and Robert P Mecham. Vascular extracellular matrix and arterial mechanics. *Physiological reviews*, 89(3):957–989, 2009.

[61] Jiang Zhang, Yang Liu, Rifang Luo, Si Chen, Xin Li, Shuheng Yuan, Jin Wang, and Nan Huang. In vitro hemocompatibility and cytocompatibility of dexamethasone-eluting plga stent coatings. *Applied Surface Science*, 328, 02 2015. doi: 10.1016/j.apsusc.2014.12.002.

[62] Meital Zilberman and Robert C Eberhart. Drug-eluting bioresorbable stents for various applications. *Annual review of biomedical engineering*, 8(1):153–180, 2006.